European Reviews of Chemical Research

Has been issued since 2014. ISSN 2312-7708
2015. Vol.(3). Is. 1. Issued 4 times a year

The journal is registered by Federal Service for Supervision of Mass Media, Communications and Protection of Cultural Heritage (Russian Federation). Registration Certificate **ПИ № ФС77-57042** 25.02.2014.

Journal is indexed by: **CrossRef** (UK), **Electronic scientific library** (Russia), **Journal Index** (USA), **Open Academic Journals Index** (Russia), **ResearchBib** (Japan), **Scientific Indexing Services** (USA)

All manuscripts are peer reviewed by experts in the respective field. Authors of the manuscripts bear responsibility for their content, credibility and reliability.

Editorial board doesn't expect the manuscripts' authors to always agree with its opinion.

Postal Address: 26/2 Konstitutcii, Office 6
354000 Sochi, Russian Federation

Website: http://ejournal14.com/en/index.html
E-mail: evr2010@rambler.ru
Founder and Editor: Academic Publishing House *Researcher*

Passed for printing 15.03.15.
Format 21 × 29,7/4.
Enamel-paper. Print screen.
Headset Georgia.
Ych. Izd. l. 5,1. Ysl. pech. l. 5,8.
Circulation 500 copies. Order № 103.

European Reviews of Chemical Research

2015

Is. 1

Европейские обзоры химических исследований

2015

№ 1

Европейские обзоры химических исследований

Издается с 2014 г. ISSN 2312-7708
2014. № 2 (2). Выходит 4 раза в год.

Журнал зарегистрирован Федеральной службой по надзору в сфере массовых коммуникаций, связи и охраны культурного наследия (Российская Федерация). Свидетельство о регистрации средства массовой информации **ПИ № ФС77-57042** 25.02.2014.

Журнал индексируется в: **CrossRef** (Великобритания), **Journal Index** (США), **Научная электронная библиотека** (Россия), **Open Academic Journals Index** (Россия), **ResearchBib** (Япония), **Scientific Indexing Services** (США)

Адрес редакции: 354000, Российская Федерация, г. Сочи, ул. Конституции, д. 26/2, оф. 6
Сайт журнала: **http://ejournal14.com**
E-mail: **evr2010@rambler.ru**

Учредитель и издатель: ООО «Научный издательский дом "Исследователь"» - Academic Publishing House *Researcher*

Подписано в печать 15.03.15.
Формат 21 × 29,7/4.
Бумага офсетная.
Печать трафаретная.
Гарнитура Georgia.
Уч.-изд. л. 5,1. Усл. печ. л. 5,8.
Тираж 500 экз. Заказ № 103.

C O N T E N T S

Published in the Russian Federation
European Reviews of Chemical Research
Has been issued since 2014.
ISSN: 2312-7708
Vol. 3, Is. 1, pp. 4-24, 2015

DOI: 10.13187/ercr.2015.3.4
www.ejournal14.com

UDC 538.56: 577.3: 612.6

Methods For Registering Non-Ionizing Radiation Emitted From The Human Body

[1] Ignat Ignatov
[2] Oleg Mosin
[3] Hugo Niggli
[4] Christos Drossinakis
[5] Georg Tyminski

[1] The Scientific Research Center of Medical Biophysics (SRC MB), Bulgaria
N. Kopernik Str., 32, Sofia, 1111
Professor, Doctor of Science, director of SRC MB
E-mail: mbioph@dir.bg
[2] Moscow State University of Applied Biotechnology, Russian Federation
Talalihina Str., 33, Moscow, 103316
Senior research Fellow of Biotechnology Department, PhD (Chemistry)
E-mail: mosin-oleg@yandex.ru
[3] Applied BioFotonics Inc., Albligen, Switzerland
Zelgstrasse Str., 17, 3183
Doctor of Science, consulting research employee
[4] IAWG GmbH, IAWG GmbH, Frankfurt am Main, Germany
Frankfurt am Main, 61A Königsteiner Str., 65929
Doctor of Engineering, chairman of IAWG GmbH
[5] Europäische Wissenschaftliche Gesellschaft, Germany
Hannover, 50A Sutelstr, 30659
PhD, D.M., chairman of European scientific society

Abstract

This paper presents the results of evaluation of possible biophysical methods and approaches for registering of various non-ionizing radiation (NIR) wave types of the human body in the optic and electromagnetic range. Various types of NIR (electromagnetic waves, infrared radiation, thermo radiation, bioluminiscence) emitted from the human body were reviewed. In particular the results on of spontaneous biophoton emission and delayed luminescence from the human body are submitted along with infrared thermography (IRT) results. It was shown that 1 cm^2 of skin generally emits ~85 photons for 1 s. The intensity of biophoton emission ranges from 10^{-19} to 10^{-16} W/cm^2 (approx. ~1–1000 photons·cm^{-2}·s^{-1}). The specific photon emission from part of the human thumb was detected as a spectrum of various colours with the method of Colour coronal spectral analysis on a device with an electrode made of polyethylene terephthalate (PET hostaphan) with applied electric voltage 15 kV, electric impulse duration 10 μs, and electric current frequency 15 kHz. It was established that photons corresponding to a red color emission of visible electromagnetic spectrum have energy at 1,82 eV. The orange color of visible electromagnetic spectrum has energy at 2,05 eV, yellow – 2,14 eV, blue-green (cyan) – 2,43 eV, blue – 2,64 eV, and

violet – 3,03 eV. The reliable result measurement norm was at E ≥ 2,53 eV, while the spectral range of the emission was within λ = 380–495±5 nm and λ = 570–750±5 nm. Also were estimated some important physical characteristics (energy of hydrogen bonds, wetting angle, surface tension) of water by the methods of non-equilibrium energy (NES) and differential non-equilibrium energy (DNES) spectrum of water, that helps understand in general how electromagnetic radiation interacts with water and establish the structural characteristics of water.

Keywords: electromagnetic waves; thermo-infrared radiation; bioluminescence; colour coronal spectral analysis; NES; DNES.

Introduction

All living organisms have a cellular therefore, a molecular organized structure. The living processes inside of them run on a cellular and a molecular level. Bioelectrical activity is one of the very important physical parameters of living organisms [1]. Bioelectric potentials generated by various cells are widely used in medical diagnostics [2] and are recorded as electrocardiogram, electromyogram, electroencephalogram, etc. It was proved that the human body and tissues emanate weak electromagnetic waves, the electric voltage of which is denoted as resting potential, action potential, omega-potential etc. [3]. Between the outer surface of the cell membrane and the inner contents of the cell there is always the electric potential difference which is created because of different concentrations of K^+, Na+ and Cl- inside and outside of the cell and their different permeability through the cell membrane [4]. Their value in the human body varries at ~50–80 mV and is defined by the galvanic contact of a voltmeter input with an object that indicates on the galvanic type of their source [5]. When being excited a living cell changes the membrane electric potential due to changes in membrane permeability and active ion movement through the membrane. In cells of excitable tissues (muscle, nervous), these processes can occur within a very short time intervals (milliseconds) and are called “current action” potential. Its magnitude makes up ~120 mV.

Electromagnetic fields refer to non-ionizing radiation (NIR), i.g. the radiative energy that, instead of producing charged ions when passing through matter, has sufficient energy only for excitation. Nevertheless it is known to cause biological effects [6]. The NIR spectrum is divided into two main regions, optical radiations and electromagnetic fields. The optical spectrum can be further sub-divided into ultraviolet, visible, and infra-red. The electromagnetic fields are further divided into radiofrequency (microwave, very high frequency and low frequency radio wave). NIR encompass the long wavelength (> 100 nm) and low photon energy (<12,4 eV) portion of the electromagnetic spectrum, from 1 Hz to $3 \cdot 10^{15}$ Hz.

As a result of research carried out in the 1990-s and subsequent years, it was established the property of animal and plant tissues to generate relatively strong transient NIR electric fields due to mechanical stresses and temperature changes in biological structure [7]. These electric fields are mainly due to the piezoelectric and pyroelectric voltage electric polarization of natural biological structures. Owing to cell metabolism, electric dipoles (polar and ionized molecules) involved in polarization of biostructures are continuously destroyed and restored, i.e. this is a non-equilibrium polarization. Such type of non-equilibrium electric polarization is known as a main characteristic of electrets [8]. Electrets include dielectric insulators and semiconductors, which under certain conditions, i.g. under the influence of a strong electrostatic field or ionizing radiation, light and other factors acquire property to generate an external electric field, existing for a long time (days, years) and slowly diminishes because the destruction of their substance by polarization [9]. Along with the electromagnetic field electrets generate specific elecric currents produced by heating – thermally stimulated current (TSC) [10]. Electrets belong to the non-galvanic type of electrical sources, which tend to a strong electric field (up to 10^6 V/m) and the infinitesimal electric current (~10^{-14} A/mm^2). By analogy with the physical fields the electric field emitted from the human body on its physical characteristics resembles the electric field generated by electrets. The electrets play an important role in functioning of many biological structures as they themselves possess electret properties. The bioelectret fild registered on the surface of the human body basically are generated by the basal cells of the epidermis. Dermis cells adjacent to the bottom layer of basal cells are surrounded by a conductive interstitial fluid, which electric voltage while grounding of the human body is close to zero (so called ground potential). This interstitial fluid screens off electromagnetic

fields of underlying tissues. With the average thickness of the epidermis (~0,1 mm) and the maximum value of electric voltage (~30,0 V), the electric field strength can reach significant values at ~300000 V/m [11]. The strength of the electric field is quiet sufficient for its influence on the biological processes in cells and surrounding tissues, including the synthesis of proteins and nucleic acids [12]. This electric field along with the field of transmembrane assymetry of ions concentrated at inside and outside of the membrane (~10^5 V/cm^2) can participate in the cooperative effects in cell membrane structures [13]. Thus owing to the bioelectret condition of certain subcellular structures in the cell and its surroundings is generated slowly oscillating electric field that is strong enough to influence the biological processes. This field and the electric field due to the piezoelectric voltage and intramembrane electric field formes the total electromagnetic field of the cell and its supracellular structures.

It is known that the human skin emanates electromagnetic waves in close ultraviolet range, optic range and also in close infrared range. Infrared thermal bioradiation is found in the middle infrared range at wavelengths from 8 to 14 μm. At wavelength of 9,7 μm infrared bioradiation has its maximum value at t = 36,6 ^{o}C. At this temperature the skin emission is closest to the emission of absolute black body (ABB) being at the same temperature. Infrared emission penetrates the skin surface at a depth of ~0,1 mm, and is reflected in accordance with the physical laws of reflection of the visible part of the electromagnetic spectrum. Evidently, radiation energy influences tissues while being absorbed by them. Yu.V. Gulyaev and E.E. Godik [14] determined that the threshold of skin sensitivity for infrared radiation compiled ~10^{-14} W/cm^2. When thermal influence is applied to the point of threshold skin sensitivity, there is developed a physiological reaction toward the thermal current. The intensity of the radiated thermal current generated by skin makes up ~$2{,}6 \cdot 10^{-2}$ W/cm^2.

The second component of electromagnetic waves is bioluminescence. It is supposed that biophotons, or ultraweak photon emissions of biological objects, are weak electromagnetic waves in the optical range of the spectrum [15]. The typical observed emission of biological tissues in the visible and ultraviolet frequencies ranges from 10^{-19} to 10^{-16} W/cm^2 (~1–1000 photons·cm^{-2}·sec^{-1}) [16]. This light intensity is much weaker than that one to be seen in the perceptually visible and well studied spectrum of normal bioluminescence detectable above the background of thermal radiation emitted by tissues at their normal temperature [17].

Bioelectric emission from parts of the human body as thumbs can be easily detected with the method of Color coronal spectral analysis under applying gas electrical discharge of high voltage and friquency developed by I. Ignatov [18]. This method has big scientific and practical prospects in biophysics and medical diagnostics. Its advantages include safety, sterility, clarity and interpretability of the data obtained, ease of storage and subsequent computer data processing, the ability to monitor the development of processes in time, comparing the structural, functional and temporal processes etc.

The purpose of this research was studying of possible biophysical methods and approaches for registering various NIR wave's types emitted from the human body (electromagnetic waves, infrared radiation, thermoradiation) and methods of their visualization by different technique including magnetography, infrared thermography, chemiluminescence and coronal gas discharge spectral analysis.

Material and methods

Infrared thermography (IRT)

The research was made with using infrared thermography (IRT) method according to M. Marinov. The range of the infrared thermal-imaging camera was in the middle infrared range from 9 μm to 14 μm. The temperature range was from 24,0 ^{o}C to 38,0 ^{o}C. The first camera was of Inframetrics/FLIR ThermaCam PM 290 wave type. FLIR ThermaCam PM 290, FLIR 390, Inframetrics PM 250 and Inframetrics PM 350 thermal infrared cameras were of FLIR short wave type, handheld, Focal Plane Array cameras that are capable of temperature measurement. These cameras stored images on a PCMCIA Card, and the images were further analyzed using one of several available FLIR software packages (Thermogram 95, FLIR Reporter 2000 Software, Researcher 2000). The second camera (D.I.T.I.) was a totally non-invasive clinical imaging camera for detecting and monitoring a number of diseases and physical injuries, by revealing the thermal

abnormalities present in the human body's patterns. It was used as a tool for diagnosis and prognosis, as well as monitoring therapy progress; the type of this device was TB 04 K.

Registration of electromagnetic fields

The registration of electromagnetic fields was used with super conductive detectors based on Joseffson junctions – divice made by sandwiching a thin layer of insulating nonsuperconducting material between two layers of superconducting cooper pairs (S-I-S).This allows the registering of magnetic fields 10^{10} times weaker than the Earth's magnetic field. The study of electric field nearly the human body was done using a standard Faraday cage formed by conducting material (aluminium foil) blocks external static and non-static electric fields by channeling electricity through the conducting material, providing constant voltage on all sides of the enclosure.

Biophoton detection

The measurement was made with using photoemission detector with photomultiplier (EMI9558QA selected type) in impervious to the light dark room wherein the light was minimized about ~5 cps. This was 4 times lower than the noise of the cooled photomultiplier – 20 cps. The photomultiplier was connected through an amplifier and other intermediate devices with potentiometer recorder or a personal computer. The detection of biophoton emission was performed within time interval with real count rate 3 cps, for 30 min, with reliability according to *t* criterion of Student at $p < 0,05$. The registration was performed from area of the skin with average diameter 7 cm within time interval of 100 ms or 1 s. The calculation of biophoton emission was measured in count/100 ms/count. The irradiation time of the 150 W-tungsten lamp was 5 s. Within 100 ms after switching off the external lamp the first measurement of delayed luminescence was recorded; after then were recorded 256 units of the delayed luminescence. Delayed luminescence of biological objects and tissues in terms of coherent states was detected within time intervals of 100 ms. Relaxation function was of 25,6 units.

Colour coronal gas discharge spectral analysis

Experiments were caried out by using selective high-frequency electric discharge (SHFED) on a device with the electrode made of polyethylene terephthalate (PET, hostafan) with an electric voltage on the electrode 15 kV, electric impulse duration 10 μs, and electric current frequency 15 kHz. The electrode of the device was made of hostafan, and was filled up with electro-conductive fluid. The spectral range of the emission was in the range at λ = 380–495±5 nm and λ = 570–750±5 nm. The measurements were measured in electronvolts (eV). Detection of gas disharge glowing was conducted in a dark room equipped with a red filter. On the electrode put a photosensitive paper or color film. The object under study (human thumb) was placed on top of a sheet of photo paper or color film. Between the object and the electrode were generated impulses of the electric voltage 15 kV and electric current frequency – 15–24 kHz; on the reverse side of the electrode was applied the transparent electrically conductive thin copper coating. Under these conditions in the thin contact gas space between the studied object and electrode was generated gas electric discharge in the form of characteristic glow around the object – a corona gas electric discharge in the range at λ = 280–760 nm, illuminates a color photo or a photographic film on which was judged about the bioelectric properties of the studied object. Along with the visible range, for this method were obtained color spectra in UV and IR range. Evaluation of the characteristic parameters of snapshots was based on the analysis of images treated by standard software package. Statistical processing of the experimental data was performed using the statistical package STATISTISA 6 using Student's *t*-criterion (at $p < 0,05$).

NES and DNES experiments on interaction of electromagnetic field with water

The research was made with the method of non-equilibrium spectrum (NES) and differential non-equilibrium spectrum (DNES). The device measures the angle of evaporation of water drops from 72 ° to 0 °. As the main estimation criterion was used the average energy ($\Delta E_{H...O}$) of hydrogen O...H-bonds between H_2O molecules in water's samples. The spectrum of water was measured in the range of energy of hydrogen bonds 0,08–0,387 eV or λ = 8,9–13,8 μm with using a specially designed computer program.

Results and Discussion

Electric fields

The electric field surrounding the human body with frequency $\nu = 1 \cdot 10^3$ Hz is created by electrochemical processes in the organism and is modulated by the rhythm of internal organs [19]. The spatial distribution of the electric field around the body reflects the teamwork of the different organs and systems in the organism. There are also electric fields, which are generated by accumulation of triboelectric (caused by friction) charge on the epidermis, which depends on epidermal electric resistance and varies from 10^9 to 10^{11} Ω/cm^2. Radiothermal emission is being detected in the centimetre and decimetre range of the spectrum. This type of emission is connected with the temperature and the biorhythms of the internal organs, and is being absorbed by surface layer of skin at depth from 5 cm to 10 cm [20]. Long persistent electric field nearby the human body can be detected with using an electrometer voltmeter after neutralizing electric charges on the skin caused by triboelectric charges. The electric strength of this field is undergoing slow oscillations, and most patients exert its value within the range of 100–1000 V/m at a distance of 5–10 cm from the body. People in a state of clinical death usually have the electric field strength's value reduced to 10–20 V/m after 2–3 hours of cardiac arrest. Intensity vector of the detected electric field is found to be normal to the surface of the skin, and the electric voltage is inversely proportional to the distance. On the skin surface the electric voltage of the field (the difference of its electric potential with respect to ground potential) reaches essential values of ~10000 mV or more, i.e., is about 1000 times greater than the source electric voltage of the electric unit above the bioelectric potentials. This allows us to characterize the electric field detected nearby the human body as relatively strong electric field emitted from living tissues. Its electric voltage was measured by electrometric methods, indicating on non-galvanic type of its source.

If the physical basis of the generation of a relatively strong electric field in the human tissue is non-equilibrium electric polarization of the substance due to metabolic processes, the electric field strength should depend on these processes. As noted above, this dependence is actually observed: inhibition of tissue metabolism due to hypoxia during cardiac arrest was accompanied by drop in the electric field strength. This relationship is confirmed in experiments on animals [21]. For example, in rats inhibition of metabolism of the tissue due to cardiac arrest (death of the animal) or by general anesthesia is accompanied by a significant drop in the electric field strength [22].

Electric fields depend on the magnitude of the electric voltage and the distance from the source. Generally, the electric voltages are stable and remain the same; however electric fields are easily perturbed and distorted by many surounding objects.

Relatively strong electric field investigated in humans and animals is being formed evidently by skin's biostructures, since the electric fields of the underlying tissues are largely shielded by conductive interstitial fluid [23]. The greatest contribution to the detected electric field makes the basal cells of the epidermis – the top layer of the skin. Electric polarization vector of these cells is normal to the surface of the skin, i.e., coincides with the electric voltage's vector field, and yet it is inherent in the metabolism intensity, conditioning the generation of the electric field.

Magnetic fields

Magnetic field of a living organism can be caused by three following reasons. First of all, it is ion channels arising from electrical activity of cell membranes (primarily muscle and nervous cells). Another source of magnetic fields is tiny ferromagnetic particles, trapped or specially introduced into the human body. These two sources create their own magnetic fields. In addition, at imposition of external magnetic field there appears inhomogeneity of the magnetic susceptibility of different organs and tissues distorting the external magnetic field. The magnetic field in the last two cases is not accompanied by the appearance of the electric field, so the study of the behavior of magnetic particles in the human body and the magnetic properties of various organs are applicable only with using of magnetometric methods. Biocurrents on the contrary except for the magnetic fields create the distribution of electric potentials on a body's surface. Registration of these electric potentials has long been used in research and clinical diagnostics – in electrocardiography, electroencephalography etc. It would seem that their magnetic counterparts, i.e. magnetocardiography and magnetoencephalography recording the signals from the same electrical processes in the body, will give almost the same information about the studied organs. However, as follows from the

theory of electromagnetism, the structure of the electric current source in the electric conductive medium (the body) and the heterogeneity of the medium have significantly different impact on the distribution of magnetic and electric fields: some types of bioelectric activity manifest themselves primarily in the electric field, giving a weak magnetic signal, while the others – on the contrary create rather strong magnetic signal [24]. Therefore, there are many biophysical processes which observation is preferable by using of magnetographic methods.

Magnetography does not require the direct contact with the investigated object, i.e., it allows carry out measurements over a bandage or other obstructions. It is not only practically useful for diagnostics, but is fundamental advantage over electrical methods towards data recording, as the attachment of the electrodes on the skin can be a source of slowly varying contact electric potentials. There are no such spurious noises while using magnetographic methods, therefore, magnetography allows, in particular, reliably explore slowly occurring processes (with the characteristic time of tens of minutes).

Magnetic fields rapidly diminish with distance from the source of the activity, as they are caused by relatively strong currents running in the body, while the surface potentials are determined mainly by the weaker and "smeared" electric currents in the skin. Therefore, magnetography is more convenient for accurate determination (localization) of bioelectric activity parts on the human body. And finally, the magnetic field vector is characterized as not only by the absolute value but also by the direction, which also may provide additional useful information. However, it should not be assumed that the electricity and magnetographic methods compete with each other. On the contrary, it is their combination that gives the most complete information about the processes being investigated. But for each of the individual methods, there are practical areas wherein the use of any one of them is preferable.

Water is the main substance of all living organisms and the magnetic field exerts a certain influence on water. This influence is a complex multivariate influence, which the magnetic field exerts on dissolved in water metal cations (Fe^{2+}, Fe^{3+}) and the structure of the hydrates and water associates [25]. Experimentally was proved that the magnetic field acts much weaker on still unmoved water, because water has conductivity; as water moves in the electromagnetic field it is generated a small electric current.

The research performed with superconductive detectors based on Joseffson junctions shows that magnetic fields around the human body are in the range from 1 to 100 Hz. The magnetic activity of the brain for example makes up $\sim 30 \cdot 10^{15}$ T/Hz$^{1/2}$. The magnetometric system has a sensitivity of $10 \cdot 10^{15}$ T/Hz$^{1/2}$ in the range of 1 to 100 Hz [26].

Chemiluminescence

Chemiluminescence denotes luminescence accompanying chemical reactions, detected in the near infrared, the optical and the near UV-range of the electromagnetic spectrum. When chemiluminescence takes place in living organisms, the phenomenon is called bioluminescence. The term is generally used for higher luminance ATP-dependent luciferin/luciferase systems observed in *Lampyridae* lightning bugs [27]. Although there bacterial, latia and dinoflagellate luciferin, and coelenterazine found in some bacteria, freshwater snails, dinoflagellates, radiolarians, shrimp, squid and deep-sea fish species [28].

Chemiluminescence is observed in reactions accompanied by allocation of large amounts of energy, such as the reaction of combining of two radicals, or in reactions involving peroxides, e.g. peroxide oxidation of lipids [29]. Peculiar ("ultra-weak") glow of cells and tissues of animals and mammals is caused by free radical reactions: lipid radicals and oxygen, and nitrogen oxides – compounds that play an essential role in cell metabolism, and under certain conditions in the development of a number of pathological conditions.

It is suggested that the major radicals responsible for the light emission are excited triplet carbonyl and excited singlet oxygen, and that these radicals arise through the decomposition of hydroperoxides formed in the process of lipid oxidation [30]. The process of lipid peroxidation (LPO) is an important cause of the accumulation of cellular defects caused by radicals. LPO main substrate is polyunsaturated fatty acids in composition of cell membranes and lipoproteins. Their attack by oxygen radicals leads to the formation of hydrophobic radicals, interacting with each other [31]. Many different mechanisms have been suggested for the oxidative lipid

fragmentation that produce biologically active aldehydes as 4-hydroxynon-2-enal (HNE), oxononanoyl phosphatidylcholine (ON-PC) from linoleic acid (LA) esters, or HNE and oxovaleroyl phosphatidylcholine (OV-PC) [32].

Processes of life are almost always accompanied by a very weak radiation, which is sometimes called ultra-low illumination or radiation of cells and tissues. Some organisms possess the ability to emit bright light at photon fluxes below about 10^4 photons·cm^{-2}·s^{-1}, visible to the naked eye, this phenomenon is denoted "bioluminescence". In biochemical systems, i.e. in tissue's homogenates, cell suspensions or cell organelles, mixtures of enzymes and substrates, chemiluminescence in most cases has an extremely low intensity, and requires particularly sensitive equipment for its detection and measurement [33]. Some substances – enhancers, have the ability to essentially enhance the chemiluminescence, sometimes many thousands of times (activated, or enhanced chemiluminescence). In addition, weak luminescence is accompanied by the formation of free radicals under the action of a number of physical factors on the object: at ionizing radiation is observed radiochimoluminescence, at ultraviolet or visible light illumination – photochimoluminescence, at passing an electric current – electroluminescence, with ultrasound – sonoluminescence, under the influence of friction forces – triboluminescence.

Chemiluminescence differs from fluorescence in that the electronic excited state is derived from the product of a chemical reaction rather than the more typical way of creating electronic excited states, namely adsorbtion. It photomemical reactions, in which light is used to drive an endothermic chemical reaction, light is generated from a chemically exothermic reaction.

At present time it is known quite a lot of chemical reactions involving the formation of luminescence glow. In most cases they are generally quite a complex processes having many intermediate stages, but the basic processes leading to luminescence glowing in general are similar. They include the separation and transfer of charged particles (electrons and free radicals), the electron transfer (redox reactions) at one of the higher energy levels with the formation of the reaction product in an electron-excited state and further releasing of a photon in the transition of the molecule to the low excited electronic ground state with a lower energy level (luminescence). Theoretically, in this process on each molecule of the reactant should be allocated one photon.

Chemiluminescence accompanies many chemical reactions (ozonation and fluorination reactions, the oxidation of phosphorus and complex organic substances, lipids) and has an impulse mode; the signals of this process usually are very week. Thus, the human skin dissociates few photons per 1 sec. with emission power level ~10 mW/cm^2 [34].

Luminescence of cells and tissues are accompanied by three types of reactions:

- Reactions with active oxygen;
- Chain reactions of lipid peroxidation;
- Reactions involving nitric oxide (NO·).

The more lipid radicals contain the system, e.g. the more energetically occurs the chain reaction of lipid oxidation, the higher the intensity of chemiluminescence accompanying the reaction of radicals. Substances reacting with free radicals and thereby inhibiting the chain lipid oxidation (so-called antioxidants) simultaneously inhibit chemiluminescence. That inhibition of chemiluminescence by cells and tissues by such antioxidants as tocopherol (vitamin E), indicating that chemiluminescence is stipulated by lipid oxidation chain reactions. On the other hand, studying the impact of various natural and synthetic compounds on the time (kinetics) of chemiluminescence, it can be judged on the ability of these substances to protect our body from the harmful effects of free radicals and thereby select candidates to certain medications.

Chemiluminescent methods are used for recording of ultra-weak light wave accopmanying from the chemical and biobiochemical reactions involving the formation of free radicals. They do not require special laboratory conditions and special material preparation for analysis and characterised by high sensitivity, reliability, meet the requirements for rapid methods of express research. Chemiluminescent methods are widely used in biomedical diagnostics for studying of the molecular basis of physiological processes in biological systems and general mechanisms of development of pathological conditions.

Biophoton emission

The term biophoton emission means a photon of non-thermal origin spontaneous emission in the visible and UV-spectrum emitted from all biological objects and tissues and covered over a wide range of wavelengths, from 200 to 800 nm. Biophoton emission was discovered by the Soviet biologist Alexander Gurwitsch (USSR) who was among the first discovered that in the process of cell mitogenesis cells emited ultra-weak UV waves, named mitogenetic or Gurwitsch rays [35]. The biophoton emission evidently is linked to the endogenous production of excited states within the biological system. As a possible carrier of biophotone emission A. Gurvitsh offered chromatin – the complex of DNA with special proteins that during eukaryotic cell division formes chromosomes – thread-like structures inside the cell's nucleus, consisting of DNA, RNA and proteins. Cells that do not contain chromatin do not possess the ability to emit biophotones. It was found that if the other surrounding cells were under mitogenetic rays, the mitosis was being increased, i.e. stimulated the cell growth [36]. It was also demonstrated that mitogenetic radiation can not only stimulate, but also inhibit the cell growth. Further F.A. Popp developed a biophoton theory to explain their possible biological role and the ways in which they may control biochemical processes, growth, cell differentiation etc. [37].

For many years the existence of Gurwitsch rays has been under the question because of the very contradictory experimental results for their detection. The situation has changed for the better with the development of more sensitive resolution technical devices for their precise detection [38].

Contemporary photon-emission detectors used for photon's detection are divided into two classes: photodetectors, or photon detectors and temperature detectors. In photodetectors photons absorbed by the material of the detector at interaction with electrons change the electrical characteristics of the detector, which is reflected in the measured electrical signal. In thermodetectors the absorption of photons leads to an increase of the temperature and temperature characteristics of the detector. Thus, in the pyroelectric detector is being measured the change in internal electron polarization; in bolometers – electrical resistance, etc. The photodetectors have, as a rule, better sensitivity and more widespread, whereas temperature detectors are used mainly for standard measurements.

Photodetectors are divided into three classes: photoemission, semiconductor and superconducting detectors. These types of photodetectors may be used in hybrid devices; photoemission electrons may be recorded when they are exposed to a semiconductor CCD (EBCCD type detectors and ICSD).

In photoemission detectors incident photon knocks an electron from the surface of the photocathode, which is accelerated under electric field in vacuum and moves to the anode when an electric potential. The resulting electric current of the detector is proportional to the number of photoelectrons, i.e. the intensity of the incident radiation. The effectiveness of photoemission and spectral energy characteristics of such a detector are defined by the working surface of the photocathode. Advantages of such photodetectors are: high sensitivity and convenience; disadvantages: low quantum efficiency, the spectral dependence of the detector response and the dependence of its efficiency on surface cleanliness.

In semiconductor detectors, photons are absorbed within the volume of the semiconductor material, creating a pair of "electron-hole" and the corresponding conductivity. This class of detectors uses an internal photoelectric effect, in which the photon energy must be large enough to overcome the photoelectron band gap to be moved to the conduction band. In photodiodes, Schottky diodes and metal-insulator-semiconductors to overcome the potential barrier the external electric field is applied. External detector photocurrent is proportional to the number of detected photons. Advantages of such photodetectors: a wide operating range, linearity, high quantum efficiency, wide dynamic range, large image matrices; disadvantages – aging effects by UV radiation.

Superconducting photon detectors – are temperature detectors based on the change in the physical state of matter at increased internal energy of the material due to the absorption of UV photons.

To photodetectors usually put forward the following demands:

• Low sensitivity to visible light (solar-blind). Outside the Earth's atmosphere per one photon in the range of 100–200 nm corresponds ~104–106 photons in the visible and infrared ranges.

This ratio is increased on the surface of the Earth. Therefore, the use of transmissive UV-filters with attenuation of signal on 10^{-4}–10^{-3} level is not enough, if the detector has good sensitivity in the visible and/or infrared ranges;

• High detection quantum efficiency (DQE). In optical systems, the UV range, where are large losses in transmission, this value may differ from the quantum efficiency of the photocathode, or CCD. As a result, the use of special filters and windows to block of visible light DQE of photoemission detectors decreases by an order from ~50 % to ~2–5 %;

• Wide local dynamic range: a maximum value of the ratio of flux in a given point of the detector to a minimum signal level composed ~3 units of the noise signal. At the integration over the detector area is obtained integral dynamic range of the detector. This option is especially important for sensitive photomultiplier detectors and the development of high-speed position-sensitive detectors;

• Low level of background noise and signal that determines the practical sensitivity of the device and the image contrast.

It shold be mentioned that biophotonic emition is measured to be much weaker compared to other types of radiation. Biophotons according to recent studies have a wavelength from λ = 200 nm to λ = 800 nm (0,2–0,8 μm). They are usually being observed in the close UV range (from 300 nm to 400 nm) and visible optic range (from λ = 0,38 μm to λ = 0,75 μm) with frequencies ranges from 10^{-19} to 10^{-16} W/cm^2 (approx. ~1–1000 photons·cm^{-2}·sec^{-1}). This light intensity is much weaker than that one may be seen in the perceptually visible and normal bioluminescence, but is detectable above the background of thermal or infrared (0,74–2,5 μm) radiation emitted by tissues at their normal temperature.

F.A. Popp proposed that this type of light is not radiated in a dispersed way as daylight, but quiet coherently maintaining order in the flow oscillations, stability and continuity of the phase difference of the amplitude of the total wave, i.e. it might be both semi-periodic and coherent [39]. It is known that coherence is an ideal property of waves that enables stationary (i.e. temporally and spatially constant) interference. More generally, coherence describes all properties of the correlation between physical quantities of a single wave, or between several waves or wave packets. This may signify that biophotones in the light's beam vibrating simultaneously, like in a laser beam that can indicate on information characteristics of the signal.

The photon emission in its turn is weaker than normal bioluminescence because during that process are being emanated individual photons. The "delayed luminescence" is connected with hyperbolic relaxation of biological objects that is a characteristic active response of coherent states. In recent years has been found the evidence that the light has a high degree of coherence because of its photon count statistics, the spectral distribution and unstable decay behavior after exposure to light illumination, and its transparency through optically thick materials. Moreover, DNA is apparently an important source of biophoton emission, since conformational changes of DNA induced with 3,8-diamino-5-ethyl-6-phenylphenanthridinium bromide *in vivo* are clearly reflected by changes of photon emission in cells [40]. The physical properties of the emission are described, using the DNA molecule as an exciplex ultraviolet laser system, where a stable state can be reached far from thermal equilibrium at threshold [41].

One of us, Ch. Drossinakis has performed the scrutinized studying of luminescence emission in over 30 scientific laboratories, and part of them on the topic of bioluminescence. He used special photoemission detector for detection of strongly expressed biophotone radiation emitted from the human body. These results are shown on Figure 1 and Figure 2. The registration was performed from area of the skin with average diameter 7 cm within time interval of 100 ms or 1 s. The calculation of biophoton emission was measured in count/100 ms/count. The measurement was made using EMI9558QA photoemission detector in impervious to the light dark room wherein the light was minimized about ~5 cps. The photomultiplier was connected through an amplifier and other intermediate devices with potentiometer recorder or a personal computer. The detection of biophoton emission was performed within time interval with real count rate 3 cps, for 30 min, with reliability according to *t*-criterion of Student at $p < 0,05$. The irradiation time of 150 W-tungsten lamp was 5 s. Within 100 ms after switching off the external lamp the first measurement of delayed luminescence was recorded; after then were recorded 256 units of the delayed luminescence. Delayed luminescence of biological objects and tissues in terms of coherent states was detected

within time intervals of 100 ms. The relaxation function was of 25,6 units. These dates are the object of further scrutinized analysis.

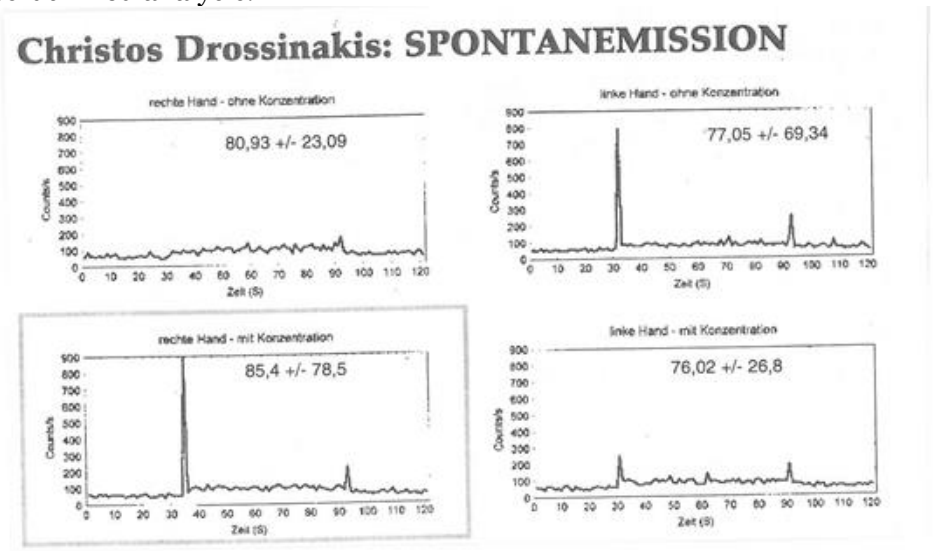

Figure 1. The results of Ch. Drossinakis on research of spontaneous biophoton emission of the human body with using EMI9558QA photoemission detector: figures represent the graphs with different intensities; left graphs – left hand, right graphs – right hand; the calculation of biophoton emission was measured in count/100 ms/count; reading interval – 100 ms; the irradiation time – 5 s; an average diameter of the skin area – 7 cm; axis X – time; axis Y – counts/cm²

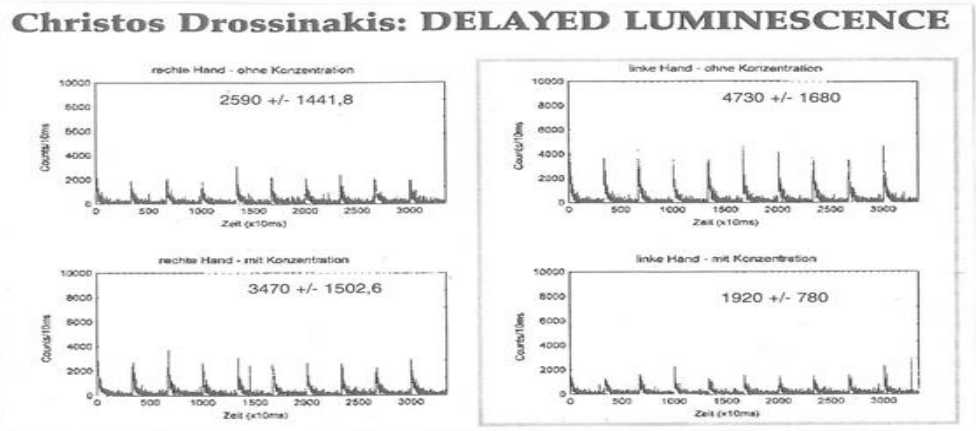

Figure 2. The results of Ch. Drossinakis on research of delayed luminescence of the human body with using EMI9558QA photoemission detector: left graphs – left hand, right graphs – right hand; figures represent the graphs with different intensities; axis X – time; axis Y – counts/cm²

It was established that 1 cm² of human skin generally emits ~85 photones for 1 s. The intensity of biophoton emission ranges from 10^{-19} to 10^{-16} W/cm² (approx. ~1–1000 photons·cm^{-2}·s^{-1}) and depends on a number of conditions as intensity of biochemical processes, metabolism, temperature etc. The result of Ch. Drossinakis shows ~900 biophotons from 1 cm² of the skin for 1 s. However, there still has not been reliable proof that this method has consistent results for medical diagnostics.

Color coronal gas discharge spectral analysis

Coronal gas discharge effect is indicated by the glow corona electrical discharge (flooding, crown, streamer) on the surface of objects being placed in the alternating electric field of high frequency (10–150 kHz) and electric voltage (5–30 kV) [42]. In this process in the ionization zone develops the gas corona discharge sliding on dielectric surface, occurring in a nonuniform electric field near the electrode with a small radius of curvature.

In the thin air layer with thickness of ~10–100 μm between the studied object and the electrode are developed the following processes:

1) Excitation, polarization and ionization by electric field of high frequency the main components of air – the molecules of nitrogen (78 % N_2), oxygen (21 % O_2) and carbon dioxide (0,046 % CO_2). In the result of this is formed an ionized gas, i.e. gas with separated electrons having negative charges, creating a conductive medium as plasma;

2) Formation of a weak electric current in the form of free electrons separated from molecules of N_2, O_2 and CO_2, which generate gas discharge between the studied object and the electrode. The form of gas discharge glowing, its density and surface brightness distribution is determined mainly by electromagnetic properties of the object;

3) The transition of electrons from the lower to higher energy levels and back again, during which there appears a discrete quantum of light radiation in the form of photon radiation. The transition energy of electrons depends on the external electric field and the electronic state of the studied object. Therefore, in different areas surrounding the electric field, the electrons receive different energy impulses, i.e. "skipping" at different energy levels which results in emission of photons with different wavelengths (frequencies) and the energy, coloring the contour of the glow in various spectral colors.

Processes outlined above form the total gas electric effect, allows study the electrical properties of the object at its interaction with an external electromagnetic field [43]. It was shown that the electrical conductivity of the object has almost no effect on the formation of the electric images, which mostly depends on the dielectric constant [44].

There is a relationship (1) of the electric discharge per unit area of the recording medium on the following parameters:

$$\sigma = a - [U_p \frac{(d_2 + \delta)}{\delta \cdot d_2} \varepsilon_0 \frac{(d_2 + \delta)}{\delta \cdot d_2}], \quad (1)$$

where: $\delta = d_1/\varepsilon_1 + d_3/\varepsilon_3$
α – slope rate of electrical pulse;
U_p – breakdown voltage of the air layer between the sobject and the recording medium;
d_1 – the width of the object;
d_2 – width of the zone of influence of the electromagnetic field;
d_3 – width of the recording medium;
ε_0 – dielectric permittivity of the air (ε_0 = 1,00057 F/m);
ε_1 – dielectric permittivity of the studied object;
ε_3 – dielectric permittivity of the medium.
To calculate the breakdown voltage of the air layer is used this formula:

$$U_p = 312 + 6{,}2d_2 \quad (2)$$

As a result of mathematical transformations is obtained a quadratic equation describing the width of the air layer:

$$6{,}2d_2^2 - (\alpha T - 6{,}2\delta - 312)d_2 + 312\delta = 0 \quad (3)$$

Which reduces to the standard quadratic equation:

$$ax^2 + bx + c = 0 \quad (4)$$

where a = 6,2; b = $\alpha T - 6{,}2\delta - 312$; c = 312δ

This quadratic equation has to solutions:

$$x_{1,2} = \frac{-b \pm \sqrt{b^2 - 4ac}}{2a} \quad (5)$$

Accordingly:

$$d_{1,2} = \frac{-[a \cdot T - 6,2\delta - 312] \pm \sqrt{[a \cdot T - 6,2\delta - 312)]^2 - 77,376\delta}}{12,4} \quad (6)$$

The above equations allow calculate maximum and minimum width of the air layer for the occurrence of elecric discharge under which is being formed the electrical image of the studied object.

Gas discharge characteristics for various biological objects vary in character and light intensity, size of contour glow and color spectrum and depend both on its own electromagnetic radiation and the dielectric constant of the object. The intensity depends on the electric voltage applied on the electrode.

Studies have shown that the contours of gas discharge glow at 12 kHz and 15 kHz are homogeneous in their structure. The contour at kHz is 55 % of the contour at 15 kHz and at 24 kHz – only 15 % of the contour at 15 kHz that is important for further analysis and identification of images. The incidence of bioelectrical activity of the body reducing the intensity of gas discharge glow. Pathology in the organism and surrounding tissues also alter the bioelectric activity and the shape and color of gas discharge glow, which is determined mainly by energy of photon emission at the transition of electrons from higher energy levels to the lower ones when being excited by the external electric field. Thus, for red colour of the electromagnetic spectrum this energy compiles 1,82 eV, for orange color – 2,05 eV, yellow – 2,14 eV, blue-green (cyan) – 2,43 eV, blue – 2,64 eV, and violet – 3,03 eV. The reliable result norm is at E ≥ 2,53 eV. The spectral range of the photon emission for different colors is within λ = 380–495±5 nm and λ = 570–750±5 nm. The photons, corresponding to the emission with green color in the visible electromagnetic spectrum, are not being detected under those experimental conditions. Thus, the more predominant in the color spectrum yellow, orange, blue, blue-green and purple colors, the more pronounced is gas discharge glow and bioelectric properties of the object. According to the data obtained, the incidence of bioelectrical activity of the body reducing the intensity of gas disharge glow.

Studies carried out by A. Antonov and I. Ignatov on 1120 patients shown that the overall drop in the bioelectric activity of the body, as well as pathology in organism alter the bioelectric activity and reduce the apparent size of the gas disharge glow. This dependence is observed for many disorders, although there are not statistical reliable results that this method can be applied in medical diagnostics.

Figure 3 shows the results on bioelectrical discharge images of thumbs of various biotherapists detected on color photofilm under coronal gas discharge conditions. The research area was from part of the thumb contacted with transparent electrode. The norm of energy of photon emission compiles 2,54 eV. If the value is over than 2,54 eV this is an indicator of normal bioelectrical status. Some people with high energy status possess the values of photon emission over 2,90 eV. The high values of this parameter are possible with practicing of yoga, sport etc. The emission less than 2,53 eV is characteristic for people with low bioelectrical status. These results are interesting from scientific point of view, because they may provide brilliant prospects for further using of this method for biophysical studies.

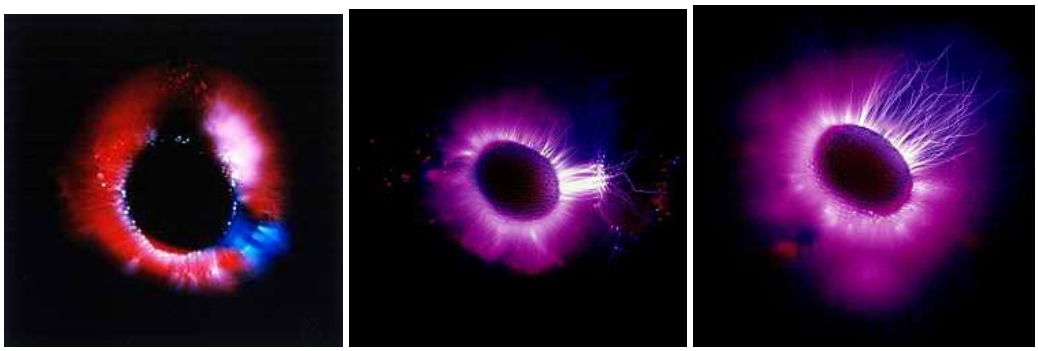

a) *b*) *c*)

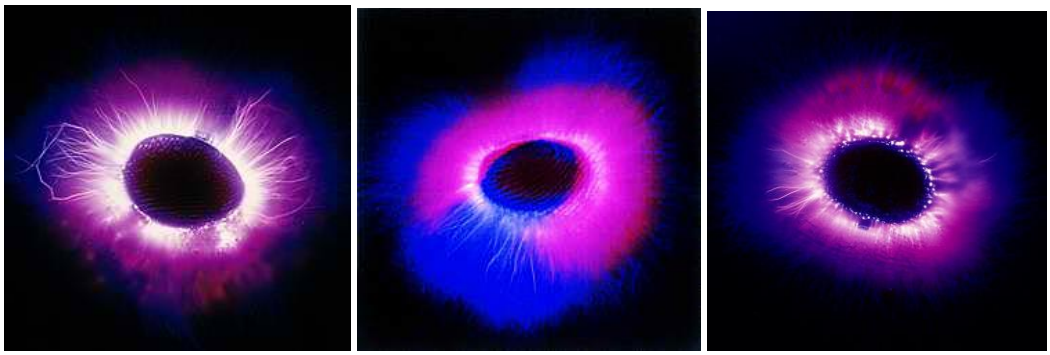

d) *e)* *f)*

Figure 3. Bioelectrical discharge images of thumbs of various biotherapists relative to the bioelectrical discharge image of a normal person (according to I. Ignatov): the snapshots were obtained using colour coronal spectral analysis on a device with the polyethylene PET-electrode with an electric voltage on the electrode 15 kV, electric impulse duration 10 μs, and electric current frequency 15 kHz; *a*) – normal bioelectrical discharge of the human body (1,94 eV); *b*) – bioelectrical image of Laura Weigman (3,00 eV); *c*) – bioelectrical image of Pascal Bosinger (2,95 eV); *d*) – bioelectrical image of Enrico Bauer (3,03 eV); *e*) – bioelectrical image of Lieselotte Eder (2,84 eV); *f*) – bioelectrical image of Elisabeth Caggiano (3,97 eV)

NES and DNES analysis of water

Water seems to be a good model system for studying the interaction with electromagnetic field and structural research. The recent data indicated that water is a complex associated non-equilibrium liquid consisting of associative groups (clusters) containing from 3 to 50 individual H_2O molecules [45]. These associates can be described as unstable groups (dimers, trimers, tetramers, pentamers, hexamers etc.) in which individual H_2O molecules are linked by van der Waals forces, dipole-dipole and other charge-transfer interactions, including hydrogen bonding. At room temperature, the degree of association of H_2O molecules may vary from 2 to 21 units.

The measurements were performed with using NES and DNES methods. It was established experimentally that the process of evaporation of water drops, the wetting angle θ decreases discreetly to 0, and the diameter of water drop basis is only slightly altered, that is a new physical effect [46]. Based on this effect, by means of measurement of the wetting angle within equal intervals of time is determined the function of distribution of H_2O molecules according to the value of f(θ). The distribution function is denoted as the energy spectrum of the water state. A theoretical research established the dependence between the surface tension of water and the energy of hydrogen bonds among individual H_2O-molecules. The hydrogen bonding results from interaction between electron-deficient H-atom of one H_2O molecule (hydrogen donor) and unshared electron pair of an electronegative O-atom (hydrogen acceptor) on the neighboring H_2O molecule; the structure of hydrogen bonding may be defined as $O\cdots H^{\delta+}-O^{\delta-}$.

For calculation of the function f(E) represented the energy spectrum of water, the experimental dependence between the wetting angle (θ) and the energy of hydrogen bonds (E) is established:

$$f(E) = bf(\theta)/[1 - (1 + bE)^2]^{1/2} \quad (7)$$

where $b = 14{,}33\ eV^{-1}$

The relation between the wetting angle (θ) and the energy (E) of the hydrogen bonds between H_2O molecules is calculated by the formula:

$$\theta = \arccos(-1 - 14{,}33E) \quad (8)$$

The energy spectrum of water is characterized by a non-equilibrium process of water droplets evaporation, therefore, the term non-equilibrium spectrum (NES) of water is used. The energy of hydrogen bonds measured by NES is determined as $E = -0{,}1067 \pm 0{,}0011$ eV.

The difference Δf(E) = f (samples of water) – f (control sample of water) – is called the "differential non-equilibrium energy spectrum of water" (DNES).

Thus, DNES spectrum is an indicator of structural changes of water as a result of various external factors. Figure 4 shows NES-spectrum of deionized water that was used as a model system for studying the interaction of electromagnetic field with water. On the X-axis are given three scales. The energies of hydrogen bonds among H_2O molecules are calculated in eV. On the Y-axis is shown the energy distribution function f(E) of H_2O molecules measured in eV^{-1}. It was shown that the window of transparency of the earth atmosphere for the electromagnetic radiation in the middle IR-range almost covers NES-spectrum of water. Arrows A and B designate the energy of hydrogen bonds among H_2O molecules. Arrow C designates the energy at which the human body behaves itself as absolute black body (ABB) at optimum temperature 36,6 °C and adsorbs the thermal radiation. A horizontal arrow designates the window of transparency of the earth atmosphere for the electromagnetic radiation in the middle IR-range.

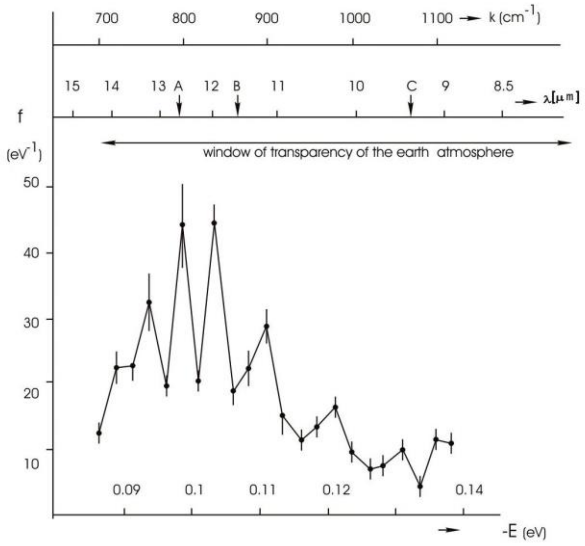

Figure 4. Non-equilibrium energy spectrum (NES) of water as a result of measurement for 1 year: on the X-axis is shown the average energy of H…O-bonds between H_2O measured in eV; on the Y-axis is shown the energy distribution function f(E) of H_2O molecules measured in eV^{-1}; λ – wavelength (μm), *k* – wave number, (cm^{-1})

Another important physical parameter was calculated with using NES and DNES methods – the average energy ($\Delta E_{H...O}$) of H…O-bonds between H_2O compiled –0,1067±0,0011 eV. The most remarkable peculiarity of H…O-bond consists in its relatively low strength; it is 5–10 times weaker than chemical covalent bond. In respect of energy hydrogen bond has an intermediate position between covalent bonds and intermolecular van der Waals forces, based on dipole-dipole interactions, holding the neutral molecules together in gasses or liquefied or solidified gasses. Hydrogen bonding produces interatomic distances shorter than the sum of van der Waals radii, and usually involves a limited number of interaction partners. These characteristics become more substantial when acceptors bind H atoms from more electronegative donors. Hydrogen bonds hold H_2O molecules on 15 % closer than if water was a simple liquid with van der Waals interactions. The hydrogen bond energy compiles 5–10 kcal/mole, while the energy of covalent O–H-bonds in H_2O molecule – 109 kcal/mole. With fluctuations of water temperature the average energy of hydrogen H…O-bonds in H_2O molecule associates changes. That is why hydrogen bonds in liquid state are relatively weak and unstable: it is thought that they can easily form and disappear as the result of temperature fluctuations. The next conclusion that can be drawn from our research is that there is the distribution of energies among individual H_2O molecules.

Further we performed two types of temperature-dependent experiments on heat exchange from the surface of the human body by DNES-method. In first experiment we studied heat exchange when the temperature of the human body was higher than the temperature of the surrounding environment (curve 1a and 1b on Fig. 5). In second experiment there was heat

exchange when the temperature of the human body was lower than that of the surrounding environment (curve 2a and 2b on Fig. 5). In both experiments it was detected a local maximum at 9,7 μm on curve 1 and curve 2 (Fig. 5). This local maximum corresponds to the maximal level of heat emission from the surface of the human body and lays within the "transparency window" of Earth atmosphere to electromagnetic radiation in the mid IR-range of the electromagnetic spectrum. In this range, the electromagnetic radiation emitted by the earth in the surrounding space is being absorbed by the Earth atmosphere. There is a statistical difference between the results of heat emission from the surface of the human body to the surrounding environment and back to the human body according to the *t*-criterion of Student at $p < 0{,}01$. The local maximum on curve 1a is detected at 7,3 eV^{-1}, while the local maximum on curve 2a – at 2,4 eV^{-1} (Fig. 5).

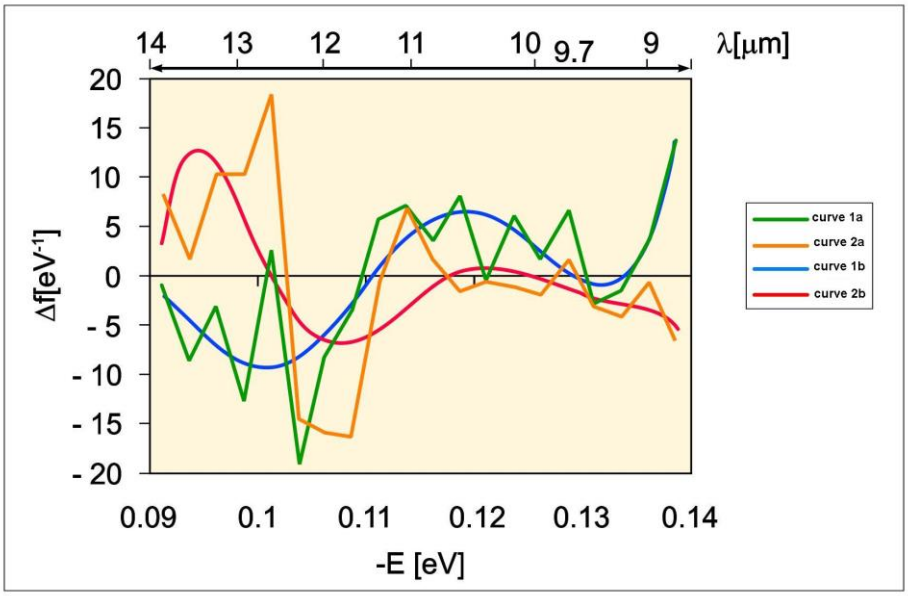

Figure 5. Differential non-equilibrium energy spectrum (DNES) reflecting the heat exchange of the human body with surrounding environment: curve 1a – normal heat exchange at normal temperature; curve 1b – heat exchange at the temperature of the human body higher than the temperature of the surrounding environment; curve 2a – normal heat exchange; curve 2b – heat exchange at the temperature of the human body lower than the temperature of the surrounding environment; on the X-axis is shown the average energy of H…O-bonds between H_2O measured in eV; on the Y-axis is shown the energy distribution function f(E) of H_2O molecules measured in eV^{-1}; λ – wavelength, μm

Infrared thermography (IRT)

The human body as a biological body having temperature in the range from 31 °C to 42 °C, therefore being preferably a source of infrared radiation that percieves by organism as thermoradiation. The main part of this radiation predominantly falls on human skin with a long wavelength range from λ = 4 μm to λ = 50 μm. Maximum of spectral density covers the range approx. ~10 μm i.e. the long wavelength IR range. Specifically the infrared radiation of the human skin can be distributed as follows: radiation with a wavelength of up to 5 μm covers 1 %, the radiation with a wavelength of 5 μm to 9 μm – 20 %, the radiation with a wavelength of 9 μm to 16 μm – 30 % and at a long wavelength – 41 %.

The physical essence of the thermal radiation consists in the presence of charged particles (electrons and ions), which are in random motion and have the properties of electrical or magnetic polarity. Infrared radiation is emitted or absorbed by excited atoms or ions when they change their rotational-vibrational movements. Electromagnetic waves propagate throughout the body and reach the surface, passing through the skin and partly emitted into the environment. The intensity of these processes is proportional to the body temperature. That is why any heated body having temperature above absolute zero (273 °K) emits electromagnetic waves in a broad frequency spectrum. Because particle motion is random, they generate different wavelengths. The wavelength

of infrared radiation emitted by the body depends on the heating temperature: the higher the temperature, the shorter is the wavelength and therefore the higher the emission intensity.

Studies have shown that in the long wavelength infrared region (8–14 μm) the human skin radiates as a black body, regardless of age, degree of pigmentation and other features. Therefore, the emissivity of the human skin can be considered equal to 1 absolute unit. In practice, it is proved that the difference between the emission characteristics of the human skin and blackbody still exist, however, it is small and depends essentially on the influence of the surrounding background.

The limit of effective temperature measurement is equal to the thickness of the emitting layer (skin layer) and is defined as the distance at which electromagnetic waves propagate from the object's surface before the layer in which the intensity decreases in ~2,5 times. Under equal conditions the greater is the wavelength, the greater is the depth, which can detect the temperature perturbations. The maximum intensity of thermal radiation at normal ambient temperature is located in infrared rage of the spectrum (wavelength ~10 μm at t = 36,6 ^{o}C). The threshold of the skin sensitivity according to Yu.V. Gulyaev and E.E. Godik compiles ~10^{-14} W/cm^2 [47]. This led to the feasibility of establishing IR thermal imaging (thermography) for the study of the temperature anomalies. However, the measurement of the thermal radiation of the human body in the IR range gives the true temperature for only the top layer of skin with thickness of ~1 mm; after that the thermal radiation is reflected back into the environment. The temperature of the underlying tissues and organs can be judged indirectly when the temperature changes are “projected” on the skin.

Infrared thermography is a scientific method for registering the thermogram – infrared image showing the distribution pattern of infrared waves emitted from the objects. Thermographic cameras detect radiation in the infrared range of the electromagnetic spectrum (approx. ~0,9–14,0 μm), and on its basis are obtained thermographic images (thermograms) allowing to determine the locations of patterns having different temperatures. Thermograms, therefore are actually visual displays of the amount of infrared energy emitted, transmitted, and reflected from the surface of the object. Since infrared radiation is emitted by all objects with the temperature according to Planck's formula for black body radiation, thermography allows “see” the environment with or without visible illumination. The intensity of the thermal radiation of the body increases with the temperature, therefore thermography allows to see the temperature distribution on the surface of the body. As a result warm objects are seen better on the cooler environment background; mammals and warm-blooded animals are better visible on the environment. That is why the thermography may find many diagnostic applications and is often being used for breast diagnostics, tumour detection etc.

Most thermographic cameras use CCD and CMOS image sensors having most of their spectral sensitivity in the visible light wavelength range. The most commonly used is a matrix of indium antimonide (InSb), gallium arsenide (GaAs), mercury telluride (HgTe), indium (In) and cadmium (Cd). The latest technology allows use the inexpensive uncooled microbolometer sensors. Their resolution is varried from 160×120 pixels or 320×240 up to 768×1024 pixels in the most advanced camera’s models. Often the thermogram reveals temperature variations so clearly that a photograph is not necessary for further analysis. Usually a block of the focal planes of thermo imager can detect radiation in the medium (3 μm to 5 μm) and long (8 μm to 15 μm) infrared wave band, designated as MWIR and LWIR corresponding to two infrared windows with high coeficient of transmittance. Improperly selected temperature range on the surface of the objects, indicates a potential problem.

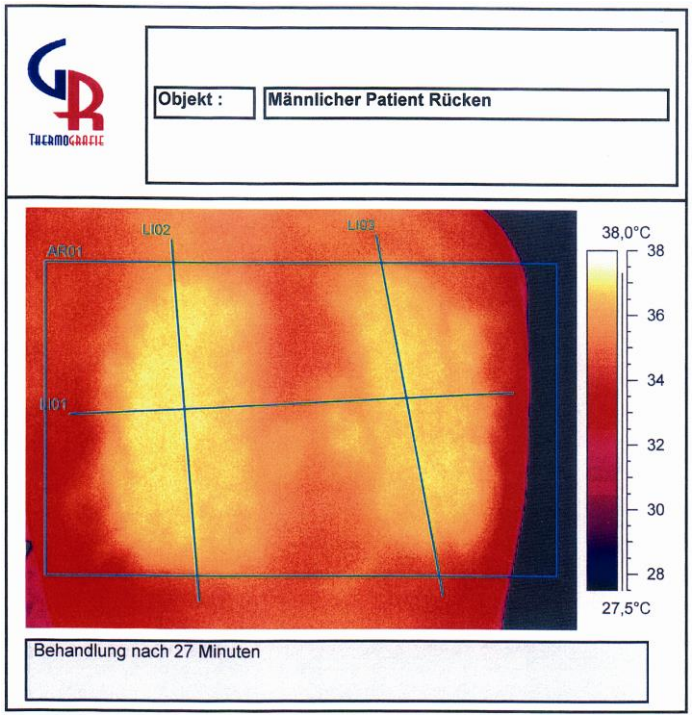

Figure 6. Thermovisual snapshot of the result of bioinfluence of Ch. Drossinakis on the skin back section of a patient suffering radiculitis after 27 min of bioinfluence: different colors show the temperature area of the human body corresponding to different temperatures from 27,5 ^{o}C to 38,0 ^{o}C

It should be noted that the intensity of the thermal radiation of the human body in the microwave (MW) range is much smaller on magnitude than in the infrared part of the spectrum. In particular at a wavelength of 17 cm the intensity is less in ~10 times, so the heat reception of signals in this range of the spectrum requires equipment with higher sensitivity. However, the advantage of this method is that the measurement range and the depth of radiation penetration is much greater, therefore it is possible to obtain data on the temperature parameters of the internal organs and structures of the human body, but the resolution is significantly reduced, therefore it is impossible to obtain reliable thermal image of the study area. Infrared thermography registered a thermal infrared radiation emitted by the capillary network of the skin, which is used in medicine for thermovisual diagnostics. The closer an ailing organ is to the skin, the more accurate the diagnosis based on a thermal signal.

Today it seems to be an established fact that some biotherapists possess the ability to increase the temperature of the treated area of the human body. Figure 6 shows the thermovisual result of the temperature difference between the initial (t = 35,6 ^{o}C) and final skin section temperature (t = 37,3 ^{o}C) of the patient before and after the treatment of the biotherapist. It was calculated that the temperature of the skin part was increased after the treatment on 1,7 ^{o}C.

In this connection there should be noted two important empirical thermography results obtained by M. Marinov [48], which allow carry out the medical diagnostics of various human organs and monitor their condition and malfunction by this method. Figure 7*a* shows the thermography snapshot of a patient having the benign tumour growth in the mammary gland, which has highest temperature than the surrounding tissues lower temperature than the surrounding tissues at 0,54 ^{o}C. Figure 7*b* shows a patient having hyperfunction of thyroid glands, which has highest temperature than the surrounding tissues lower temperature than the surrounding tissues at 0,76 ^{o}C. The middle value on the scale is 36,6 ^{o}C. In the left side of the scale there are temperatures less than 36,6 ^{o}C. In the right side of the scale there are temperatures more than 36,6 ^{o}C.

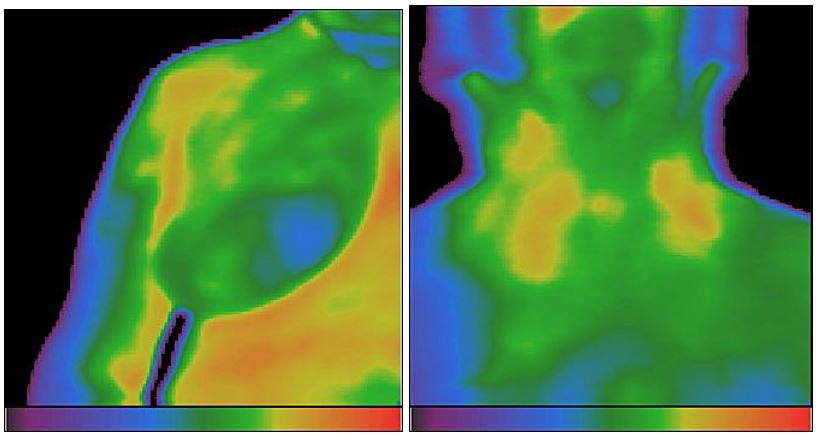

a) b)

Figure 7. Thermovisual snapshots of the human body by IRT method (Marinov & Ignatov, 2008): the spectral range of the infrared thermal-imaging camera was in the middle infrared range from 9 μm to 14 μm; the temperature range – from 24,0 °C to 38,0 °C; different colors show the temperature regions of the body corresponding to different temperatures: *a*) – patient having the benign tumour growth in the mammary gland; *b*) – patient having hyperfunction of thyroid glands

Conclusion

In frames of this research various types of NIR radiation (electromagnetic waves, infrared radiation, thermo radiation, bioluminiscence) emitted from the human body were studied and carefully scrutinized. It was established taht the intensity of biophoton emission of the human body ranges from 10^{-19} to 10^{-16} W/cm² (approx. ~1–1000 photons·cm^{-2}·s^{-1}). The specific photon emission from part of the human thumb was detected as a spectrum of various colours with the method of Colour coronal spectral analysis on a device with an electrode made of PET (hostaphan) with applied electric voltage 15 kV, electric impulse duration 10 μs, and electric current frequency 15 kHz. The photons corresponding to a red color emission of visible electromagnetic spectrum have energy at 1,82 eV. The orange color of visible electromagnetic spectrum has energy at 2,05 eV, yellow – 2,14 eV, blue-green (cyan) – 2,43 eV, blue – 2,64 eV, and violet – 3,03 eV. The approaches and methods for detecting of various types of radiation employed in this research as magnetography, infrared thermography, chemiluminescence and coronal gas discharge spectral analysis may find further application in many branches of applied science and medical diagnostics, while other methods as NES and DNES may be applied for studying the interaction of electromagnetic fields with water and structural studies.

Acknowledgements

The authors wish to thank Alexander Popp for kindly providing the scientific correspondence and letters of his father, Prof. Fritz-Albert Popp.

References:

1. Ignatov I. Energy Biomedicine / I. Ignatov. Sofia: Gea Libris, 2005, 88 p.

2. Rubik B. The biofield hypothesis: its biophysical basis and role in medicine / B. Rubik / J. Altern. Complement Med. 2002. V. 8. № 6. P. 703–717.

3. Dobrin R. Experimental measurements of the human energy field / R. Dobrin, C. Kirsch, S. Kirsch. In S. Krippner (ed.), Psychoenergetic Systems: The Interface of Consciousness, Energy and Matter. New York: Gordon & Breach, 1979, 230 p.

4. Kiang J.G. External bioenergy-induced increases in intracellular free calcium concentrations are mediated by Na^+/Ca^{2+} exchanger and L-type calcium channel / J.G. Kiang, J.A. Ives, W.B. Jonas / Mol. Cell Biochem. 2005. V. 271. P. 51–57.

5. Miller M.W. Extremely low frequency (ELF) electric fields: experimental work on biological effects / M.W. Miller, ed. In: CRC Handbook of biological effects of electromagnetic fields. New York: Academy Press, 1986, P. 138–168.

6. Kwan-Hoong Ng. Non-ionizing radiations – sources, biological effects, emissions and exposures / Ng. Kwan-Hoong. Proceedings of the International Conference on Non-Ionizing Radiation at UNITEN (ICNIR 2003). Electromagnetic Fields and Our Health. 20–22 October 2003.

7. Anderson L.E. Biological effect of extremely low frequency electromagnetic fields: in vivo studies / L.E. Anderson / Am. Ind. Hig. Assoc. J. 1993. V. 54. P. 186–196.

8. Gubkin A.N. Electrets / A.N. Gubkin. Moscow: Nauka. 1978, 192 p.

9. Sessler G.M. Electrets / G.M. Sessler, R. Gerhard-Multhaupt (eds). Morgan Hill, California, USA: Laplacian Press, 1998, ISBN 1–885540–07–8.

10. Barnes F.S. CRC Handbook on biological effects of electromagnetic fields / F.S. Barnes, B. Greenebaum, B. (eds.). 3d Edition. – Boca Raton: CRC Press, November 2006. V. 2. 960 p.

11. Seto A. Detection of extraordinary large bio-magnetic field strength from human hand / A. Seto, C. Kusaka, S. Nakazato / Acupuncture Electrother Res. Int. J. 1992. V. 17. P. 75–78.

12. Shimizu H. Biological effects of electromagnetic fields / H. Shimizu, Y. Suzuki, H. Okonogi / Nippon Eiseigaki Zasshi. 1995. V. 50. № 6. P. 919–931.

13. Holzel R. Wirkungen elektromagnetischer Felder auf biologische Systeme / R. Holzel, I. Lamprecht / Nachrichtentech Elektron. 1994. V. 44. № 2. P. 28–32.

14. Gulyaev Yu.V. On the possibilities of the functional diagnostics of the biological subjects via their temporal dynamics of the infrared images / Yu.V. Gulyaev, E.E. Godik / USSR Academy Nauk Proceedings/Biophysics. 1984. V. 277. P. 1486–1491.

15. Cohen S. Biophoton emission of the human body / S. Cohen, F.A. Popp / Journal of Photochemistry and Photobiology B: Biology. 1997. V. 40. № 2. P. 187–189.

16. Choi C. Biophoton emission from the hands / C. Choi, W.M. Woo, M.B. Lee / J. Korean Physical. Soc. 2002. V. 41. P. 275–278.

17. Niggli H. Artificial sunlight irradiation induces ultra weak photon emission in human skin fibroblasts / H. Niggli / Journal of Photochemistry and Photobiology B: Biology. 1993. V. 18. № 2–3. P. 281–285.

18. Ignatov I. Kirlian effect in biomedical diagnostics and study of bioenergetical properties of biological objects and water / I. Ignatov, O.V. Mosin / Biomedical Radio electronics, Biomedical Technologies and Radio Electronics. 2012. V. 12. P. 13–21 [in Russian].

19. Ignatov I. Medical Biophysics – Biophysical Fields of Man / I. Ignatov, A. Antonov, T. Galabova. – Sofia: Gea Libris, 1998, P. 1–71.

20. Gulyaev Yu.V. Human and animal physical fields / Yu.V. Gulyaev, E.E. Godik / Scientific American. 1990. V. 5. P. 74–83.

21. Gerardi, G., De Ninno A., Prosdocimi, M. et al. (2008) Effects of electromagnetic fields of low frequency and low intensity on rat metabolism / G. Gerardi, A. De Ninno, M. Prosdocimi / Biomagnetic Research and Technology. 2008. V. 6. P. 3–12.

22. Bars Le. Biological effects of electric fields on rats and rabbits / Le. Bars, G. Andre / Red. Gen. Elect. (special issue). July 1976. P. 91–97.

23. Goodman R. Effects of electromagnetic fields on molecules and cells / R. Goodman, B. Greenbaum, M.T. Marron / Int. Rev. Cytol. 1995. V. 158. P. 279–338.

24. Zhadin M.N. Review of Russian literature on biological action of DC and low-frequency AC magnetic fields / M.N. Zhadin / Bioelectromagnetics. 2001. V. 22. P. 27–45.

25. Mosin O.V. Advanced technologies and equipment for magnetic water treatment (review) / O.V. Mosin / Water supply and sanitary technique. V. 8. P. 12–32 [in Russian].

26. Anosov V.N. A new approach to the problem of weak magnetic fields: An effect on living objects / V.N. Anosov, E.M. Trukhan / Doklady Biochemistry and Biophysics. 2003. V. 392. № 1–6. P. 274–278.

27. Rauhut M.M. Chemiluminescence. In: M. Grayson (Ed). Kirk-Othmer Concise Encyclopedia of Chemical Technology. 3rd ed. New York: John Wiley and Sons, 1985, 247 p, ISBN 0-471-51700-3.

28. Hastings J.W. Biological diversity, chemical mechanisms, and the evolutionary origins of bioluminescent systems / J.W. Hastings / J. Mol. Evol. 1983. V. 19. № 5. P. 309–321.

29. Halliwell B. Free Radicals in Biology and Medicine (2nd ed.) / B. Halliwell, J.M.C. Gutteridge. Oxford: Clarendon Press, 1989.

30. Zlatkevich L. Analysis of Lipid Oxidation / L. Zlatkevich, A. Kamal-Eldin. In: A. Kamal-Eldin & J. Pokorn (Eds.). New York: AOCS Publishing, 2005, 281 p.

31. Vladimirov Y.A. Studies of antioxidants with chemiluminescence. In: Proceedings of the International Symposium on Natural Antioxidants. Molecular Mechanisms and Health Effects / L. Packer, M.G. Traber & W. Xin (eds.). 1996. P. 125–144.

32. Esterbauer H. Aldehydes formed by lipid peroxidation: mechanisms of formation, occurrence, and determination / H. Esterbauer, H. Zollner, R.J. Schaur. In: Membrane Lipid Oxidation. Boca Raton: CRC Press, 1990. 283 p.

33. Popp F.A. Evidence of non-classical (squeezed) light in biological systems / F.A. Popp, J.J. Chang, A. Herzog, Z. Yan, Y. Yan / Physics Letters A. 2002. V. 293. № 1–2. P. 98–102.

34. Beloussov L. Biophotonics and Coherent Systems / L. Beloussov, F.A. Popp, V. Voeikov, R. van Wijk, (eds). Moscow: Moscow University Press, 2000. 133 p.

35. Gurwitsch A.G. A historical review of the problem of mitogenetic radiation / A.G. Gurwitsch A.G. / Experientia. 1988. V. 44. P. 545–550.

36. Nikolaev Y.A. (2000) Distant Interactions in Bacteria / Y.A. Nikolaev. Microbiology. 2000. V. 69. № 5. P. 497–503.

37. Popp F.A. Recent advances in biophoton research and its application / F.A. Popp, K. Li, Q. Gu / World scientific. 1992. V. 2. P. 1–18.

38. Inaba H. Super-high sensitivity systems for detection and spectral analysis of ultraweak photon emission from biological cells and tissues / H. Inaba // Experientia. 1988. V. 44. P. 550–559.

39. Popp F.A. Biophoton emission: experimental background and theoretical approaches / F.A. Popp, G. Quao, L. Ke-Hsuen / Modern physics Letters B. 1994. V. 8. P. 21–22.

40. Rattemeyer M. Evidence of photon emission from DNA in living systems / M. Rattemeyer, F.A. Popp, W. Nagl / Nature Wissenshanften. 1981. V. 68. № 11. P. 572–573.

41. Popp F.A. Essential differences between coherent and non-coherent effects of photon emission from living organisms / F.A. Popp, ed. In: X. Shen, R. van Wijk (eds) Biophotonics. New York: Springer, 2005, 124 p.

42. Kirlian S.D. Method for receiving photographic pictures of different types of objects / S.D. Kirlian. USSR Patent № 106401, 1949.

43. Ignatov I. Method for Color coronal (Kirlian) spectral analysis / I. Ignatov, O.V. Mosin / Biomedical Radio electronics, Biomedical Technologies and Radio Electronics. 2013. V. 1. P. 38–47 [in Russian].

44. Ignatov I. Colour crown spectral Kirlian analysis in the modeling of non-equilibrium conditions with a gas electric discharge that simulates the primary atmosphere / I. Ignatov, O.V. Mosin / Nano engineering. 2013. V. 12. № 30. P. 3–13 [in Russian].

45. Ignatov I. Structural mathematical models describing water clusters / I. Ignatov, O.V. Mosin / Journal of Mathematical Theory and Modeling. V. 3. № 11. P. 72–87.

46. Antonov A. Selective high frequency discharge (Kirlian effect) / A. Antonov, L. Yuskesselieva / Acta Hydrophysica. 1985. P. 5–29.

47. Gulyaev Yu.V. Functional Imaging of the Human Body / Yu.V. Gulyaev, E.E. Godik / IEEE Engineering in Medicine and Biology. 1991. V. 10. P. 21–29.

48. Marinov M. Color Kirlian spectral analysis Color observation with visual analyzer / M. Marinov, I. Ignatov. Hanover: Euromedica, 2008. p. 57–59.

УДК 538.56: 577.3: 612.6

Методы регистрации неионизирующих излучений, испускаемых человеческим телом

[1] Игнат Игнатов
[2] Олег Викторович Мосин
[3] Хюго Ниггли
[4] Кристос Дроссинакис
[5] Георгий Тыминский

[1] Научно-исследовательский центр медицинской биофизики (РИЦ МБ), Болгария

Професcор, доктор наук Европейской академии естественных наук (ФРГ), директор НИЦ МБ
1111, София, ул. Н. Коперника, 32/6
E-mail: mbioph@dir.bg
[2] Московский государственный университет прикладной биотехнологии, Российская Федерация
Старший научный сотрудник кафедры биотехнологии, кандидат химических наук
103316, Москва, ул. Талалихина, 33
E-mail: mosin-oleg@yandex.ru
[3] НПО «Прикладная Биофотоника», Швейцария
Sc.D., научный консультант
17, Цельгштрассе, Альблиген, 3183
[4] IAWG-GmbH, IAWG-GmbH, Германия
Дипломированный инженер, председатель IAWG-GmbH
Франкфурт на Майне, 61A, Кёнигштайнер штрассе, 65929
[5] Европейское научное Общество (ЕНО), Германия
PhD, M.D., председатель ЕНО
Ганновер, 50A Сутел штрассе, 30659

Аннотация. В статье представлены результаты оценки возможных биофизических методов и подходов для регистрации различных неионизирующих излучений (NIR), испускаемых человеческим телом в оптическом и электромагнитном диапазоне. Рассмотрены различные виды NIR-излучений (электромагнитные волны, инфракрасное излучение, тепловое излучение, биолюминесценция), испускаемые человеческим телом. В частности, показаны результаты по спонтанному биофотонному излучению и замедленной люминесценции человеческого тела и данные инфракрасной термографии (ИКТ). Показано, что 1 см^2 кожи человека, в среднем испускает ~85 фотонов в 1 сек. Интенсивность биофотонного излучения в среднем варьирует от 10^{-19} to 10^{-16} W/cm^2 (~1–1000 фотонов·см$^{-2}$·с$^{-1}$). Специфическое фотонное излучение органов человеческого тела регистрировалось в виде спектра различных цветов методом цветного коронного спектрального анализа на устройстве с электродом из полиэтилентерефталата (ПЭТ, хостафан) с напряжением 15 кВ, длительность электрического импульса 10 мс, и частотой электрического тока 15 кГц. Было установлено, что фотоны, соответствующие видимому излучению красного цвета электромагнитного спектра имеют энергию 1,82 еВ. Оранжевый цвет электромагнитного спектра имеет энергию 2,05 эВ, желтый – 2,14 эВ, сине-зеленый (голубой) – 2,43 эВ, синий – 2,64 эВ, а фиолетовый – 3,03 эВ. Уровень достоверности полученных результатов находится в пределах E ≥ 2,53 эВ, а спектральный диапазон излучения – в пределах длин волн λ = 380–495±5 нм и λ = 570–750±5 нм. Также определены некоторые важные физические характеристики (энергия водородных связей, угол смачивания, величина поверхностного натяжения) воды методами неравновесного энергетического (НЭС) и дифференциального неравновесного энергетического (ДНЭС) спектра воды, что помогает понять, как электромагнитное излучение взаимодействует с водой и установить структурные характеристики воды.

Ключевые слова: электромагнитные поля; инфрактрасная термография; биолюминисценция; цветной коронный спектральный анализ; НЭС; ДНЭС.

Published in the Russian Federation
European Reviews of Chemical Research
Has been issued since 2014.
ISSN: 2312-7708
Vol. 3, Is. 1, pp. 25-42, 2015

DOI: 10.13187/ercr.2015.3.25
www.ejournal14.com

UDC 546.212

Studying of Isotopic Effects of Deuterium in Biological Objects

[1] Oleg Mosin
[2] Ignat Ignatov

[1] Moscow State University of Applied Biotechnology, Russian Federation
Senior research Fellow of Biotechnology Department, PhD (Chemistry)
Talalihina Str., 33, Moscow, 103316
E-mail: mosin-oleg@yandex.ru
[2] The Scientific Research Center of Medical Biophysics (SRC MB), Bulgaria
Professor, Doctor of Science, director of SRC MB.
N. Kopernik Str., 32, Sofia, 1111
E-mail: mbioph@dir.bg

Abstract

This article describes the data on isotopic effects of deuterium in various biological objects as the cells of methylotrophic, chemoheterotrophic, photoorganotrophic microorganisms, green algae as well as animal cells. It was demonstrated that the increased content of deuterium in water leads to physiological, morphological and cytology alterations of the cell, and also renders negative influence on cellular metabolism, while deuterium depleted water (DDW) with decreased deuterium content on 20–30 % exerts beneficial effects on organism. The maximum kinetic isotopic effect measured at ordinary temperatures in chemical reactions leading to rupture of bonds involving hydrogen and deuterium lies in the range k_H/k_D = 6–8 for C–H versus C–D, N–D versus N–D, and O–H versus O–D-bonds. By IR-spectroscopy method water samples with varying content of deuterium were investigated.

Keywords: deuterium; heavy water; deuterium depleted water; isotopic effects; biological systems; IR-spectroscopy.

Introduction

The most interesting biological phenomenon is the ability of some microorganisms to grow on D_2O media in which all hydrogen atoms are replaced with deuterium [1, 2]. The average ratio of H/D in nature makes up approximately 1:5700 [3]. In mixtures D_2O–H_2O with high speed occurs the dissociation reactions and isotopic (H–D) exchange with the formation of semi-heavy water (HDO). For this reason deuterium presents in smaller content in aqueous solutions in form of HDO, while in the higher content – in form of D_2O.

The chemical structure of D_2O molecule is analogous to that one for H_2O, with small differences in the length of the covalent H–O-bonds and the angles between them. The difference in nuclear masses stipulates the isotopic effects, which may be sufficiently essential for H/D pair [4].

With the development of new biotechnological approaches, there appears an opportunity to use adapted to deuterium cells for preparation of deuterium-labeled natural compounds [5, 6]. The traditional method for production of deuterium labeled compounds consists in the growth on

media containing maximal concentrations of D_2O and deuterated substrates as [D]methanol, [D]glucose etc. [7]. During growth of cells on D_2O are synthesized molecules of biologically important natural compounds (DNA, proteins, amino acids, nucleosides, carbohydrates, fatty acids), which hydrogen atoms at the carbon backbones are completely substituted with deuterium. They are being isolated from deuterated biomass obtained on growth media with high D_2O content with using a combination of physical-chemical methods of separation – hydrolysis, precipitation and extraction with organic solvents and chromatographic purification by column chromatography on different adsorbents. These deuterium labeled molecules evidently undergo structural adaptation modifications necessary for the normal functioning in D_2O.

The adaptation to D_2O is interested not only from scientific point, but allows obtain the unique biological material for the studying of molecular structure by ^{1}H-NMR [8]. Trend towards the use of deuterium as an isotopic label are stipulated by the absence of radioactivity and possibility of determination the deuterium localization in the molecule by high resolution NMR spectroscopy [9], IR spectroscopy [10] and mass spectrometry [11]. The recent advances in the technical and computing capabilities of analytical methods have allowed to considerable increase the efficiency of de novo biomedical studies, as well as to carry out structural-functional studies with deuterium labeled molecules on a molecular level.

The aim of this research was to study the isotopic effects of water in biological objects represented by methylotrophic bacteria, chemoheterotrophic bacteria, photo-organotrophic bacteria and microalgae.

Material and methods

The objects of the study

In this study were used various cells of procaryotic and eucaryotic microorganisms, realizing methylotrophic, chemoheterotrophic, photo-organotrophic and photosynthesizing pathways of carbon assimilation.

Chemical reagents

For preparation of growth media was used D_2O (99,9 at.%) and DCl (95,5 at.%) received from the “Isotope” Russian Research Centre (St. Petersburg, Russian Federation). Inorganic salts and glucose were preliminary crystallized in D_2O and dried in vacuum before using. D_2O was distilled over $KMnO_4$ with the subsequent control of isotope enrichment by ^{1}H-NMR-spectroscopy on a Brucker WM-250 device (“Brucker”, Germany) (working frequency – 70 MHz, internal standard – Me_4Si).

Isolation of natural compounds

Cellular growth was carried out in 500 ml Erlenmeyer flasks containing 100 ml of growth media with 99,9 at.% D_2O at 32–34 ^{0}C and vigorously aerated on an orbital shaker Biorad (“Biorad Labs”, Poland). Photo-organotrophic bacteria and blue-green algae were grown at illumination by fluorescent monochromatic lamps LDS-40-2 (40 W) ("Alfa-Electro", Russia). Growing of microalgae was carried out at 32 ^{0}C in a photoreactor with CO_2 bubbling. After 6–7 days the cells were harvested and separated by centrifugation (10000 g, 20 min) on T-24 centrifuge ("Heracules Sepatech", Germany). The biomass was washed with D_2O and extracted with a mixture of organic solvents: chloroform-methanol-acetone = 2:1:1, % (v/v) for isolating of lipids and pigments. The resulting precipitate (10–12 mg) was dried in vacuum and used as a protein fraction, while the liquid extract – as a lipid fraction. Hydrolysis of polysaccharides and amino acids was performed according to standard procedures using as the reactant HCl in D_2O.

Amino acid analysis

The analysis of amino acids from protein hydrolyzates was carried out on a Biotronic LC-5001 (230 × 3,2) column (“Eppendorf–Nethleler–Hinz”, Germany) with a UR-30 (“Beckman –Spinco”,

USA) sulfonated styrene (7,25% cross linked) resin as a stationary phase; 22 °C; 3,2×230 mm; the granule diameter was 25 μm; 0,2 N sodium–citrate buffer (pH = 2,5) was used as an eluent; the working pressure – 50–60 atm; the eluent input rate – 18,5 ml/h; the ninhydrin input rate – 9,25 ml/h; detection at λ = 570 and λ = 440 nm (for proline).

Analysis of carbohydrates

Carbohydrates were analyzed on a Knauer Smartline chromatograph ("Knauer GmbH", Germany) equipped with a Gilson pump ("Gilson Inc.", USA) and a Waters K-401 refractometer ("Waters Corp.", USA) using Separon NH_2 as a stationary phase: 22 °C; the column size – 4,5 × 250 mm; the granule diameter – 10 μm; the mobile phase – acetonitrile–water (75:25, % (w/w); the input rate – 0,6 ml/min.

Fatty acid analysis

Fatty acids were analyzed on a Beckman Gold System 166 chromatograph (Beckman Coulter, USA), equipped with Model 166 and UV-detector LCD 2563 (Beckman Coulter, USA). Stationary phase: Ultrasphere ODS, 22 °C; particel size 5 μm, 4,6 × 250 mm; mobile phase: linear gradient of 5 mM KH_2PO_4-acetonitrile, elution rate 0,5 ml/min, detection at λ = 210 nm.

Mass-spectrometry

FAB-mass spectra were recorded on pulse mass spectrometer VG-70 SEQ ("Fisons VG Analytical", USA), supplied with caesium source Cs^+ on a glyceric matrix with accelerating pressure 5 кВ and an ionic current 8 мА. EI mass spectra were recorded on MB-80A device ("Hitachi", Japan) with double focusing (the energy of ionizing electrons, 70 eV; the accelerating voltage, 8 kV; the cathode temperature, 180–200 °C) after amino acid modification into methyl esters of N-5-dimethylamino(naphthalene)-1-sulfonyl (dansyl) amino acid derivatives according to an earlier elaborated protocol [12]. Calculation of levels of deuterium enrichment of molecules was carried by the contribution ratio of the peaks of the molecular ions $[M]^+$ for deuterated derivatives of amino acids, isolated from D_2O-media and protonated amino acids obtained in H_2O-medium (control).

IR-spectroscopy

IR-spectra of water with varying deuterium content were registered on Brucker Vertex ("Brucker", Germany) IR spectrometer (a spectral range: average IR – 370–7800 cm^{-1}; visible – 2500–8000 cm^{-1}; the permission – 0,5 cm^{-1}; accuracy of wave number – 0,1 cm^{-1} on 2000 cm^{-1}).

Results and discussion

Isotopic effects of deuterium in biological objects

When biological objects being exposed to water with different deuterium content, their reaction varies depending on the isotopic composition of water and magnitude of isotope effects determined by the difference of constants of chemical reactions rates k_H/k_D in H_2O and D_2O. The maximum kinetic isotopic effect measured at ordinary temperatures in chemical reactions leading to rupture of chemical bonds involving hydrogen and deuterium lies in the range k_H/k_D = 6–8 for C–H versus C–D, N–D versus N–D, and O–H versus O–D-bonds. Water is a solvent in chemical reactions, so at the calculation of isotopic effects of deuterium it is necessary to take into consideration the effect of a solvent. As a universal solvent in which all biological reactions take place, deuterium depleted water increases the rate of these reactions compared with water with natural isotopic composition. This effect is known as kinetic isotopic effect of a solvent. The natural water consists on 99,7 mol.% of $H_2{}^{16}O$, which molecules are formed by ^1H and ^{16}O atoms. The remaining 0,3 mol.% is represented by isotope varieties (isotopologues) of water molecules, wherein deuterium forms

6 configurations of isotopologues – $HD^{16}O$, $HD^{17}O$, $HD^{18}O$, $D_2{}^{16}O$, $D_2{}^{17}O$, $D_2{}^{18}O$, while 3 configuration are formed by isotopologues of oxygen – $H_2{}^{16}O$, $H_2{}^{17}O$, $H_2{}^{18}O$.

The average ratio of atoms of deuterium and hydrogen in natural waters compiles ~1:5700. In natural waters, the deuterium content is distributed irregularly: from 0,02–0,03 mol.% for river and sea water, to 0,015 mol.% for water of Antarctic ice – the most purified from deuterium natural water containing deuterium in 1,5 times less than that of seawater. The concentration of water molecules containing heavy isotopes of D, ^{17}O and ^{18}O, in natural water varies within the limits laid down in the basic standards of the isotopic composition of the hydrosphere SNOW and SLAP (Table 1). According to the international SMOW standard the absolute content of D (isotopic shift, δ, ppm) in sea water: D/H = $(155,76\pm0,05)\cdot10^{-6}$ (155,76 ppm) [13]. For SLAP standard isotopic shifts for D in seawater: D/H = $89\cdot10^{-6}$ (89 ppm). Content of the lightest isotopologue – $H_2{}^{16}O$ in water corresponding to SMOW standard is 997,0325 g/kg (99,73 mol.%), and for SLAP standard – 997,3179 g/kg (99,76 mol.%). In surface waters, the ratio D/H = $(1,32–1,51)\cdot10^{-4}$, while in the coastal seawater – $(1,55–1,56)\cdot10^{-4}$. The natural waters of CIS countries are characterized by negative deviations from SMOW standard to $(1,0–1,5)\cdot10^{-5}$, in some places up to $(6,0–6,7)\cdot10^{-5}$, but there are also observed positive deviations at $2,0\cdot10^{-5}$. Waters of other underground and surface water sources contain varied amounts of deuterium (isotopic shifts) – from δ = +5,0 D,%, SMOW (Mediterranean Sea) up to δ = -105 D,%, SMOW (Volga River).

Table 1

The calculated mass concentrations of isotopologues in natural water corresponding to international standards of SMOW* and SLAP**

Isotopologue	Molecular mass, u	Isotopic content, g/kg	
		SMOW	SLAP
$^1H_2{}^{16}O$	18,01056470	997,032536356	997,317982662
$^1HD^{16}O$	19,01684144	0,328000097	0,187668379
$D_2{}^{16}O$	20,02311819	0,000026900	0,000008804
$^1H_2{}^{17}O$	19,01478127	0,411509070	0,388988825
$^1HD^{17}O$	20,02105801	0,000134998	0,000072993
$D_2{}^{17}O$	21,02733476	0,000000011	0,000000003
$^1H_2{}^{18}O$	20,01481037	2,227063738	2,104884332
$^1HD^{18}O$	21,02108711	0,000728769	0,000393984
$D_2{}^{18}O$	22,02736386	0,000000059	0,000000018

Notes:
*SMOW (average molecular weight = 18,01528873u)
**SLAP (average molecular weight = 18,01491202 u)

The equilibrium vapor pressure of water isotopologues is differed quite significantly. The smaller the mass of the water molecule, the higher the vapor pressure, meaning that the vapor being in equilibrium with water, is always enriched with light isotopes of oxygen and hydrogen. Due to relatively low-mass of elements the difference between the mass of isotopes is large, therefore they are fractionated in natural processes: D/H → 100%, $^{18}O/^{16}O$ → 12,5%. Isotopes of hydrogen and oxygen are more efficiently fractionated via the processes of evaporation-condensation and water crystallization. The isotopic fractionation is carried out by following methods – isotopic exchange in the presence of Pd and Pt, the electrolysis of water in combination with a catalytic isotopic exchange between H_2O and H_2, column rectification of cooled gaseous H_2, vacuum freezing of cold vapor followed by thawing and other [14].

Our previous studies demonstrated that D_2O of high concentration is toxic for the organism, chemical reactions are slower in D_2O, compared with ordinary water, the hydrogen bonds formed with participation of deuterium are somewhat more stronger than those ones formed from hydrogen due to the isotopic effect [15, 16]. In mixtures $D_2O–H_2O$ with high rates occurs isotopic (H–D) exchange resulting in formation of semi-heavy water (HDO): $D_2O + H_2O = 2HDO$. For this reason deuterium presents in smaller content in aqueous solutions in form of HDO, while in the higher content – in form of D_2O.

The chemical structure of D_2O molecule is analogous to that one for H_2O, with small differences in the length of the covalent H–O-bonds and the angles between them. The bonds formed by deuterium atoms are differed in strength and energy from similar bonds formed by hydrogen. D_2O boils at +101,44 °C, freezes at +3,82 °C, has density at 1,1053 g/cm^3 at 20 °C, and the maximum density occurs not at +4 °C as in H_2O, but at +11,2 °C (1,1060 g/cm^3). These effects are reflected in the chemical bond energy, kinetics, and the rate of chemical reactions in D_2O [17]. The chemical reactions and biochemical processes in the presence of D_2O are slower compared to H_2O. D_2O is less ionized, the dissociation constant of D_2O is smaller, and the solubility of the organic and inorganic substances in D_2O is smaller compared to these ones in H_2O. However, there are also such reactions which rates in D_2O are higher than in H_2O. In general these reactions are catalyzed by D_3O^+ or H_3O^+ ions or OD^- and OH^- ions.

Table 2

Changes in the physical properties of water with isotopic substitution

Physical properties	$H_2{}^{16}O$	$D_2{}^{16}O$	$H_2{}^{18}O$
Density at 20 °C, g/cm^3	0,997	1,105	1,111
Temperature of maximum density, °C	3,98	11,24	4,30
Melting point under 1 atm, °C	0	3,81	0,28
Boiling point temperature at 1 atm, °C	100,00	101,42	100,14
The vapor pressure at 100 °C, mm Hg	760,00	721,60	758,10
Viscosity at 20 °C, cP	1,002	1,47	1,056

According to the theory of a chemical bond the breaking up of covalent C–H bonds can occur faster than C–D bonds, the mobility of D_3O^+ ion is lower on 28,5 % than H_3O^+ ion, and OD^- ion is lower on 39,8 % than OH^- ion, the constant of ionization of D_2O is less than that of H_2O. Thus the substitution of H with D affects the stability and geometry of hydrogen bonds in an apparently rather complex way and may through the changes in the hydrogen bond zero-point vibration energies, alter the conformational dynamics of hydrogen (deuterium)-bonded structures of DNA and proteins in D_2O. It may cause disturbances in the DNA-synthesis, leading to permanent changes on DNA structure and consequently on cell genotype.

Animal cells are capable of withstanding up to 25–30% D_2O, plants – up to 60% D_2O, whereas cells of protozoa can live up to 90% D_2O. Deuterium induces physiological, morphological and cytological alterations on the cell on D_2O-media. Cells grown on D_2O-media were ~2–3 times larger in size and had thicker cell walls, than the control cells grown on a conventional protonated growth media with H_2O, the distribution of DNA in them was non-uniform. The most sensitive to the replacement of H^+ on D^+ are cell systems, using high mobility of protons and high speed of breaking up of hydrogen bonds, as the apparatus of biosynthesis of macromolecules and a respiratory chain. Last fact allows consider the biological effects of D_2O, as complex multifactor influence acting simultaneously on the functional state of a large number of cell systems: metabolism, biosynthesis, transport agents, the structure and function of macromolecules. This results in inhibition of cell growth and cell death followed by gradually increasing the concentration of D_2O in the growth medium. In some cases this occurs even when using aqueous solutions of H_2O with D_2O.

Isotopic effects of deuterium, which occur in macromolecules of even a small difference between hydrogen and deuterium, having the effect upon the structure. The sensitivity of enzyme function to the structure and the sensitivity of nucleic acid function (genetic and mitotic) may lead to a noticeable effect on the metabolic pathways and reproductive behaviour of an organism in the presence of D_2O [18]. The changes in dissociation constants of DNA and protein ionizable groups when transferring the macromolecule from H_2O to D_2O may perturb the charge state of the DNA and protein molecules [19]. All this can cause variations in nucleic acid synthesis, which can lead to structural changes and functional differences in the cell and its organelles. Thus, the structural and dynamic properties of the cell membrane, which depends on qualitative and quantitative composition of membrane fatty acids, can also be modified in the presence of D_2O. The cellular

membrane in the bacteria is one of the most important organelles for metabolic regulation, combining apparatus of biosynthesis of polysaccharides, transformation of energy, supplying cells with nutrients and involvement in the biosynthesis of proteins, nucleic acids and fatty acids. Obviously, the cell membrane plays an important role in the adaptation to D_2O. But it is not clearly known what occurs with the membranes – how they react to the replacement of H to D and how it concerns the survival of cells in D_2O-media devoid of protons. As a rule, even highly deuterated growth media contain remaining protons ~0,2–10 atom.%. These remaining protons facilitate the restructuring to the changed conditions during the adaptation to ^2H_2O, presumably integrating into those sites, which are the most sensitive to the replacement of hydrogen by deuterium. The evidence has been obtained that cells evidently are able to regulate the $^2H/^1H$ ratios, while its changes trigger distinct molecular processes. One possibility to modify intracellular $^2H/^1H$ ratios is the activation of the H^+-transport system, which preferentially eliminates H^+, resulting in increased $^2H/^1H$ ratios within cells [20].

Comparative HPLC method analysis of the fatty acid composition of deuterated cells of the chemoheterotrophic bacterium *B. subtilis*, obtained on the maximum deuterated medium with 99,8 at.% D_2O, revealed significant quantitative differences in the fatty acid composition compared to the control obtained in ordinary water (Figure 3 *a, b*). Characteristically, in a deuterated sample fatty acids having retention times at 33,38; 33,74; 33,26 and 36,03 min are not detected in HPLC-chromatogram (Figure 3*b*). This result is apparently due to the fact that the cell membrane is one of the first cell organelles, sensitive to the effects of D_2O, that is why the biosynthesis of fatty acids in the presence of D_2O is inhibited by deuterium, and thus compensates the changes in rheological properties of a membrane (viscosity, fluidity, structuredness) not only by quantitative but also by qualitative composition of membrane fatty acids. Similar results were observed with the separation of other natural compounds (proteins, amino acids, carbohydrates) extracted from deutero-biomass obtained from maximally deuterated D_2O-medium.

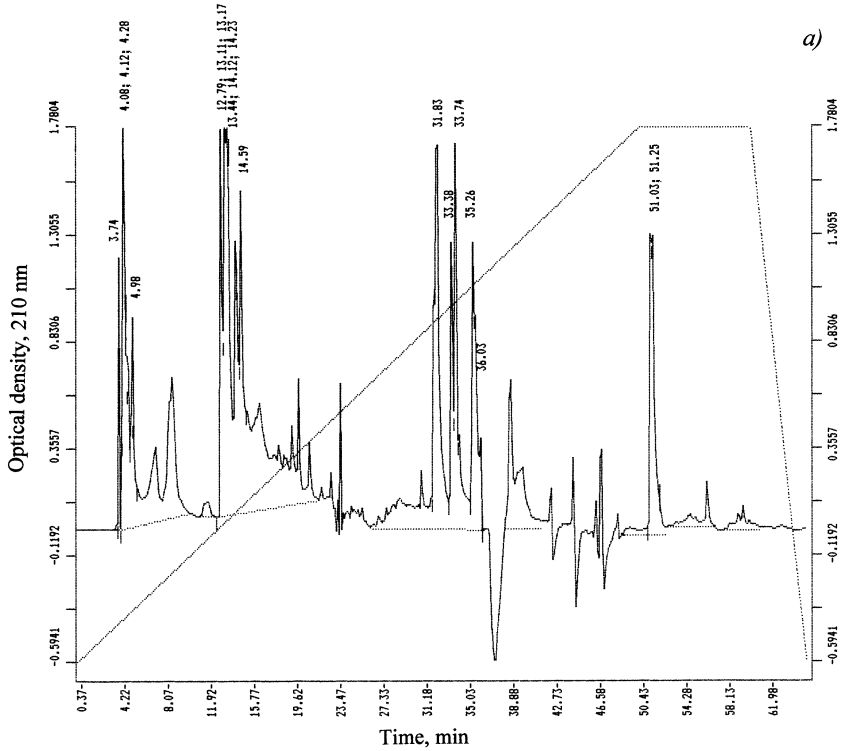

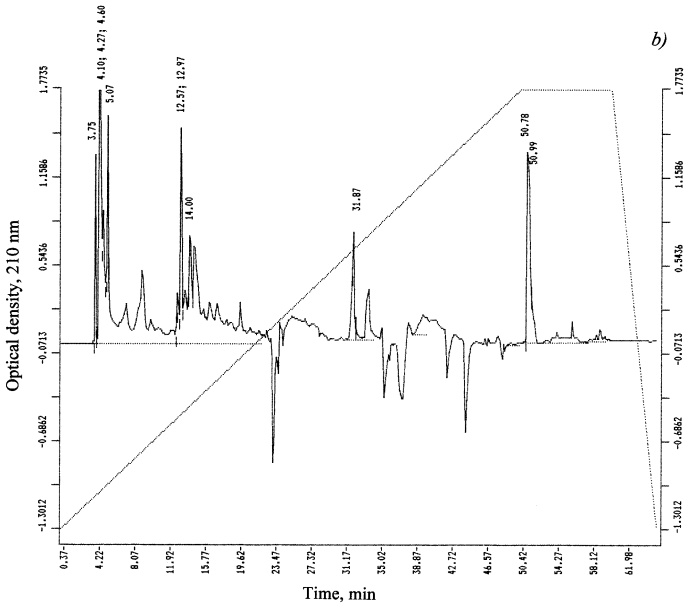

Figure 1. HPLC-chromatograms of fatty acids obtained from protonated (*a*) and deuterated (*b*) cells *B. subtilis* on the maximally deuterated D_2O-medium. The peaks on chromatograms with retention time 3,75 min (instead of 3,74 minutes in the control), 4,10; 4,27; 4,60 (instead of 4,08; 4,12; 4,28 in the control), 5,07 (instead of 4,98 in control) 12,57; 12,97 (instead of 12,79; 13,11; 13,17 in control) 14,00 (instead of 14,59 in the control), 31,87 (instead of 31,83 in the control); 33,38; 33,74; 33,26; 36,03; 50,78; 50,99 (instead of 51,03; 51,25 for control) correspond to individual intracellular fatty acids

Amino acid analysis of protein hydrolysates and intracellular carbohydrates isolated from deuterated cells of *B. subtilis*, also revealed the differences in quantitative composition of amino acids synthesized in D_2O-medium (Figure 2). Protein hydrolyzates contains fifteen identified amino acids (except proline, which was detected at λ = 440 nm) (Table 3). An indicator that determines a high efficiency of deuterium inclusion into amino acid molecules of protein hydrolyzates are high levels of deuterium enrichment of amino acid molecules, which are varied from 50 at.% for leucine/isoleucine to 97,5 at.% for alanine.

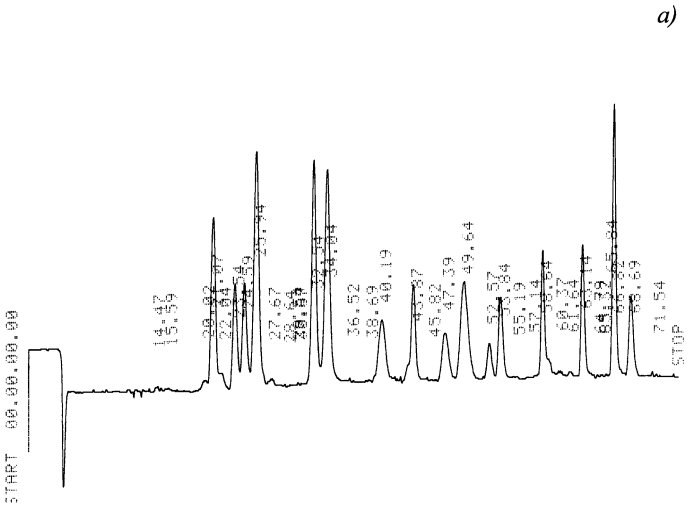

b)

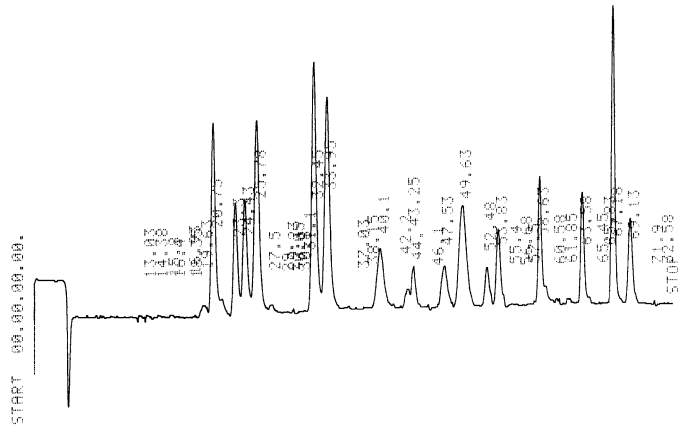

Figure 2. Ion-exchange chromatograms of amino acids obtained from hydrolizates of protonated (a) and deuterated (b) cells of *B. subtilis* on the maximally deuterated D_2O-medium: Biotronic LC-5001 (230×3,2 mm) column ("Eppendorf–Nethleler–Hinz", Germany); stationary phase: UR-30 sulfonated styrene resin ("Beckman–Spinco", USA); 25 μm; 50–60 atm; mobile phase: 0,2 N sodium–citrate buffer (pH = 2,5); the eluent input rate: 18.5 ml/h; the ninhydrin input rate: 9,25 ml/h; detection at λ = 570 and λ = 440 nm (for proline)

Table 3

Amino acid composition of the protein hydrolysates of B. subtilis, obtained on the maximum deuterated medium and levels of deuterium enrichment of molecules*

Amino acid	Yield, % (w/w) dry weight per 1 gram of biomass		Number of deuterium atoms incorporated into the carbon backbone of a molecule**	Level of deuterium enrichment of molecules, % of the total number of hydrogen atoms***
	Protonated sample (control)	The sample obtained in 99,8 % D_2O		
Glycine	8,03	9,69	2	90,0
Alanine	12,95	13,98	4	97,5
Valine	3,54	3,74	4	50,0
Leucine	8,62	7,33	5	50,0
Isoleucine	4,14	3,64	5	50,0
Phenylalanine	3,88	3,94	8	95,0
Tyrosine	1,56	1,83	7	92,8
Serine	4,18	4,90	3	86,6
Threonine	4,81	5,51	–	–
Methionine	4,94	2,25	–	–
Asparagine	7,88	9,59	2	66,6
Glutamic acid	11,68	10,38	4	70,0
Lysine	4,34	3,98	5	58,9
Arginine	4,63	5,28	–	–
Histidine	3,43	3,73	–	–

Notes:

* The data obtained on growth medium with 99,8% D_2O and 2% hydrolysate of deutero-biomass *B. methylicum*.

** While calculating the level of deuterium enrichment protons (deuterons) at the carboxyl (COOH-) and NH_2-groups of amino acid molecules are not taken into account because of their easy dissociation in H_2O/D_2O.

*** A dash means absence of data.

Qualitative and quantitative composition of the intracellular carbohydrates of *B. subtilis* obtained on maximally deuterated D_2O-medium shown in Figure 3 (the numbering is given to the sequence of their elution from the column), contained monosaccharides (glucose, fructose, rhamnose, arabinose), disaccharides (maltose, sucrose), and four other unidentified carbohydrates with retention time 3,08 min (15,63%); 4,26 min (7,46%); 7,23 min (11,72%) and 9,14 min (7,95%) (not shown) (Table). Yield of glucose in deuterated sample makes up 21,4 % by dry weight, i.e. higher than for fructose (6,82%), rhamnose (3,47%), arabinose (3,69%), and maltose (11,62%). Their outputs are not significantly different from control in H_2O except for sucrose in deuterated sample that was not detected (Table 4). The deuterium enrichment levels of carbohydrates were varied from 90,7 at.% for arabinose to 80,6 at.% for glucose. Thus, the observed changes in the qualitative and quantitative composition of various natural compounds synthesized in the presence of D_2O is a common phenomenon observed for the studied microbial cells.

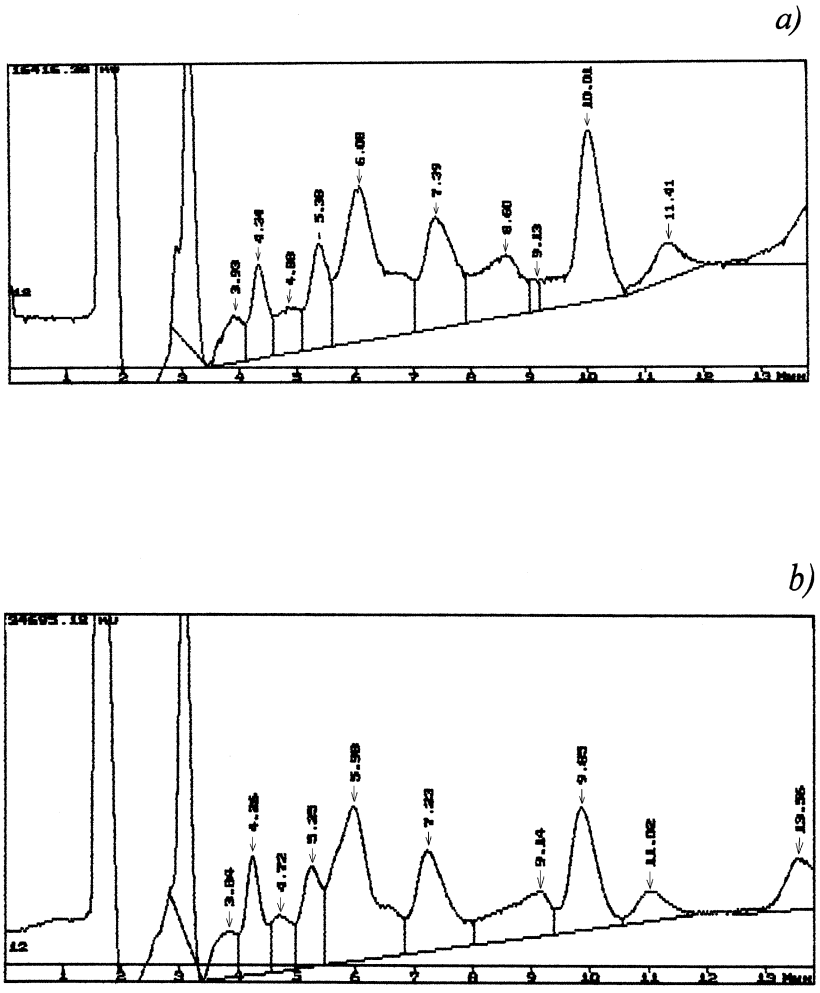

Figure 3. HPLC-chromatograms of intracellular carbohydrates obtained from protonated (a) and deuterated (b) cells of *B. subtilis* on the maximally deuterated D_2O-medium: Knauer Smartline chromatograph (250×10 mm) (“Knauer”, Germany); stationary phase: Ultrasorb CN; 10 μm; mobile phase: acetonitrile–water (75:25, % (w/w); the input rate: 0,6 ml/min

Table 4

Qualitative and quantitative composition of intracellular carbohydrates of B. subtilis obtained on the maximally deuterated medium* and levels of deuterium enrichment of molecules

Carbohydrate	Content in the biomass, % of the dry weight of 1 g biomass		Level of deuterium enrichment, % of the total number of hydrogen atoms
	Protonated sample (control)	The sample obtained in 99,8 % D_2O**	
Glucose	20,01	21,40	80,6
Fructose	6,12	6,82	85,5
Rhamnose	2,91	3,47	90,3
Arabinose	3,26	3,69	90,7
Maltose	15,30	11,62	–
Sucrose	8,62	not detected	–

Notes:

* The data were obtained on growth medium with 99,8% D_2O and 2% hydrolysate of deutero-biomass *B. methylicum*.

Biological effects of DDW

Contrary to D_2O, water with the reduced deuterium content (deuterium depleted water, DDW) exerts a positive effect on metabolism. Experiments on animals [21] demonstrated that at the consumption of water with decreased content of deuterium pigs, rats and mice provide a larger number of offspring, upkeep of poultry from 6 day old to puberty on DDW leads to the accelerated development of reproductive organs (size and weight) and strengthen the process of spermatogenesis, egg laying by hens is increased by almost half, wheat ripens earlier and gives higher yields. DDW delays the appearance of the first metastasis nodules on the spot of inoculation of cervical cancer, and exerts immunomodulatory and radioprotective effect [22].

Radioprotective effects of DDW were studied by W. Bild [23], V.S. Turusov [24] and D.V. Rakov [25] at irradiation of mice's cells by γ-radiation at semimortal dose LD50. Survival level of animals treated with deuterium depleted water for 15 days prior to γ-radiation, was 2,5-fold higher than in control group (dose of 850 R). The surviving experimental group of mice has the number of leukocytes and erythrocytes in the blood remained within the normal range, while in the control group the number of leukocytes and erythrocytes was significantly decreased.

Consumption of DDW by cancer patients during or after radiation therapy treatments allows restore the composition of blood and relieve nausea [26]. According to G. Shomlai, the results of clinical trials with DDW conducted in 1998–2010 in Hungary showed that the survival rate for patients drinking DDW in combination with traditional therapies was significantly higher than for patients who only were treated with chemotherapy or radiation therapy [27].

Biological experiments with DDW carried out in Moscow Research Oncological Institute after P.A. Herzen and N.N. Blokhin with Institute of Biomedical Problems [28, 29], confirmed the inhibitory effects of deuterium depleted water on the process of growth of various tumors, i.g. division of breast adenocarcinoma MCF-7 tumor cells being placed in deuterium depleted water started with a delay of ~5–10 hours. In 60% of mice with immunosuppressed immunity and transplanted human breast tumor MDA and MCF-7 consumption of deuterium depleted water caused tumor regression. A group of mice with transplanted human prostate tumor PC-3 consumed deuterium depleted water showed the increase in the survival rate by ~40%; the ratio number of dividing cells in tumors of dead animals in experimental group was 1.5:3.0, and in control group – 3.6:1.0 [30]. In this regard special attention deserves two indicators: the delay of metastasis and loss of animal's weight during experiments. Stimulating action of deuterium depleted water on the immune system of animals has led to delay of development of metastasis by 40% in comparison with the control group, and weight loss in animals that consumed deuterium depleted water at the end of the experiment was 2 times less. It was also reported that deuterium depleted water may delay the progression of prostate cancer [31] and inhibit human lung

carcinoma cell growth by apoptosis [32] – the programmed cell death, resulting in fragmentation of the cell into separate apoptotic bodies bounded by the plasma membrane.

Preliminary experimental results on motility of human sperm [33], indicated that in DDW (4 ppm) spermatozoa longer retain their functional activity, and it increases with a decrease in the deuterium content of water, whereas the sperm motility is by 40% higher for 5 hours after registration. However, the effect depends on initial properties of a sperm sample. These data indicated that deuterium content variation in water including deep deuterium depletion produces various non-linear isotopic effects on key processes in the cell: enzyme action of Na, K-ATPase, regeneration, motility, fertilizing effectiveness and embryo developing. It should be noted that for any deuterium concentration dependence there should be an optimal condition for the best result.

One prominent effect of deuterium depletion is the inhibition of fatty acids as well as the synthesis, chain elongation and desaturation. These anabolic reactions utilize acetyl-CoA, as well as hydrogen of water for new fatty acid biosynthesis [34]. Fatty acids then are used for new membrane formation in the rapidly proliferating cell. The complex structure and molecular organization of the mammalian fatty acid synthase (EC 2.3.1) offer remarkable opportunities with altered morphology and flux handling properties.

The positive influence of drinking deuterium depleted water on blood chemistry included a significant reduction of glucose, cholesterol, erythrocyte sedimentation rates, leukocyte counts and cortisol (stress hormone) levels, while also revealed an increase in antioxidant capacities [35–37]. These data evidence the significance of deuterium depleted water to increase energy resources even in a healthy cohort, while decreasing risks of psycho-emotional stress, which is known to pose a negative influence on blood biochemistries that often lead to psychosomatic diseases and shorten life. It was also noted the positive impact of water on indicators of saturation the liver tissue by oxygen: the observed increase in pO_2 was ~15%, i.e., cell respiration increased 1,3 times [38]. On beneficial effect on health of experimental mice evidenced the increased resistance and weight increase compared with the control group.

The main impact of DDW on organism is explained by a gradual reduction of deuterium content in physiological fluids due to the reactions of isotopic (H–D) exchange: $D_2O + H_2O = 2HDO$. It was recorded the change in the isotopic composition of urine and Ca^{2+} content as well. Thus, the regular consumption of DDW provides a natural way to reduce the deuterium content in the human body to a value of 110 ppm.

Clinical trials of DDW with a residual content of deuterium 60–100 ppm, showed [39] that it can be recommended as an adjunct in the treatment of patients having metabolic syndrome (hypertension, obesity, impaired glucose metabolism) and diabetes. In addition DDW improves the quality of life for patients having renal stone disease (nephrolithiasis) and various disorders in the gastrointestinal tract (colitis and gastritis), cleanses the body of toxins, enhances the action of drugs and promotes weight correction. DDW can be recommended for fast and deep cleaning of the human body from deuterium that is essential for metabolic disturbances. Taking into consideration the dynamics of the distribution of water in the human body, the reaction of isotopic (H/D and $^{16}O/^{18}O$) exchange and the results obtained with DDW, it can be expected that the greatest effect the isotopic purification of water will have on the regulatory system and metabolism.

The total effects of DDW depend on total body mass, total mass of intracellular water, the amount of daily consumption of DDW and the degree of its isotope purification [40]. The results on the calculation of gradual increasing of deuterium content in the human body at regular consumption of DDW with varied residual deuterium content are shown in Table 5. These results demonstrate that the content of deuterium in the human body decreases while consuming DDW. Thus, at the consumption of water with a residual deuterium content of 60 ppm deuterium content in the body decreases after 45 days to 117,3 ppm, and at the consumption of water with a residual content of deuterium 100 ppm – to 131 ppm at 1 liter of water consumption per a day, to 122,6 ppm at water consumption of 1,5 liters of water a day. Hence, the regular taking of DDW provides a natural way to reduce the content of HDO in the human body to a value of ~117 ppm.

Table 5.

Gradual decreasing of deuterium content in the human body over time, with regular consumption of DDW*

Number of days	The residual content of deuterium in water, ppm		
	60	100	100
	Daily consumption of DDW, liters		
0	1	1	1,5
1	150,5	150,7	150,8
2	145,5	147,9	146,9
7	136,5	143,6	140,5
14	130,6	138,3	134,7
21	120,8	135,6	129,6
28	120,0	133,9	126,6
35	119,6	132,6	124,5
45	117,3	131,5	122,6

*Notes:
The calculation was performed based on the following data:
- daily consumption of DDW – 1 or 1,5 liter;
- daily water exchange rate – 2,5 liters;
- deuterium content in the body corresponds to its content in natural water ~ 150 ppm;
- the average volume of water in the body – 45 liters (average body weight ~ 75 kg).

IR-spectroscopy of D_2O-solutions.

The comparative analysis of IR-spectra of H_2O solutions and its deuterated analogues (D_2O, HDO) is of considerable interest for biophysical studies, because at changing of the atomic mass of hydrogen by deuterium atoms in H_2O molecule their interaction will also change, although the electronic structure of the molecule and its ability to form H-bonds remains the same. The IR spectra of water usually contain three absorption bands, which can be identified as 1 – absorption band of the stretching vibration of OH^- group; 2 – absorption band of the first overtone of the bending vibration of the molecule HDO; 3 – absorption band of stretching vibration of OD^- group. OH^- group is able to absorb much infrared radiation in the infrared region of the IR-spectrum. Because of its polarity, these groups typically react with each other or with other polar groups to form intra-and intermolecular hydrogen bonds. The hydroxyl groups not involved in formation of hydrogen bonds are usually given the narrow bands in IR spectrum and the associated groups – broad intense absorption bands at lower frequencies. The magnitude of the frequency shift is determined by the strength of the hydrogen bond. Complication of the IR spectrum in the area of OH^- stretching vibrations can be explained by the existence of different types of associations, a manifestation of overtones and combination frequencies of OH^- groups in hydrogen bonding, as well as the proton tunneling effect (on the relay mechanism. Such complexity makes it difficult to interpret the IR spectrum and partly explains the discrepancy in the literature available on this subject.

The local maximums in IR-spectra reflect vibrational-rotational transitions in the ground electronic state; the substitution with deuterium changes the vibration-rotational transitions in H_2O molecule that is why there appear other local maximums in IR-spectra. In the water vapor state, the vibrations involve combinations of symmetric stretch (v_1), asymmetric stretch (v_3) and bending (v_2) of the covalent bonds with absorption intensity (H_2O) $\boldsymbol{\upsilon}_1;v_2;v_3$ = 2671; 1178,4; 2787,7 cm^{-1}. For liquid water absorption bands are observed in other regions of the IR-spectrum, the most intense of which are located at 2100, cm^{-1} and 710–645 cm^{-1}. For D_2O molecule these ratio compiles 2723,7; 1403,5 and 3707,5 cm^{-1}, while for HDO molecule – 2671,6; 1178,4 and 2787,7 cm^{-1}. HDO (50 mole% H_2O + 50 mole% ^2H_2O; ~50 % HDO, ~25 % H_2O, ~25 % D_2O) has local maxima in IR-spectra at 3415 cm^{-1}, 2495 cm^{-1} 1850 cm^{-1} and 1450 cm^{-1} assigned to OH^- -stretch, OD^- -stretch, as well as combination of bending and libration and HDO bending respectively.

In the IR-spectrum of liquid water absorbance band considerably broadened and shifted relative to the corresponding bands in the spectrum of water vapor. Their position depends on the temperature [41]. The temperature dependence of individual spectral bands of liquid water is very complex. Furthermore, the complexity of the IR-spectrum in the area of OH^- stretching vibration can be explained by the existence of different types of H_2O associations, manifestation of overtones and composite frequencies of OH^- groups in the hydrogen bonds, and the tunneling effect of the proton (for relay mechanism). Such complexity makes it difficult to interpret the spectrum and partly explains the discrepancy in the literature available on this subject.

In liquid water and ice the IR-spectra are far more complex than those ones of the vapor due to vibration overtones and combinations with librations (restricted rotations, e.g. rocking motions). These librations are due to the restrictions imposed by hydrogen bonding (minor L_1 band at 395,5 cm^{-1}; major L_2 band at 686,3 cm^{-1}; for liquid water at 0 ^oC, the absorbance of L_1 increasing with increasing temperature, while L_2 absorbance decreases but broadens with reduced wave number with increasing temperature [42]. The IR spectra of liquid water usually contain three absorbance bands, which can be identified on absorption band of the stretching vibration of OH^- group; absorption band of the first overtone of the bending vibration of the molecule H^2HO and absorption band of stretching vibration of OD^- group [43]. Hydroxyl group OH^- is able to absorb much infrared radiation in the infrared region of the IR-spectrum. Because of its polarity, these groups typically react with each other or with other polar groups to form intra-and intermolecular hydrogen bonds. The hydroxyl groups, which are not involved in formation of hydrogen bonds, usually produce the narrow bands in IR spectrum, while the associated groups – broad intense absorbance bands at lower frequencies. The magnitude of the frequency shift is determined by the strength of the hydrogen bond. Complication of the IR spectrum in the area of OH^- stretching vibrations can be explained by the existence of different types of associations of H_2O molecules, a manifestation of overtones and combination frequencies of OH^- groups in hydrogen bonding, as well as the proton tunneling effect (on the relay mechanism).

Assignment of main absorption bands in the IR-spectrum of liquid water is given in Table 4. The IR spectrum of H_2O molecule was examined in detail from the microwave till the middle (4–17500 cm^{-1}) visible region and the ultraviolet region – from 200 nm^{-1} to ionization limit at 98 nm^{-1} [44]. In the middle visible region at 4–7500 cm^{-1} are located rotational spectrum and the bands corresponding to the vibration-rotational transitions in the ground electronic state. In the ultraviolet region (200 to 98 nm^{-1}) are located bands corresponding to transitions from the excited electronic states close to the ionization limit in the electronic ground state. The intermediate region of the IR-spectrum – from 570 nm to 200 nm corresponds to transitions to higher vibration levels of the ground electronic state.

Results of IR-spectroscopy with device Infra Spec VFA-IR show that at 4,1 μm, even at low concentrations of deuterium of 0,35 and 0,71 %, there is observed a decline in the local maximums relative to the local maximum of 100 % pure water (the local maximums in IR-spectra reflect vibration-rotational transitions in the ground electronic state because at changing the atomic mass of hydrogen and deuterium atoms in the water molecule their interaction will also change, although the electronic structure of the molecule and its ability to form H-bonds, however, remains the same; with the substitution with deuterium the vibration-rotational transitions are changed, that is why it appears other local maximums in IR-spectra. These data are shown in Figure 2. The result is reliable regarding the content of deuterium in natural waters at 0,015–0,03 %.

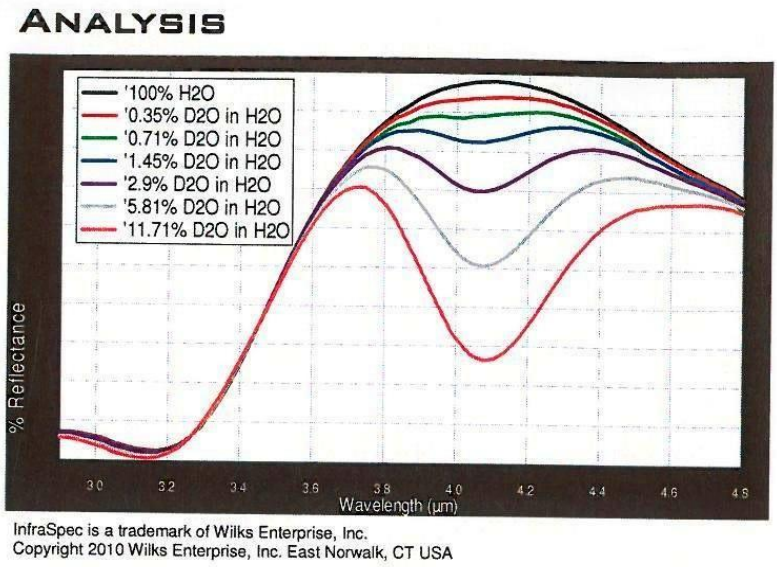

Figure 4. The typical IR-spectra of water with varying content of deuterium

At further transition from H_2O monomers to H_4O_2 dimer and H_6O_3 trimer absorption maximum of valent stretching vibrations of the O-H bond is shifted toward lower frequencies (ν_3 = 3490 cm^{-1} and ν_1 = 3280 cm^{-1}) and the bending frequency increased (ν_2 = 1644 cm^{-1}) because of hydrogen bonding [45]. The increased strength of hydrogen bonding typically shifts the stretch vibration to lower frequencies (red-shift) with greatly increased intensity in the infrared region due to the increased dipoles. In contrast, for the deformation vibrations of the H–O–H, it is observed a shift towards higher frequencies. Absorption bands at 3546 and 3691 cm^{-1} were attributed to the stretching modes of the dimer [$(H_2O)_2$]. These frequencies are significantly lower than the valence modes of ν_1 and ν_3 vibrations of isolated H_2O molecules at 3657 and 3756 cm^{-1} respectively). The absorption band at 3250 cm^{-1} represents overtones of deformation vibrations. Among frequencies between 3250 and 3420 cm^{-1} is possible Fermi resonance (this resonance is a single substitution of intensity of one fluctuation by another fluctuation when they accidentally overlap each other). The absorption band at 1620 cm^{-1} is attributed to the deformation mode of the dimer. This frequency is slightly higher than the deformation mode of the isolated H_2O molecule (1596 cm^{-1}). A shift of the band of deformation vibration of water in the direction of high frequencies at the transition from a liquid to a solid state is attributed by the appearance of additional force, preventing O-H bond bending. Deformation absorption band in IR-spectum of water has a frequency at 1645 cm^{-1} and very weak temperature dependence. It changes little in the transition to the individual H_2O molecule at a frequency of 1595 cm^{-1}. This frequency is found to be sufficiently stable, while all other frequencies are greatly affected by temperature changes, the dissolution of the salts and phase transitions. It is believed that the persistence of deformation oscillations is stipulated by processes of intermolecular interactions, e.g. by the change in bond angle as a result of interaction of H_2O molecules with each other, as well as with various cations and anions.

Table 6

The assignment of main frequencies in IR-spectra of liquid H_2O and D_2O

Main vibrations of liquid H_2O and ^2H_2O				
Vibration(s)	H_2O (t = 25 °C)		D_2O (t = 25 °C)	
	$\boldsymbol{\upsilon}$, cm^{-1}	E_o, M^{-1} cm^{-1}	v, cm^{-1}	E_o, M^{-1} cm^{-1}
Spinning ν_1 + deformation ν_2	780–1645	21,65	1210	17,10
Composite $\nu_1 + \nu_2$	2150	3,46	1555	1,88
Valence symmetrical ν_1, valence asymmetrical ν_3, and overtone $2\nu_2$	3290–3450	100,65	2510	69,70

Thus the study of the characteristics of IR spectra of water allows to answer the question not only on the physical parameters of the molecule and the covalent bonds at isotopic substitution with deuterium, but also to make a certain conclusion on associative environment in water. The latter fact is important in the study of structural and functional properties of water associates and its isotopologues at the isotopic substitution with deuterium.

Conclusion

Isotopic effects are determined by an increase in the nuclear mass of deuterium relative to protium, which may be sufficiently essential for the $^1H/^2H$ pair. The maximum kinetic isotopic effect measured at ordinary temperatures in chemical reactions leading to rupture of bonds involving hydrogen and deuterium lies in the range k_H/k_D = 6–8 for C–H versus C–D, N–D versus N–D, and O–H versus O–D-bonds. D_2O of high content of deuterium (99,8 at.%) leads to physiological, morphological and cytology alterations of the cell, and also renders negative influence on cellular metabolism, while DDW with decreased deuterium content on 20–30% exerts beneficial effects on metabolism. The most sensitive to replacement of H on D are the apparatus of biosynthesis of macromolecules and a respiratory chain, i.e., those cellular systems which use high mobility of protons and high speed of breaking up of hydrogen bonds.

References:

1. I. Ignatov, O.V. Mosin. Modeling of possible processes for origin of life and living matter in hot mineral and seawater with deuterium // Journal of Environment and Earth Science. 2013. V. 3. № 14. P. 103–118.

2. I. Ignatov, O.V. Mosin. Possible processes for origin of life and living matter with modeling of physiological processes of bacterium *Basillus subtilis* as model system in heavy water // Journal of Natural Sciences Research. 2013. V. 3. № 9. P. 65–76.

3. G. Lis, L.I, Wassenaar, M.J. Hendry. High-Precision Laser Spectroscopy D/H and $^{18}O/^{16}O$ Measurements of Microliter Natural Water Samples // Anal. Chem. 2008. V. 80. № 1. P. 287–293.

4. V.N. Lobishev, L.P. Kalinichenko. Isotopic effects of D_2O in biological systems. M.: Nauka. 1978. 215 p.

5. O.V. Mosin, I. Ignatov, D.A. Skladnev, V.I. Shvets. A strain of Gram-positive chemoheterotrophic bacterium *Basillus subtilis* – producer of [^{2}H]riboxine // Drug development & registration. 2013. № 4(5). P. 110-119.

6. O.V. Mosin, I. Ignatov, D.A. Skladnev, V.I. Shvets. A strain of Gram-positive facultative methylotrophic bacterium *Brevibacterium methylicum* – producer of [^{2}H]phenylalanine // Drug Development & Registration. 2014. № 1(6). P. 58-67.

7. O.V. Mosin, V.I. Shvets, D.A. Skladnev, I. Ignatov. Microbial synthesis of ^{2}H-labelled *L-p*henylalanine with different levels of isotopic enrichment by a facultative methylotrophic bacterium *Brevibacterium methylicum* with RuMP assimilation of Carbon // Biochemistry (Moscow) Supplement Series B: Biomedical Chemistry. 2013. V. 7. №. 3. P. 249–260.

8. H.L. Crespi. Fully deuterated microorganisms: tools in magnetic resonance and neutron scattering. *Synthesis and Applications of Isotopically Labeled Compounds*. in: Proceedings of an International Symposium / Eds. T. Baillie, J.R. Jones. Amsterdam: Elsevier. 1989. P. 329–332.

9. D.M. LeMaster D.M. Uniform and selective deuteration in two-dimensional NMR studies of proteins // Ann. Rev. Biophys. Chem. 1990. V. 19. P. 243–266.

10. P. MacCarthy. Infrared spectroscopy of deuterated compounds: an undergraduate experiment // J. Chem. Educ. 1985. V. 62. № 7. P. 633–638.

11. O.V. Mosin, D.A. Skladnev, T.A. Egorova, V.I. Shvets. Mass-spectrometric determination of levels of enrichment of ^{2}H and ^{13}C in molecules of amino acids of various bacterial objects // Bioorganic Chemistry. 1996. V. 22, № 10–11. P 856–869.

12. O.V. Mosin, I. Ignatov. Microbiological synthesis of ^{2}H-labeled phenylalanine, valine, and leucine/isoleucine with different degrees of deuterium enrichment by the Gram-posiitive facultative methylotrophic bacterium *Brevibacterium methylicum* // International Journal of Biomedicine. 2013. V. 3(2). P. 132-138.

13. I. Ignatov, O.V. Mosin. Structural mathematical models describing water clusters // Journal of Mathematical Theory and Modeling. 2013. V. 3. № 11. P. 72–87.

14. O.V. Mosin. Purification of water from heavy isotopes deuterium, tritium and oxygen // S.O.K. Moscow: izdat. “Midia Tehnolodzhi”. 2012. № 9. S. 18–19. [in Russian].

15. O.V. Mosin, I. Ignatov. Isotopic effects of deuterium in cells of bacteria and microalgae // Voda: chemistry and ecology. 2012. № 3. P. 83–94. [in Russian].

16. O.V. Mosin, I. Ignatov. Biological influence of deuterium on procariotic and eukaryotic cells // European Journal of Molecular Biotechnology. 2014. V.3. № 11–24.

17. O.V. Mosin. Development of methods of biotechnological preparation of proteins, amino acids and nucleosides, labeled with stable isotopes ^{2}H, ^{13}C и ^{15}N with high levels of isotopic enrichment: autoref. diss. ... Ph. D. – Moscow: M.V. Lomonosov Moscow State academy of fine chemical technology, 1996. 26 p.

18. W.N. Cleland, M.N. O'Leary, D.D. Northrop. *Isotope Effects on Enzyme-Catalyzed Reactions*. Baltimore, London, Tokyo: University Park Press. 1976. 303 p.

19. P. Cioni, G.B. Strambini. Effect of Heavy Water on Protein Flexibility // Biophysical J. 2002. V. 82(6). P. 3246–3253.

20. Somlyai, G. The biological effect of deuterium depletion, Budapest: Akademiai Klado. – 2002, 130 p.

21. V.I. Bad'in, G.N. Gasteva, Ju.V. Drobyshevskij. Issledovanie povedenija vody s negativnym izotopicheskim sdvigom dejterija na organizm teljat // Izv. Akad. Prom. Ekol. 2004. №. 3. S. 73–78.

22. D.V. Rakov. Effects of water with a low content of deuterium and oxygen ^{18}O on the development of radiation injury after gamma irradiation // Aerospace and Environmental Medicine J. 2007. V. 41. P. 36–39.

23. W. Bild, I. Stefanescu, I. Haulica. Research concerning the radioprotective and immunostimulating effects of deuterium-depleted water // Rom. J. Physiol. 1999. V. 36. № 3–4. P. 205–218.

24. V.S. Turusov, Y.E. Sinyak, E.E. Antoshina. Study of radioprotective action of water with a low content of deuterium with a single exposure to high doses of radiation // Rus. Biotherapeutic Journal. 2005. V. 4. № 1. P. 92–98.

25. D.V. Rakov, L.M. Erofeev, D.E. Grigorenko. Influence of water with low content of heavy stable hydrogen isotope deuterium and oxygen (^{18}O) on the development of radiation damage in gamma-irradiated at low dose // Radiation Biology. Radioecology. 2006. V. 46. № 4. P. 475–479.

26. L. Olariu, M. Petcu, S. Cuna. The role of deuterium depleted water (ddw) administration in blood deuterium concentration in Cr(VI) intoxicated rats // Lucrari stiinlifice medicină veterinară (Timişoara). 2010. V. XLIII. № 2. P. 193–196.

27. G. Somlyai. The biological effect of deuterium-depleted water. A possible new tool in cancer therapy // Anticancer Research Intern. J. 2001. V. 21. № 3. P. 23–33.

28. Y.E. Sinyak, A.I. Grigoriev, V.V. Gaydadymov. The method of obtaining water and bezdeyterievoy study its effect on the physiological status of the Japanese quail. Space Biology and Aerospace Medicine / in: Proceedings of XI Conference, Moscow, Russia, 1998. V. 2. P. 201.

29. A.I. Grigoriev, D.G. Zaridze, V.S. Turusov. The effect of water with a low content of deuterium on transplantable tumors // Problems of Oncology. 2005. V. 1. P. 99–102 [in Russian].

30. V.S. Turusov, E.E. Antoshina, L.S. Trukhanova, T.G. Gorkova, Y.E. Sinyak. Growth of transplanted tumors in mice after injecting into them water with decreased deuterium content // Problems of Oncology. 2006. V. 1. P. 59–62 [in Russian].

31. A. Kovács, I. Guller, K. Krempels. Deuterium depletion may delay the progression of prostate cancer // Journal of Cancer Therapy. 2011. V. 2. P. 548–556.

32. F. Cong, Y. Zhang, H. Sheng. Deuterium-depleted water inhibits human lung carcinoma cell growth by apoptosis // Experimental and therapeutic medicine. 2010. V. 1. P. 277–283.

33. V.I. Lobyshev, A.A. Kirkina. Biological effects of deuterium content variation in water / in: 2nd International Congress on Deuterium Depletion. Budapest, Hungary, 17–18 May, 2012.

34. L.G. Boros, G. Somlyai. Tracer substrate-based metabolic profiling, phenotypic phase plane and regression matrix analyses of pancreatic cancer cells under deuterium depleted growth environment / in: 2nd International Congress on Deuterium Depletion. Budapest, Hungary, 17–18 May, 2012.

35. E.I. Andreeva, N.A. Konstantinova, L.B. Burovkova, Y.E. Sinyak. Effect of different isotopic composition of water on the proliferative activity of endothelial cells in vitro // Aerospace and Environmental Medicine. 2005. V. 39. № 3. P. 46–52.

36. T.N. Burdeynaya, A.S. Chernopyatko A.S. Physiological effects of drinking water enriched with ^{1}H and ^{16}O /in: 2nd International Congress on Deuterium Depletion. Budapest, Hungary, 17–18 May, 2012.

37. L. Olariu, M. Petcu, S. Cuna. The role of deuterium depleted water (ddw) administration in blood deuterium concentration in Cr(VI) intoxicated rats // Lucrări ştiinłifice medicină veterinară (Timişoara). 2010. V. XLIII. № 2. P. 193–196.

38. O.E. Kolesov, I.A. Pomytkin. Influence of natural concentration of heavy water isotopologues on the rate of $^{2}H_2O$ generation by mitochondria // Bulletin of Experimental Biology and Medicine. 2006. V. 11. P. 514–516.

39. E.A. Turova, A.V. Holovatch, A.A. Timakov, B.K. Akimov. Influence of water with reduced isotopes of hydrogen and oxygen on the patients with metabolic syndrome / in: interdisciplinary conference with international participation "New Biocybernetic and telemedicine technologies of XXI century", Petrozavodsk, 23-25 June 2003, 28 p.

40. I. Ignatov, O.V. Mosin. Isotopic composition of water as the main factor of longevity // Drug development and registration. 2014. V 4.(9). P. 132–141.

41. I. Ignatov, O.V. Mosin. Structural models, describing cyclic nanoclusters // Nanomaterials and nanostructures. 2013. V. 4. № 9. P. 9–20.

42. J.B. Brubach, A. Mermet, A. Filabozzi, A. Gerschel, P. Roy. Signatures of the hydrogen bonding in the infrared bands of water // *J. Chem. Phys. 2005. V.* 122. P. 184509.

43. J.J. Max, C. Chapados. Isotope effects in liquid water by infrared spectroscopy. III. H_2O and D_2O spectra from 6000 to 0 cm^{-1} // J. Chem. Phys. 2009. V. 131. P. 184505.

44. G.E. Walrafen. Raman and infrared spectral investigations of water structure / in: *Water a Comprehensive Treatise*, F. Franks, ed. – New York: Plenum Press. 1972. V. 1. P. 151–214.

45. H.R. Zelsmann. Temperature dependence of the optical constants for liquid H_2O and D_2O in the far IR region // *J. Mol. Struct. 1995. V.* 350. P. 95–114.

УДК 546.212

Изучение изотопных эффектов дейтерия в биологических объектах

[1] Олег Викторович Мосин
[2] Игнат Игнатов

[1] Московский государственный университет прикладной биотехнологии, Российская Федерация
Старший научный сотрудник кафедры биотехнологии, кандидат химических наук

103316, Москва, ул. Талалихина, 33
E-mail: mosin-oleg@yandex.ru
[2] Научно-исследовательский центр медицинской биофизики (РИЦ МБ), Болгария
Профессор, доктор наук Европейской академии естественных наук (ФРГ), директор НИЦ МБ
1111, София, ул. Н. Коперника, 32/6
E-mail: mbioph@dir.bg

Аннотация. В данной статье рассмотрены данные по изотопным эффектам дейтерия в различных биологических объектах, представляющих собой клетки метилотрофных, хемогетеротрофных, фотоорганотрофных микроорганизмах, зеленых водорослях, а также животных клеток. Было показано, что повышенное содержание дейтерия в воде приводит к физиологическим, морфологическим и цитологическим изменениям в клетке, а также оказывает негативное влияние на клеточный метаболизм, в то время как вода с пониженным содержанием дейтерия на 20–30 % оказывает положительное воздействие на метаболизм. Величина максимального кинетического изотопного эффекта, измеренного при обычных температурах в химических реакциях, приводящих к разрыву химических связей с участием водорода и дейтерия, находится в диапазоне k_H/k_D = 6–8 для C–H-связей по сравнению с C–D-связями, N–H по сравнению с N–D и O–H по сравнению с O–D-связями. Методом ИК-спектроскопии исследованы образцы воды с различным содержанием дейтерия.

Ключевые слова: дейтерий; тяжелая вода; бездейтериевая вода; изотопные эффекты; биологические системы; ИК-спектроскопия.

Published in the Russian Federation
European Reviews of Chemical Research
Has been issued since 2014.
ISSN: 2312-7708
Vol. 3, Is. 1, pp. 43-50, 2015

DOI: 10.13187/ercr.2015.3.43
www.ejournal14.com

UDC 547.7: 547.152.3

A Sensitive and Selective Chromogenic Organic Reagent 4-hydroxy-3,5-dimethoxy benzaldehyde-4-hydroxy benzoyl hydrazone (HDMBHBH) for the Direct and Derivative Spectrophotometric Determination of Lead (II)

[1] N. Radhakrishna
[2] C. Viswanatha
[3] K. Ramakrishna Reddy
[4] N. Devanna

[1] M.L.A. College for women, Department of Chemistry, Bangalore, India
Associate professor
[2] Arba Minch University, Department of Chemistry, Ethiopia
P.O. Box 21, Arba Minch
Assistant professor
[3] Engineering College, Nandayal, Kurnool, A.P, India
Assistant professor, Professor of Chemistry
[4] College of Engineering, Kalikiri-517234, A.P, India
Professor of Chemistry JNTUA
E-mail: chamanchula.viswanatha@amu.edu.et; viswajntu@gmail.com

Abstract

4-hydroxy-3,5-dimethoxy benzaldehyde-4-hydroxy benzoyl hydrazone (HDMBHBH) is used as a novel chromogenic organic reagent for the determination of Lead (II) using spectrophotometry. The novel chromogenic organic reagent 4-hydroxy-3,5-dimethoxy benzaldehyde-4-hydroxy benzoyl hydrazone (HDMBHBH) gave yellow coloured water soluble complex with Pb (II) in basic buffer (pH = 10.0) medium. The colour complex shows maximum absorbance at 386 nm. The system obeyed beer's law in the concentration range of 0.518–5.18μg/ml. The optimum Lead (II) concentration range for accurate determination as evaluated from Ringbom plot was 1.036–4.662 μg/ml. The molar absorptivity and Sandell's sensitivity were 2.66×10^4 $L\cdot mol^{-1}\cdot cm^{-1}$ and 0.0077 $\mu g/cm^2$ respectively. The Lead (II) forms I:I colour complex with HDMBHBH and stability constant of the complex was found to be 3.42×10^6. The present developed method was successfully applied for the determination of Lead (II) in biological samples.

Keywords: novel chromogenic organic reagent; derivative spectrophotometry; lead (II); biological samples.

Introduction

Generally, lead compounds are toxic for animals. Throughout most of human history, lead was used for a wide variety of applications with little or no appreciation of the serious health hazards it poses. Today, physiologists understand that the human body is able to excrete about 2

milligrams of lead efficiently each day but excess of that can cause serious health problems. That is why lead compounds are not used in pesticides or insecticides.

Hence, the analytical methods are required with highest possible sensitivity and selectivity. One of the techniques which is simple and readily in reach of developing and developed countries is photometry. This is a nondestructive technique and it is useful for the determination of trace amounts of metal ions in different kinds of samples such as alloys, biological and industrial materials and wastes.

Experimental study

Spectrophotometric measurements were made in a shimadzu 160 a microcomputer based UV–Visible spectrophotometer equipped with 1.0 cm quartz cells, an ELICO LI-120 digital pH meter. All reagents used were of analytical reagent (AR) grade unless otherwise stated. All solutions were prepared with distilled water.

Reagent:

Synthesis, characterization and analytical properties of 4-hydroxy 3,5-dimethoxy benzaldehyde 4-hydroxy benzoyl hydrazone (HDMBHBH)

It is prepared by refluxing 1.82 g of 4-hydroxy 3,5-dimethoxy benzaldehyde and 1.52 g of 4-hydroxy benzhydrazide in 25 ml of carbinol for about 4 hours. The contents are allowed to cool and the product is separated by filtration. The crude product (yield 80 %) obtained ($C_{16}H_{16}N_2O_5$) is recrystallized twice from hot methanol. Pure light greenish coloured crystals of 4-hydroxy 3,5-dimethoxy benzaldehyde 4-hydroxy benzoyl hydrazone (HDMBHBH) (III) (m.p. 292–294 °C) are obtained (see the scheme below).

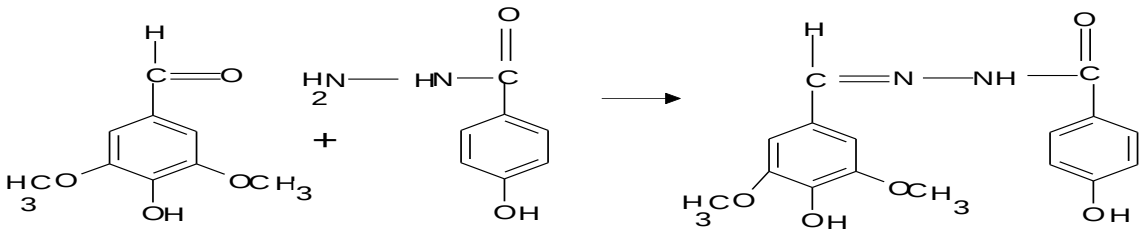

I **II** **III**

I = 4-Hydroxy 3,5-dimethoxy benzaldehyde
II = 4-Hydroxybenzhydrazide
III = 4-Hydroxy 3,5-dimethoxy benzaldehyde 4-hydoxy benzoyl hydrazone (HDMBHBH)

The reagent 4-hydroxy-3,5-dimethoxybenzaldehyde-4-hydoxy benzoyl hydrazone (HDMBHBH) was characterized with the help of Infrared, ^{1}H-NMR and mass spectral data and the structure was confirmed by the spectral data.

Analytical properties of DMAHBH

The reactions of some important metal ions were tested at different pH values. The characteristics of the most important complexes are summarized in Table 1. The samples were prepared in 10 ml standard volumetric flasks by adding 3 ml of buffer (pH = 1.0–11.0), 0.5 ml of metal ion (1×10^{-3} M) and 0.5 ml of (1×10^{-2} M) HDMBHBH solutions. The solution mixture was diluted up to the mark with distilled water. The absorbance was measured in 300–800 nm range against reagent blank.

The data obtained from appropriate spectra which were derived in the presence of 10-fold molar excess of the reagent to metal ion. The pH values, which facilitate the formation of different complexes were also included.

Table 1: Characteristics of *HDMBHBH* complexes in solution

Metal ion	λ_{max} (nm)	pH	Surfactant used	Colour of the complex
Pb(II)	386	9.0–10.0	Triton-X	Yellow
Au(III)	400	3.0–5.0	Triton-X	Brown
V(V)	392	3.0–5.0	Triton-X	Yellow

Recommended procedure

Determination of Lead (II) (zero order)

An aliquot of the solution containing 0.3178 to 3.813 µg/ml of Lead (II), 3 ml of buffer solution pH = 8.0 to 10.0 and 0.5 ml of (1×10^{-2} M) HDMBHBH reagent were taken in a 10 ml standard volumetric flask and the solution was diluted up to the mark with distilled water. The absorbance of the solution was recorded at 412 nm in a 1.0 cm cell again corresponding reagent blank prepared in the same way but without Lead (II) metal solution. The absorption spectra of HDMBHBH and its Pb (II) complex under the optimum conditions are shown in Figure 2. The [Pb(II)–HDMBHBH] complex shows the maximum absorbance at 412 nm, whereas the reagent blank does not absorb appreciably.

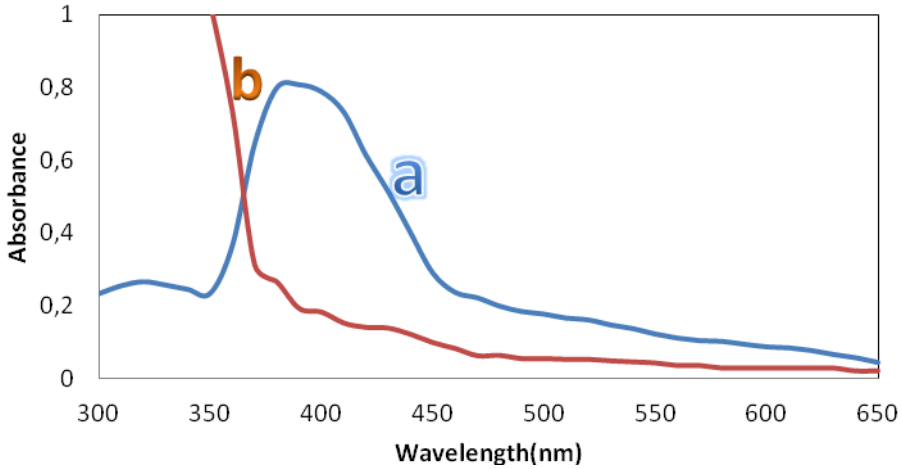

Figure 2: Absorption spectra:
(a). [Pb(II)–HDMBHBH] complex Vs. reagent blank;
(b). HDMBHBH Vs. buffer blank.

Results and discussion

4-hydroxy 3,5-dimethoxy benzaldehyde 4-hydroxy benzoyl hydrazone (HDMBHBH)

4-hydroxy 3,5-dimethoxy benzaldehyde 4-hydroxy benzoyl hydrazone (HDMBHBH) reagent is a blend of a carbonyl compound and a hydrazide. The reagent solution is stable for more than 24 hrs in presence of the buffer medium. The ligand presumably coordinates the metal ions to give a neutral water soluble complex.

Determination of Lead (II) using HDMBHBH

Copper (II) reacts with HDMBHBH in basic medium to give yellow coloured water-soluble complex. The colour reactions between Lead (II) and HDMBHBH are instantaneous even at room

temperature in the pH range 8.0 to 10.0. The absorbance of the bright yellow coloured species remains constant for five hours. The maximum colour intensity is observed at pH = 10.0. A 10-fold molar excess of reagent is adequate for full colour development. The order of addition of buffer solution, metal ion and reagent has no adverse effect on the absorbance. The complex formation reaction between Lead (II) and HDMBHBH has been studied in detail based on the composition of the complex as determined by using Job's and molar ratio methods. Important physico-chemical and analytical characteristics of Lead (II) and HDMBHBH are summarized in Table 2.

Table 2: Physico-chemical and analytical characteristics of [Pb(II)–HDMBHBH] complex

Characteristics	**Results**
λ_{max} (nm)	386
colour	yellow
pH range (optimum)	9.0 to 10.0
Mole of reagent required per mole of metal ion for full colour development	10-folds
Molar absorptivity ($L \cdot mol^{-1} \cdot cm^{-1}$)	2.66×10^4
Sandell's sensitivity ($\mu g \cdot cm^{-2}$)	0.0077
Beer's law validity range (µg/ml)	0.518–5.18
Optimum concentration range (µg/ml)	1.036–4.662
Composition of complex (M:L) obtained in Job's and mole ratio method	1 : 1
Stability constant of the complex (jobs method)	3.42×10^6
Relative standard deviation (%)	0.02
Regression coefficient	0.999

The system [Pb(II)–HDMBHBH] obeys Beers law and the calibrated values were presented in Figure 3.

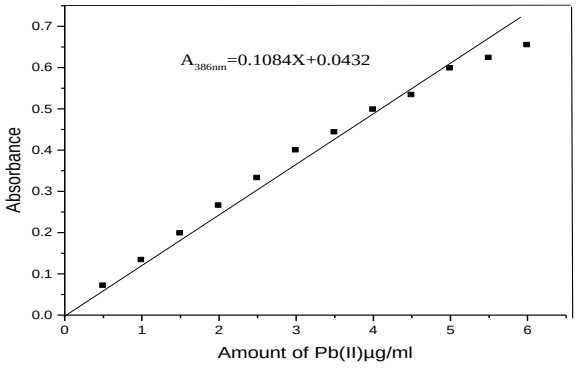

Figure 3: Absorbance Vs Amount of Pb (II) µg/ml:
[HDMBHBH] = 1×10^{-2}; pH = 9.0; wavelength = 418 nm

The first order derivative spectral graph was shown in Figure 4. This shows that the derivative amplitude is measured at 418 nm. First order was found to be proportional to the amount of Lead (II) respectively.

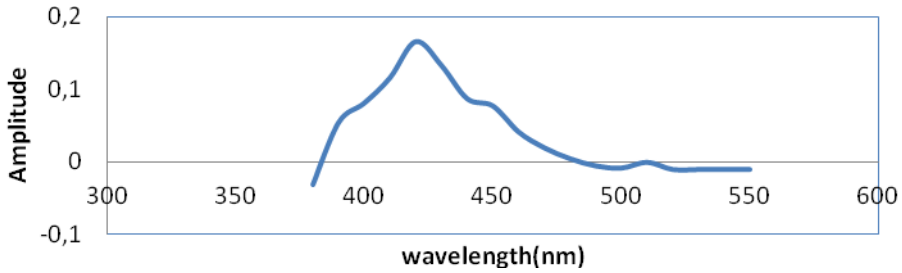

Figure 4: First derivative spectra of [Pb(II)–HDMBHBH] Vs reagent

Effect of foreign ions

Derivative spectrophotometry is a very useful technique in the sense that it decreases the interference, i.e., increases the tolerance limit value of foreign ions of metal ions having overlapping spectra. The recommended procedures have been employed for the spectrophotometric determination of Lead (II). The effect of various diverse ions in the determination of Lead (II) was studied to find out the tolerance limit of foreign ions in the present method. The tolerance limit of a foreign ion was taken as the amount of foreign ion required to cause an error of ±2 % in the absorbance or amplitude. The experimental results are given in Table 3.

Table 3: Tolerance limit of foreign ions in the determination of 5.18 µg/ml of Lead (II)

Ion added	Tolerance limit (µg/ml)	Ion added	Tolerance limit (µg/ml)
Iodide	2187	Zr(IV)	216
Sulphate	559	Zn(II)	20
Urea	723	Bi(III)	58
Thiocyanide	183	Ni(II)	33
Bromide	959	Ce(IV)	42
Thiourea	797	Fe(III)	1.6, 1.9[a]
Nitrate	1678	Cu(II)	1.7, 2.5[b]
Tetra borate	249	Ru(III)	2.6
Acetate	167	Ag(I)	12
Phosphate	293	Pt(IV)	11
Chlorides	249	Sb(II)	476
Tartarate	744	Sr(II)	25
Citrate	379	V(V)	116
Fluoride	577	Os(VIII)	8
Oxalate	269	Cd(II)	22
Thiosulphate	356	Co(II)	25
U(VI)	198	Al (III)	42
Sn(II)	47	Mo(VI)	20
La(III)	152	Cr(VI)	28
Ba(II)	267	Hg(II)	1.5, 1.3[c]
Na(I)	45	Mn(II)	55

'a' masked with 76 µg/ml of Fluoride
'b' masked with 345 µg/ml of Thiourea
'c' masked with 315 µg/ml of Ascorbic acid.

Applications:

Determination of Lead (II) in biological samples

The accuracy and applicability of the proposed method has been applied to the determination of lead in tea leaves, human hair and pond sediment by National Institute for Environment Studies (NIES). 0.1 g sample was taken in a beaker and dissolved in concentrated nitric acid (~5 ml) with heating. The solution was cooled, diluted and filtered. The filtrate was made up to 100 ml with water in a calibrated flask. Vehicle exhaust particulates (1 g) was dissolved in 18 ml of concentrated nitric acid, 18 ml of concentrated perchloric acid and 2 ml of concentrated hydrofluoric acid in a 100 ml Teflon beaker, evaporated to a small volume, filtered through a filter paper and made up to 100 ml with distilled water. An aliquot (10–50 ml) of the sample solution was taken individually and lead was determined by the general procedure. The results obtained are presented in Table 4.

Table 4: Determination of Lead (II) in biological samples

Sample	Composition	Concentration (μg g^{-1})	
		Certified value	Found*
NIES, No.1 Tea Leaves	Zn, 33; Cd, 0.030; Sb, 0.014; Ni, 6.5; Cr, 0.15; Al, 775; Mg, 1530; Ba, 5.7; K, 18600; Sc, 0.011; Na, 15.5; Sr, 3.7; Ca, 3200; Cs, 0.22l; Co, 0.12; Mn, 7.00; Cu, 7.0 μg g^{-1}	0.8	0.76±0.04
NIES, No.2 Human Hair	Zn, 169; Cd, 0.20; Sb, 0.07; Ni, 1.8; Al, 240; Fe, 225; Mg, 208; Hg, 4.4; K, 34; Rb, 0.19; Sc, 0.05; Se, 1.4; Na, 26; Sr, 2.3; Ti, 3.2; Ca, 728; Cr, 1.4; Ba, 2.2; Cu, 16.3; Co, 0.10 μg g^{-1}	6.0	5.7±0.3
NIES, No.3 Pond Sediment	Fe, 6.53±0.35; Al, 10.6±0.5; Ca, 0.81; K, 0.68; Na, 0.57% Zn, 343; Cu, 210; Cr, 75; Ni, 40; Cd, 0.82; Co, 27; As, 12 μg g^{-1}	105	104±1
NIES, No.4 Vehicle Exhaust Particulates	K, 0.115±0.008; Ca, 0.53±0.02; Mg, 0.101±0.005; Al, 0.33±0.02; Na, 0.92±0.008; Zn, 0.104±0.005%; Sr, 89±3; Co, 3.3±0.3; Cu, 67±3.5; Cd, 1.1±0.1; As, 2.6±0.2; Cr, 25.5±1.5; V, 17±2; Sb, 6.0±0.4; Ni, 18.5±1.5; Cs, (0.24); Rb, (4.6); Sc, (0.055); La, (1.2); Br, (56); Ag, (0.2); Se, (1.3); Mo, (6.4); Ce, (3.1); Th, (0.35); Sm, (0.20); Eu, (0.05); Lu, (0.02) μg g^{-1}	219±9	217±2

*Average of the best three determinations among five determinations

Conclusion

In basic medium, 4-hydroxy 3,5-dimethoxy benzaldehyde 4-hydroxy benzoyl hydrazone (HDMBHBH) reacts with Lead (II) and imparts yellow coloration water soluble complex. The colour reaction between Lead (II) and HDMBHBH is instantaneous and the absorbance of the coloured species remains constant for 3 hr. Order of addition of constituents (buffer, metal ion and reagent) has no adverse effect on the absorbance of the complex.

4-hydroxy 3,5-dimethoxy benzaldehyde 4-hydroxy benzoyl hydrazone (HDMBHBH)has been proven to be a sensitive and selective chromogenic organic reagent for the determination of Lead (II). Molar absorptivity of the colour complex was 1.65×10^4 $L{\cdot}mole^{-1}cm^{-1}$. The proposed method was especially sensitive and selective with respect to metals, which commonly seriously interfere with the determination of Lead (II) performed by literature methods. The proposed method can be successfully applied for the determination of Lead (II) in biological samples. This method was favorably compared with previously reported spectrophotometric methods.

Acknowledgement

The authors are thankful to the Jawaharlal Nehru Technological University, Anantapur (JNTUA), Anthapuramu, A.P, India, for providing research facilities to carry out the present work.

References:

1. Chandra Sekhar K.B., and Hussain Reddy, K. *Res. J. Chem. Environ*., 8 (2A), 2004, 12 p.
2. Chandra Sekhar K.B. "*Studies in the chemistry of metal pollutants*" Ph.D Thesis Sri Krishna Devaraya University, Anantapur (A.P), India, 1999.
3. Chandra Sekhar K.B., and Hussain Reddy. K., *J. Indian Chem. Soc*., 78, 2001, 340 p.
4. Narender Reddy. G, Chandrasekhar K.B., Devanna N., and Jayaveera K.N. *Asian J. Chem*., 20(3), 2008, 2257 p.
5. Nagalakshmi B.N.; vallinath G.V.S.; and Chandrasekhar K.B. *International journal of Analytical and Bioanalytical chemistry,* 1(3) 2011, pp. 83-88.
6. Peshkova, V.M., and Savoshma D.V. *Analytical Chemistry of nickel*, 48(3), 1999, pp. 511-516.
7. Taylor C.G. *Analyst*., 81, 1956, 369 p.
8. Prasad N.B.L. Hussain Reddy K., and Sreenivasula Reddy. T. *Indian. J. Chem,* 42 (A), 2003, 112 p.
9. Bao Di., Bao Guilan., Hao Xiangying, Huangjin. 22 (7) 2001, 43 p.
10. Liu, Yan-Qin, Guangpu. *Anal. Sci*. 18(94) 2001, 462 p.

УДК 547.7: 547.152.3

Чувствительный и селективный хромогенный органический реагент 4-гидрокси-3,5-диметокси бензальдегид-4-гидрокси бензоил гидразон (HDMBHBH) для прямого и производного спектрофотометрического определения свинца (II)

Н. Радхакришна[1]
С. Висватаса[2]
К. Рамакришна Редди[3]
Н. Деванна[4]

[1] ОМС Колледж для женщин, Бангалор. Индия
Ассоциированный профессор, кафедра химии
[2] Университет Арба Мынч P.O. Box 21, Арба Мынч, Эфиопия
Ассоциированный профессор, кафедра химии
[3] Инженерный колледж, Нендайл, Карнул, AP, Индия
Ассоциированный профессор, профессор химии
[4] Инженерный колледж, Каликири-517234, AP, Индия
Профессор химии
E-mail: chamanchula.viswanatha@amu.edu.et; viswajntu@gmail.com

Аннотация. 4-гидрокси-3,5-диметокси бензальдегид-4-гидрокси бензоил гидразон (HDMBHBH) используется в качестве нового хромогенного органического реагента для определения свинца (II) с использованием спектрофотометрии. Новый хромогенный органический реагент 4-гидрокси-3,5-диметокси бензальдегид-4-гидрокси бензоил гидразон (HDMBHBH) дал водорастворимый комплекс с Pb (II) желтого цвета в основном буферном растворе (pH = 10,0) среднего. Цвет комплекс показывает максимальную оптическую плотность при 386 нм. Система подчиняется закону Бера в интервале концентраций 0.518–5.18 μg/мл. Молярный коэффициент поглощения и чувствительность

составили 2.66×10^4 л·моль$^{-1}$·см$^{-1}$ и 0.0077 мкг/см^2 соответственно. Свинец (II) формирует комплекс I:I с HDMBHBH и константа устойчивости комплекса составляет 3.42×10^6. Разработанный метод был успешно применен для определения свинца (II) в биологических пробах.

Ключевые слова: новый хромогенный органический реагент; спектрофотометрия; свинец (II); биологические образцы.

Published in the Russian Federation
European Reviews of Chemical Research
Has been issued since 2014.
ISSN: 2312-7708
Vol. 3, Is. 1, pp. 51-55, 2015

DOI: 10.13187/ercr.2015.3.51
www.ejournal14.com

UDC 546.682.3,221.1

Chemical bath deposition of In_2S_3 thin films

[1] Stanislav S. Tulenin
[2] Vyacheslav F. Markov
[3] Larisa N. Maskaeva
[4] Mikhail V. Kuznetsov

[1-4] Ural Federal University, Russian Federation
Mira Str., 28, Ekaterinburg, Sverdlovskaya oblast, 620002
[1] E-mail: stast1989@mail.ru
[2] Doctor (Chemistry), Professor
E-mail: vfmarkov@list.ru
[3] Doctor (Chemistry), Professor
E-mail: mln@ural.ru
[4] Doctor (Chemistry), Professor
E-mail: kuznetsov@ihim.uran.ru

Abstract

In_2S_3 thin films were grown by means chemical bath deposition from acid solution. Calculation of ionic equilibrium with using of thermodynamic constants for systems defines boundary conditions of formation In_2S_3. Films were characterized by means of XRD, SEM, EDX and XPS methods. According to XRD films have cubic structure of In_2S_3. XPS method was shown that the surface of In_2S_3 thin film includes oxygen and carbon contained impurities. SEM confirmed ***nanosized*** nature of thin films. Optical band gap of indium(III) sulfide equal to 2.3 eV.

Keywords: boundary conditions of deposition; chemical bath deposition; indium(III) sulfide; XRD, XPS.

Introduction

Newsday indium (III) sulfide has wide application in a micro- and optoelectronics thanks to unique electrical and physical properties [1] such as picture tubes for color television, ionized radiation detectors and in the photovoltaic such as buffer layer and main material for $CuInS_2$ solar cells [2, 3]. In_2S_3 are simplest compound among chalcogenide group that possess a high energy band gap [4], n-tape conductivity, high absorption coefficient of radiation, longtime stability.

All deposition methods of In_2S_3 semiconductor material we are divide on physical and chemical methods. The physical methods include thermal evaporation in vacuum, spraying of water solutions with pyrolysis on a heating substrate [5], physical deposition from gas phase, molecular-beam epitaxy [6]. The chemical thin film methods include electrochemical deposition and chemical bath deposition [7]. As using of physical methods is being connected with composite equipments, deep vacuum and high-purity precursors but the chemical bath deposition has weak deposition condition, simple apparatus design, composition control mode and doping operations.

Materials and Methods

Deposition of indium sulfide thin films was carrying out on preliminary defatting pyroceramic substrates from reaction mixture containing indium nitrate $In(NO_3)_3$, thioacetamide CH_3NH_2CS, tartaric acid $C_4O_6H_6$, hydroxyl amine $NH_2OH{\cdot}HCl$. The optimal pH was about 1.7. Synthesis of thin films was carried out in the range of temperature 70–90 °C in Mo-glass beaker reactors. Reactors were located in thermostat TC-TB-10. Crystal structure of thin films investigated by method of X-ray diffraction (XRD) on diffractometer Shimazu XRD – 7000 with using monochromatic $Cu/K_{\alpha 1}$ radiation, λ = 1.54056 Å. Composition and main form of compounds in thin films were studied by means of X-ray photoelectron spectroscopy (XPS) method on ESCALAB MK II (VG Scientific, Great Britain) X-ray photoelectron spectrometer using magnesium cathode MgK_α (1253.6 eV). The C1*s* line was calibration line. Scanning electron microscopy (SEM) of a simple surface was occurred on Mira-3-LMY instrument in second electron (SE) with JED 2300 tool for energy dispersive X-ray (EDX) analysis. Thickness of simples has been measured on an interferometer MII-4M.

Discussion

The choice of reaction mixture composition and definition of colloidal chemical deposition conditions of indium sulfide In_2S_3 thin films is considerably facilitated after carrying out of the preliminary thermodynamic calculations.

In a basis of the deposition condition analysis from the solutions containing thioacetamide has laid a rule about reversible hydrolytic decomposition character of the sulfur-supplier [8, 9]. Thus TAA decompose in acid solution according to equal:

$$CH_3CSNH_2+2H_2O+H_3O^+ \leftrightarrow Ac^-+NH_4^++H_2S \quad (1)$$

In equal (1) yielded hydrogen sulfide quickly decompose (2) and (3) as indium-ions In^{3+} combine with sulfide-ions on equal (4):

$$H_2S + H_2O \leftrightarrow H_3O^+ + HS^- \quad (2)$$

$$HS^- + H_2O \leftrightarrow S^{2-} + H_3O^+ \quad (3)$$

$$InL_x + S^{2-} \rightarrow In_2S_3 + xL \quad (4)$$

The content of Me^{n+} ions had been calculated by means of the analysis ionic balances in system with the complexing account with present ligands. Result of calculation which characterized placed balance in $InCl_3$ – $C_4O_6H_6$ – $NH_2OH{\cdot}HCl$ – CH_3NH_2CS system between a sediment In_2S_3 (curve 1), $In(OH)_3$ (curve 2) and indium complex compounds in a solution are showed on Fig. 1. Deposition of this sulfide in investigated system is placed in a wide range pH from 3 to 15. Also indium hydroxide form at the same conditions. The region pH less then 3 without formation of indium hydroxide for synthesis is optimal.

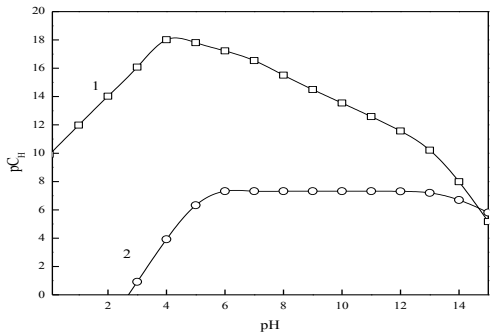

Figure 1. The region of In_2S_3 solid phase deposition in system $In(NO_3)_3$ – $C_4O_6H_6$ – $NH_2OH{\cdot}HCl$– TAA (1), $In(OH)_3$ line (2). The calculation carried out at 80 °C

According to calculation it was deposited uniform orange films which were observed on pyroceramic substrates and walls of beakers with good adherent. Thin films were washed and dried. Thickness of obtained thin films was up to 3500 nm.

The XRD patterns of the deposited In_2S_3 thin films confirmed that it crystallized in cubic structure (XRD patterns no shown). Diffraction peaks (311), (400), (422) and (440) observed on typical XRD pattern of the In_2S_3 prepared on pyroceramic at 80 ºC (a film thickness 700 nm) indicate about this [10]. It is noticed that lines with least *hkl* indexes on XRD pattern of thin film are absent because of the strong substrate background is presence, and also the accurate crystal structure is not formed completely.

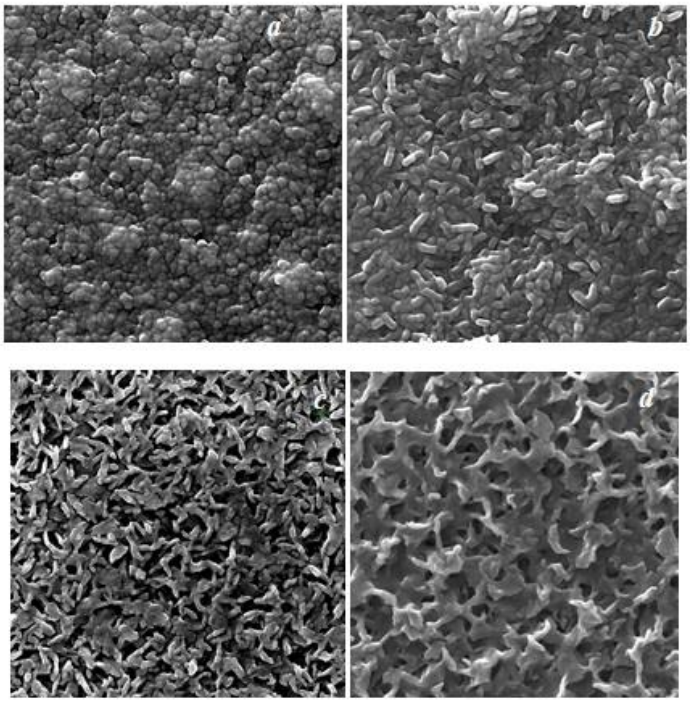

Figure 2. SEM images of as-deposited (*a, b, c*) and heat treatment at 300 ºC (*d*) In_2S_3 thin films prepared at, ºC: 70 (*a*), 80 (*b, d*), 90 (*c*). Magnification is 50000

SEM micrographs of the deposited films at different synthesis temperature are presented on Fig. 2. The study of as-deposited indium(III) sulfide thin films at 70 ºC (Fig. 2*a*) shown that it has a fine-crystalline structure with an average crystal size to 70-120 nm. It is a good agreement with literature date to deposition in a more acid solution [11]. The modification of film surface and mesh fractal structure were observed at increasing of a synthesis temperature (Fig. 2*b,c*) [12]. The average size of thread-crystals is 90-150 nm. We can see a particular flash-off of crystals after heat treatment on air condition in the SNOL furnace. The EDX-analysis shown that films contain up to 10 at.% of oxygen by means of oxidation process.

The In_2S_3 films were investigated by XPS using Ar^+ etching on 12 nm into depth. All films include characteristic In4*d*, S2*p*, C1*s*, In3*d* and O1*s* core levels of indium, sulfur, carbon and oxygen (Fig. 3*a*). We can see that overview XSP spectra after etching not contain C1*s* and O1*s* core levels. It means that volume material is pure. We obtained by means of XPS that surface of thin films include some oxidation phases (no more 8.5 at.% of oxygen) on surface. For example, it is may be different carbonates and organic impurities. Opposite EDX-analysis shown absents of oxygen in thin films and confirmed formation of In_2S_3 with small indium excess [13].

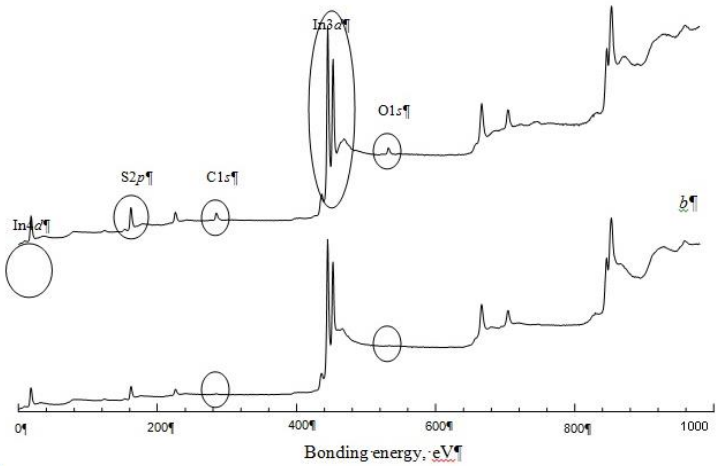

Figure 3. Overview XPS spectra of the simples with shown In4*d*, S2*p*, C1*s*, In3*d* and O1*s* core level spectrum of In_2S_3 before (*a*) and after (*b*) etching on 12 nm.

As can be observed (Fig. 3) all peaks are accurate and good define. The In3$d_{5/2}$ core shall with energy approximately 444.9 eV correspond to nonoxide form and it is correspond to In_2S_3 (444.7 eV). We cannot see any width and asymmetry of the In3*d* peak which indicate purity of compound. S2*p* peak is accurate and good define. Its bonding energy (161.4 eV) interquartile correspond to sulfide phases. The α-parameter gave us more information about compound. This value is 852.2 eV but it is some less then literature date for In_2S_3 (852.5 eV) and we refer this α-parameter to indium(III) sulfide.

The measure of optical properties of In_2S_3 thin films carried out from 300 to 1000 nm. The thin layers with 300 nm thickness for these measurements were deposited on glass substrates.

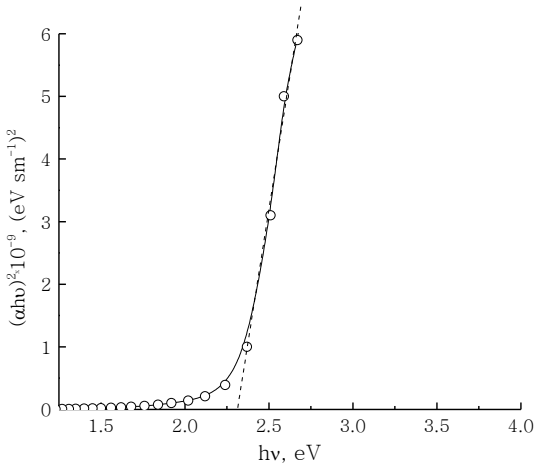

Figure 4. The plot of $(\alpha h\upsilon)^2$ versus hυ of thin film deposited at 80 ºC by CBD.

The dependence of $(\alpha h\upsilon)^2$ on energy of incident photons hυ show on Fig. 4. The E_g for as-prepared In_2S_3 thin film has been determined by extrapolating the linear portion of $(\alpha h\upsilon)^2$ vs. hυ on x-line and has made 2.3 eV that have good agreement with literature data. The increasing of the E_g more then 2.03 eV for In_2S_3 material is explained by the smaller size of crystal and chemical composition of a film. The oxygen on film surface indicates on thin oxidation layers that increase E_g

Conclusion

The theoretical study of ion balance in $InCl_3$ – $C_4O_6H_6$ – $NH_2OH{\cdot}HCl$ – TAA system confirmed that deposition of In_2S_3 is accompany with formation of indium hydroxide $In(OH)_3$ steady in wide pH region. The In_2S_3 thin films with thickness up to 3.5 μm from tartaric solution with 1.7 pH were obtained. It was confirmed that deposited thin films has cubic structure of indium(III) sulfide by means of XRD. The surface layer of In_2S_3 thin film up to 12 nm includes a small amount of oxygen and carbon

contained impurities. Nanosized nature of thin films and modification of their morphology depend on temperature were shown by means of SEM. So, the increasing of synthesis temperature in rang from 70 to 90 ºC lead to increasing of average crystal size from 70 to 150 nm. It was obtained optical band gap of indium(III) sulfide equal to 2.3 eV.

The research was supported by the Russian Fund of Basis Research (№ 14-03-00121) "Thin films on the basis of chalcopyrite structures for solar cells – chemical bath deposition, fundamental properties and application".

References:

1. X.H. Xu, F. Wang, J.J. Liu, K.C. Park and M. Fujishige: *Sol. Energy Mat. and Sol. Cells*, 2011, 95, 791–796.
2. S.S. Kale, R.S. Manea, C.D. Lokhande, K.C. Nandi and Sung-Hwan Han: *Mat. Sci. and Eng. B.,* 2006, 133, 222–225.
3. K. Otto, A. Katerski, A. Mere, O. Volobujeva and M. Krunks: *Thin Solid Films*, 2011, 519, 3055–3060.
4. A.V. Novoselova: "Fiziko-himicheskie svoystva poluprovodnikovih vechestv", 339; 1979, Moscow, Nauka.
5. T.T. John, C.S. Kartha, K.P. Vijayakumar, T. Abe and Y. Kashiwaba: *Appl. Phys. A*, 2006, 82, 703–707.
6. Y. Xiong, Y. Xie, G. Du, X. Tian and Y. Qian: *J. of Sol. State Chem.* 2002, 166, 336–340.
7. S. Lugo-Loredo, Y. Peca-Mindez, M. Calixto-Rodriguez, S. Messina-Fernindez, A. Alvarez-Gallegos, A. Vizquez-Dimas and T. Hernindez-Garcia: *Thin Solid Films*, 2014, 550, 110–113.
8. V.P. Markov, L.N. Maskaeva and P.N. Ivanov "Gidrohimicheskoe osajdenie plenok sulfidov metallov: modelirovanie i experiment", 276. 1nd edition, 2006, Yekaterinburg, UrO RAS.
9. V.F. Markov, S.S. Tulenin, L.N. Maskaeva, M.V. Kuznetsov and N.M. Barbin: *Tech. Ph. Let.*, 2012, 38, 77–83.
10. B.Yahmadi, N.Kamoun, R. Bennaceur, M. Mnari, M. Dachraoui and K. Abdelkrim: *Thin Solid Films*, 2005, 473, 201–207.
11. S.S. Tulenin, V.F. Markov and L.N. Maskaeva: *Butlerov's reports*, 2012, 29, 79–85.
12. C. Lokhande, A. Ennaoui, P. Patil , M. Giersig, K. Diesner, M. Muller and H. Tributsch: *Thin Solid Films*, 1999, 340, 18–23.
13. S.S. Korovin, D.V. Drobot, P.I. Fedorov: "Redkie i rasseyannye elementy. Khimiya i technologiya", 461; 1999, Moscow, MISIS.

Published in the Russian Federation
European Reviews of Chemical Research
Has been issued since 2014.
ISSN: 2312-7708
Vol. 3, Is. 1, pp. 56-68, 2015

DOI: 10.13187/ercr.2015.3.56
www.ejournal14.com

UDC 546.815, 221

Composition, Structure, Morphology of thin Films Produced by Hydrochemical Deposition in PbSe-CdSe System

[1] Nina V. Zarubina
[2] Ivan V. Zarubin
[3] Larisa N. Maskaeva
[4] Vyacheslav F. Markov

[1-4] Ural federal university named after the first President of Russia B.N. Yeltsin, Russian Federation
Mira Street, 19, Ekaterinburg, 620002
[1] Post-graduate student
E-mail: nina6131@mail.ru
[2] Advanced engineer
E-mail: ivan-carevich85@mail.ru
[3] Doctor of Sciene (Chemical), Professor
E-mail: mln@ural.ru
[4] Doctor of Science (Chemical), Professor
E-mail: v.f.markov@ustu.ru

Abstract

The area of co-precipitation of lead and cadmium selenide in the reaction system "$Pb(CH_3COO)_2$ – $CdCl_2$ – $Na_3C_6H_5O_7$ – NH_4OH – $CSeN_2H_4$" was calculated taking into account the critical nucleus. Thin films of supersaturated solid solutions $Cd_xPb_{1-x}Se$ having the cubic structure *B*1 (NaCl) have been produced by hydrochemical co-deposition of lead and cadmium selenide. The patterns of formation of solid solutions $Cd_xPb_{1-x}Se$ and the kinetics of their growth depending on the composition of the reaction mixture have been determined. The structure, composition and morphology of PbSe-CdSe thin films were investigated by methods of X-ray energy dispersive analysis and electron microscopic studies.

Keywords: chemical deposition; thin films; $Cd_xPb_{1-x}Se$; supersaturated solid solutions.

Введение

Материалы на основе твердых растворов халькогенидов металлов активно применяются при производстве оптоэлектронных приборов и устройств, так как обладают широкой вариабельностью свойств при изменении состава.

Одним из наиболее востребованных полупроводниковых материалов для создания датчиков ИК-излучения продолжает оставаться селенид свинца [1-20]. Ширина его запрещенной зоны позволяет создавать фотоприемники для работы в спектральной области 2–5 мкм. В этой же области находятся молекулярные спектры поглощения воды, метана, углекислого и угарного газов, многих углеводородов. Кроме того, в рассматриваемой области спектра в той или иной степени излучают тела, нагретые от 1100 до 200 °С. Именно поэтому фотоприемники для указанного оптического диапазона находят широкое применение в металлургии, медицине, экологии для мониторинга

окружающей среды, газового анализа токсичных сред, в системах предупреждения чрезвычайны ситуаций в технике, раннего обнаружения пожаров.

Материалы на основе селенида кадмия чувствительны к излучению в видимой и ближней инфракрасной области [21, 22]. Они применяются как высокочувствительные фотоприемники при изготовлении видиконов в видимом диапазоне длин волн. Селенид кадмия – активная среда в полупроводниковых лазерах, материал для изготовления фоторезисторов, фотодиодов, солнечных батарей, пигмент для эмалей, глазурей и художественных красок [23, 24]. Также CdSe используется в бытовой технике, например, в качестве оптодатчика в пультах дистанционного управления.

Перспективность твердых растворов замещения $Cd_xPb_{1-x}Se$, в первую очередь, определяется вариабельностью свойств от состава. Они востребованы в качестве инфракрасных датчиков ближнего и среднего диапазона, полупроводниковых лазеров, матричных ПЗС структур, создания тепловизионной техники различного назначения, солнечных фотопреобразователей.

На основе $Cd_xPb_{1-x}Se$ могут быть созданы фотоприемники и источники инфракрасного излучения для оптических газоанализаторов [25-29]. Источниками излучения в таких ИК-абсорбционных газоанализаторах служат переизлучающие структуры на основе поликристаллических слоев $Cd_xPb_{1-x}Se$ благодаря наблюдаемой в них высокой фотолюминесценции.

Имеются данные о создании вакуумтермической технологии формирования тонких поликристаллических, хорошо текстурированных слоев твердых растворов в системе PbSe–CdSe [26, 27]. На основе этих структур созданы фоторезисторы и фотодиоды со временем отклика 3–50 мкс. Приборы нашли применение в извещателях пламени; пирометрах, работающих в диапазоне температур 200–1200 °С; малогабаритных тепловизорах.

Привлекательность широко используемого метода гидрохимического осаждения заключается не только в простоте его технологического оформления, отсутствии необходимости в вакууме и высоких температурах, но и в возможности получения пересыщенных твердых растворов в тонкопленочном виде, гибкости управления свойствами наносимых слоев, чего добиться другими методами крайне сложно или практически невозможно [3, 7, 13]. Авторам [30] удалось получить послойным гидрохимическим осаждением пленки CdSe – PbSe и исследовать их методами рентгенографии, растрово-электронной и сканирующей зондовой микроскопией.

В настоящей работе рассматривается возможность совместного гидрохимического осаждения селенидов кадмия и свинца в форме тонких пленок и исследование их состава, структуры и морфологии.

Экспериментальная часть

Синтез твердых растворов $Cd_xPb_{1-x}Se$ проводили на предварительно обезжираенные ситалловые подложки из ванны, содержащей ацетат свинца $Pb(CH_3COO)_2$, хлорид кадмия $CdCl_2$, трехзамещенный цитрат натрия $Na_3C_6H_5O_7$, водный раствор аммиака NH_4OH, селеномочевину $CSeN_2H_4$, йодид аммония NH_4I и сульфит натрия Na_2SO_3. В приведенной реакционной смеси комплексообразующими агентами наряду с гидроксид-ионами выступали: для свинца – цитрат-ионы, для кадмия – аммиак. Введение сульфита натрия Na_2SO_3 обеспечивало антиоксидантную составляющую, препятствующую окислению селеномочевины кислородом воздуха, а иодид аммония играл роль сенсибилизирующей добавки, т.е. повышал чувствительность осаждаемых пленок к ИК-излучению. Селеномочевина в реакционной смеси играла роль халькогенизатора, т.е. источника ионов серы.

Толщина синтезированных слоев оценивалась с помощью интерференционного микроскопа (микроинтерферометра Линника) МИИ–4М.

Кристаллическую структуру плёнок исследовали методом рентгеновской дифракции в медном-излучении на дифрактометре D/max – 2500 фирмы RIGAKU (Япония) с использованием монохроматизированного (графитовый монохроматор) $Cu/K_{\alpha 1}$ излучения, λ = 1,5406 А. Съёмку проводили при комнатной температуре в интервале углов от 20° до 80° в режиме сканирования с шагом 0,02° и временем

накопления сигнала 5 с. Измерение величины периода решетки $Pb_{x-1}Cd_xSe$ и уточнение структурных параметров проводились методом полнопрофильного анализа Ритвелда с использованием программы FULLPROF [31].

Элементный анализ синтезированных пленок и одновременное определение химического состава в локальных зонах с высоким пространственным разрешением на все элементы проводился на энерго-дисперсионном спектрометре INCA ENERGY 200. Все спектры были сняты при ускоряющем напряжении 20 кВ при наклоне образца 35°.

Электронно-микроскопические изображения пленок выполнены при помощи растрового электронного микроскопа JSM-5900 LV с различным увеличением.

Результаты и их обсуждение

Целенаправленный синтез пленок твердых растворов замещения $Cd_xPb_{1-x}Se$ требуемого состава путем гидрохимического соосаждения индивидуальных селенидов свинца и кадмия значительно облегчается после проведения предварительных термодинамических расчетов ионных равновесий в реакционной системе, содержащей ацетат свинца, хлорид кадмия, трехзамещенный цитрат натрия, водный раствор аммиака NH_4OH, селеномочевину.

На рис. 1 представлена область соосаждения индивидуальных селенидов PbSe (кривая 1) и CdSe (кривая 2) в цитратно–аммиачной системе, а также и сопутствующих их образованию труднорастворимых гидроксидов металлов, граничные условия которых рассчитаны по начальному состоянию системы, учитывая критический радиус зародышеобразования [32], по уравнению, предложенному в работе [33]. Анализ рисунка показывает, что в цитратно–аммиачной системе совместное осаждение PbSe и CdSe возможно в широком диапазоне pH= 8–14, что создает потенциальную возможность формирования на их основе твердых растворов замещения. В выбранной системе прогнозируется образование примесных фаз в виде гидроксидов металлов $CdOH)_2$ (кривая 3), $Pb(OH)_2$ (кривая 4), а осаждение цианамидов металлов не предполагается.

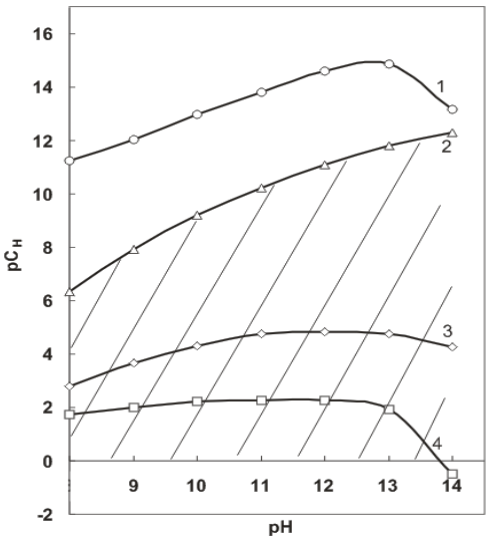

Рис. 1. Граничные условия образования CdSe (1), PbSe (2), $Cd(OH)_2$ (3), $Pb(OH)_2$ (4) в цитратно-аммиачной системе при 298 K.
Область совместного осаждения PbSe и CdSe (заштрихована)

Найденная область совместного осаждения селенидов металлов определила выбор концентраций компонентов реакционной смеси и позволила установить рабочую рецептуру.

В процессе разработки и оптимизации условий осаждения пленок в системе PbSe–CdSe из цитратно-аммиачной системы была исследована как кинетика роста пленок, полученных при соосаждении.

На рис. 2 приведены зависимости изменения толщины пленок, полученных при совместном осаждении селенидов свинца и кадмия, от температуры процесса синтеза при различном времени его протекания. Из рисунка видно, что максимальная толщина соосажденных селенидов свинца и кадмия от температуры процесса синтеза составляет ~1,05 мкм. Причем увеличение продолжительности осаждения вдвое с 45 мин до 90 мин повышает толщину пленок примерно на четверть.

Следует отметить, что существенное влияние кроме температуры процесса на толщину пленок оказывает концентрация соли свинца и селеномочевины. Увеличение содержания кадмия в реакционной смеси ингибирует процесс роста пленок.

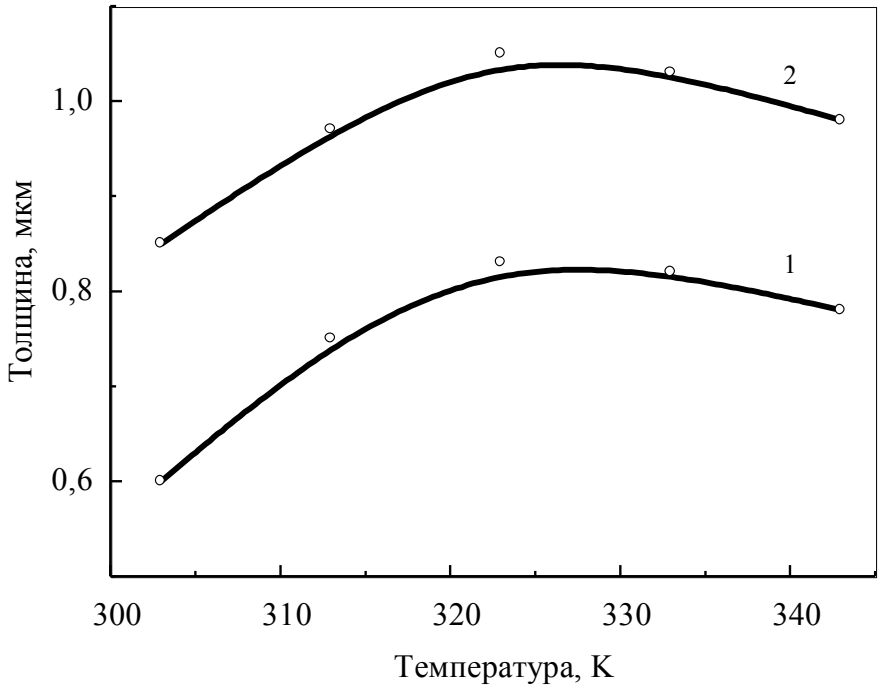

Рис. 2. Зависимость толщины совместно осажденных PbSe и CdSe пленок от температуры процесса при продолжительности синтеза 45 мин (1) и 90 мин (2)

При изучении синтезированных пленок методом рентгеновской дифракции найденная постоянная кристаллической решетки индивидуального селенида свинца составила 0,61480 нм. Это немного больше справочного значения 0,6124 нм для монокристаллического PbSe со структурой *B*1 (NaCl) [34]. На рентгенограммах пленок, полученных совместным осаждением PbSe и CdSe, обнаружена только кубическая фаза со структурой *B*1 со сдвигом рефлексов PbSe в область дальних углов. Увеличение содержания кадмия в реакционном растворе сопровождалось уменьшением периода решетки этой фазы от 0,61479(2) до 0,61313(3) нм. Это было интерпретировано нами как образованием со стороны PbSe твердых растворов $Cd_xPb_{1-x}Se$ путем замещения ионов свинца Pb^{2+} с радиусом 0,120 нм в кристаллической решетке ионами кадмия Cd^{2+} с радиусом 0,097 нм. В результате максимально достигнутое содержание CdSe составляет 21,9 моль.%.

С использованием полученных данных была построена зависимость содержания селенида кадмия в твердом растворе $Cd_xPb_{1-x}Se$ от концентрации соли кадмия в реакционной смеси (рис. 3).

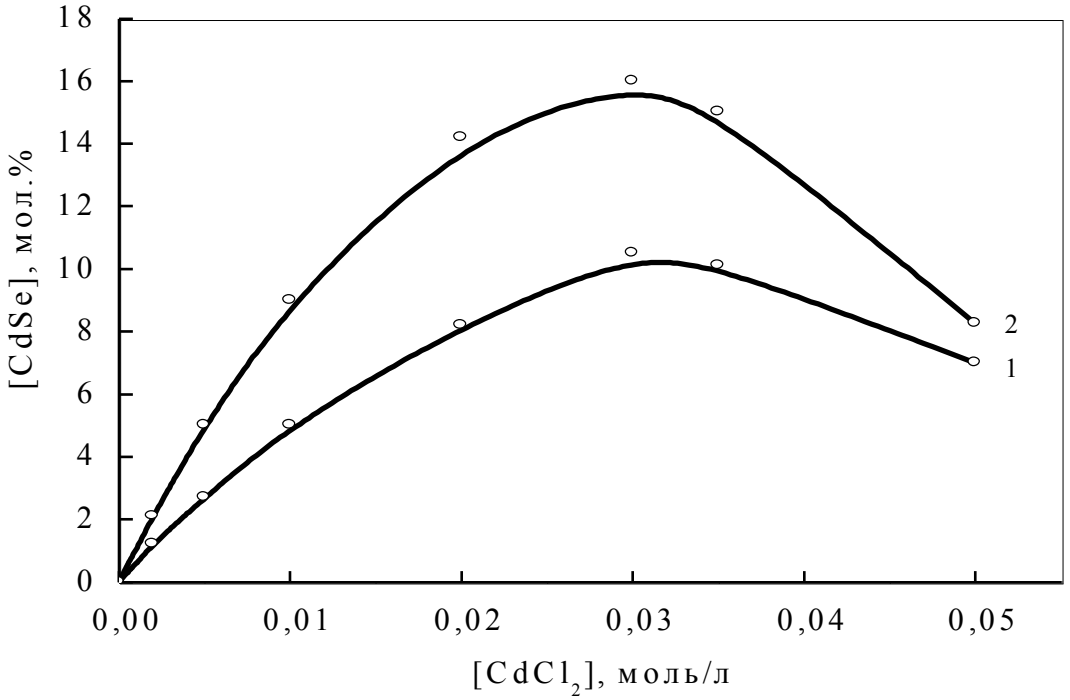

Рис. 3. Зависимость содержания селенида кадмия в пленках твердых растворов $Cd_xPb_{1-x}Se$ от концентрации соли кадмия в реакционной смеси при начальных концентрациях ацетата свинца $Pb(CH_3COO)_2$], моль/л: 0,06 (1); 0,04 (2). Температура процесса 333 K. Время осаждения – 60 мин.

Видно, что повышение концентрации хлорида кадмия в реакционной смеси ведет к постепенному увеличению содержания селенида кадмия в твердом растворе до определенного максимального значения, равного 16,0 моль. % при концентрации соли кадмия 0,35 моль/л. Дальнейшее возрастание концентрации $CdCl_2$ в реакционной смеси сопровождается обеднением твердого раствора замещения $Cd_xPb_{1-x}Se$ по кадмию. Объяснение полученной зависимости может быть связано с изменением термодинамических условий в системе, способствующих преобладающему осаждению CdSe в виде собственной индивидуальной фазы. Процесс участия кадмия в формировании твердого раствора $Cd_xPb_{1-x}Se$ становится термодинамически менее выгодным.

Большой интерес представляло оценить влияние температуры процесса на содержание CdSe в твердом растворе $Cd_xPb_{1-x}Se$. Исследования были проведены при 333, 343, 348, 353, 363 K. Полученные результаты представлены на рис. 4.

Анализ рисунка показывает, что максимальное содержание CdSe в твердом растворе $Cd_xPb_{1-x}Se$ соответствует температуре процесса 353 K и достигает 13,2 моль.% (кривая 1) при концентрации соли свинца 0,06 моль/л.

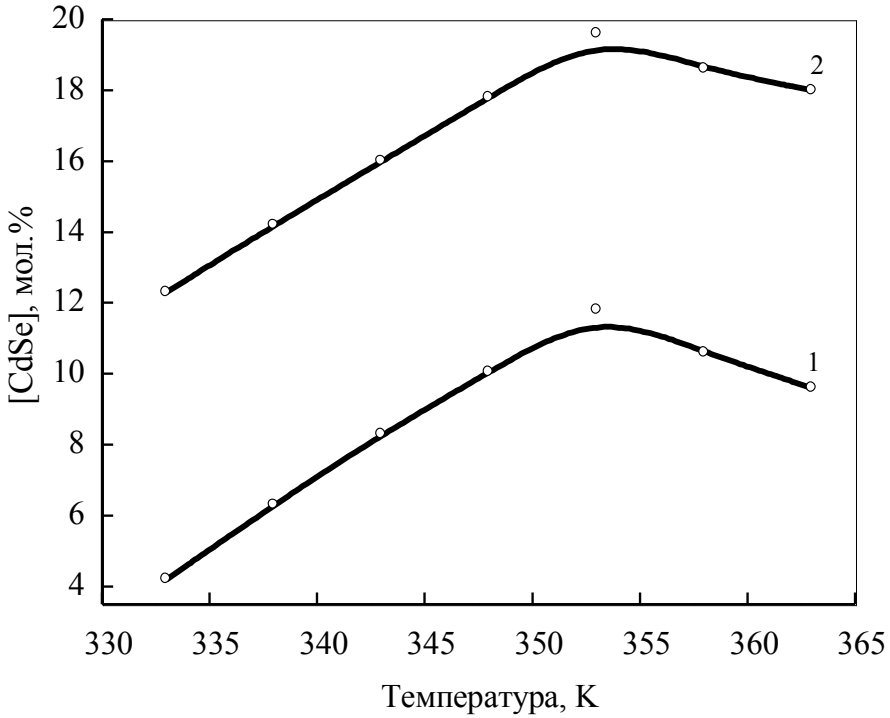

Рис. 4. Зависимость содержания селенида кадмия в твердом растворе $Cd_xPb_{1-x}Se$ от температуры процесса при концентрации соли свинца в реакционной ванне 0,06 (1) и 0,03 моль/л (2)

Уменьшение содержания ацетата свинца в реакционной ванне до 0,03 моль/л повышает процент селенида кадмия в твердом растворе (кривая 2) во всем температурном интервале.

Следует сказать, что согласно равновесной фазовой диаграмме системы CdSe–PbSe [35], синтезированные при 333–363 K твердые растворы $Cd_xPb_{1-x}Se$ являются сильно пересыщенными по замещающему компоненту и фактически не могут быть получены высокотемпературными методами.

Электронно-микроскопические исследования пленок осажденных селенидов свинца и кадмия показали, что образование твердого раствора $Cd_xPb_{1-x}Se$ сопровождается изменением морфологии пленок. При замещении ионов свинца в решетке PbSe ионами кадмия происходит уменьшение размеров кристаллитов, образующих пленку и приобретение ими выраженной зернистой структуры. На рис. 5 и 6 приведены электронно-микроскопические изображения пленок $Cd_xPb_{1-x}Se$, осажденных соответственно при варьировании соли кадмия в реакционной смеси и температуры процесса. Анализ изображений показывает, что, если пленка индивидуального PbSe (см. рис. 5) состоит из кристаллов кубической формы, размеры которых составляют 155–620 нм, то добавление соли кадмия в реакционную смесь в количестве 0,02 моль/л приводит к формированию зернистой структуры.

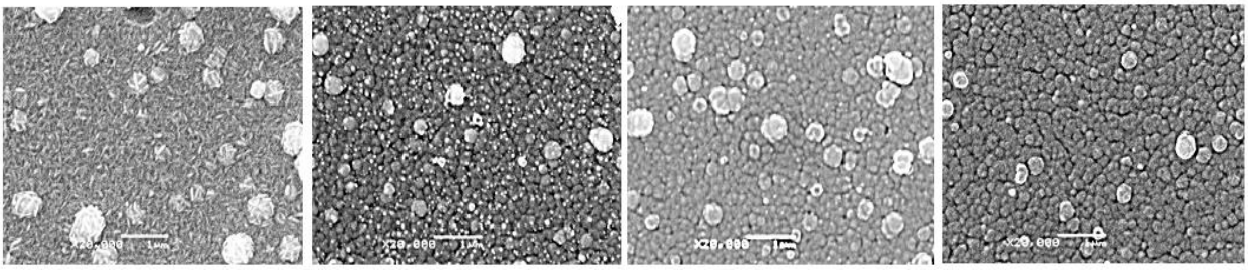

а *б* *в* *г*

Рис. 5. Электронно-микроскопическое изображение свежеосажденных пленок PbSe (*а*) и $Cd_xPb_{1-x}Se$, синтезированных из реакционной смеси с концентрацией хлорида кадмия, моль/л: 0,02 (*б*), 0,035 (*в*), 0,05 (*г*)

Кристаллиты уменьшают свои размеры до 135-500 нм. Увеличение концентрации моли кадмия до 0,035 и затем до 0,05 моль/л сопровождается дальнейшим уменьшением среднего размера частиц до 115–450 нм. Напрашивается вывод о том, что увеличение пересыщения твердого раствора по замещающему компоненту CdSe сопровождается асимбатным уменьшением размера кристаллитов. Таким образом, имеет место размерный эффект [PbCdS].

Влияние температуры синтеза демонстрируют электронно-микроско-пические изображения пленок твердых растворов $Cd_xPb_{1-x}Se$, полученных при 343 (а), 353 (б), 363 К (в) (рис. 6). Так, если при 343 К размер зерен кристаллитов составляет 130–520 нм, при 353 К наблюдается некоторое уменьшение их среднего диаметра до 115–500 нм, то при 363 К дальнейшего уменьшения размера практически не происходит, и они остаются равными 115–500 нм.

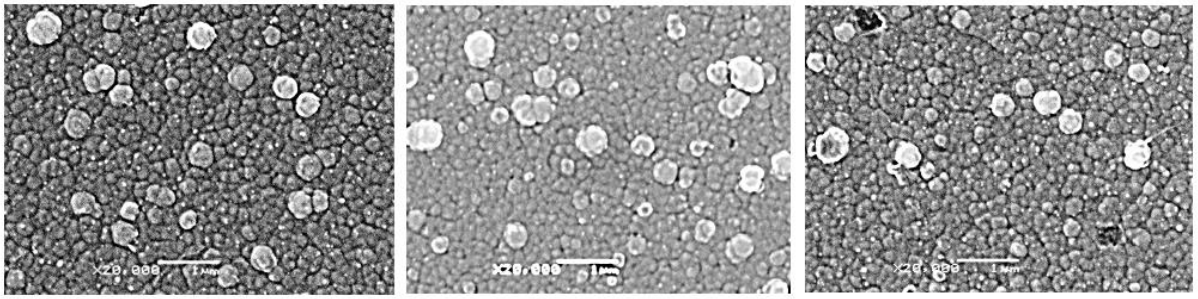

а *б* *в*

Рис. 6. Электронно-микроскопическое изображение пленок $Cd_xPb_{1-x}Se$, осажденных при 343 К (а), 353 К (б), 363 К (в). Продолжительность осаждения – 60 мин.

Для подтверждения химического состава полученных пленок $Cd_xPb_{1-x}Se$ был проведен их элементный анализ с использованием энерго-диперсионного и рентгено-спектрального методов исследования. Локальное определение химического состава с высоким пространственным разрешением на все элементы проводилось на энерго-дисперсионном спектрометре INCA ENERGY 200. Все спектры были сняты при ускоряющем напряжении 20 кВ при наклоне образца 35°. На рис. 7 приведены энерго-дисперсионные спектры пленок $Cd_xPb_{1-x}Se$ различного состава и их электронные микроизображения.

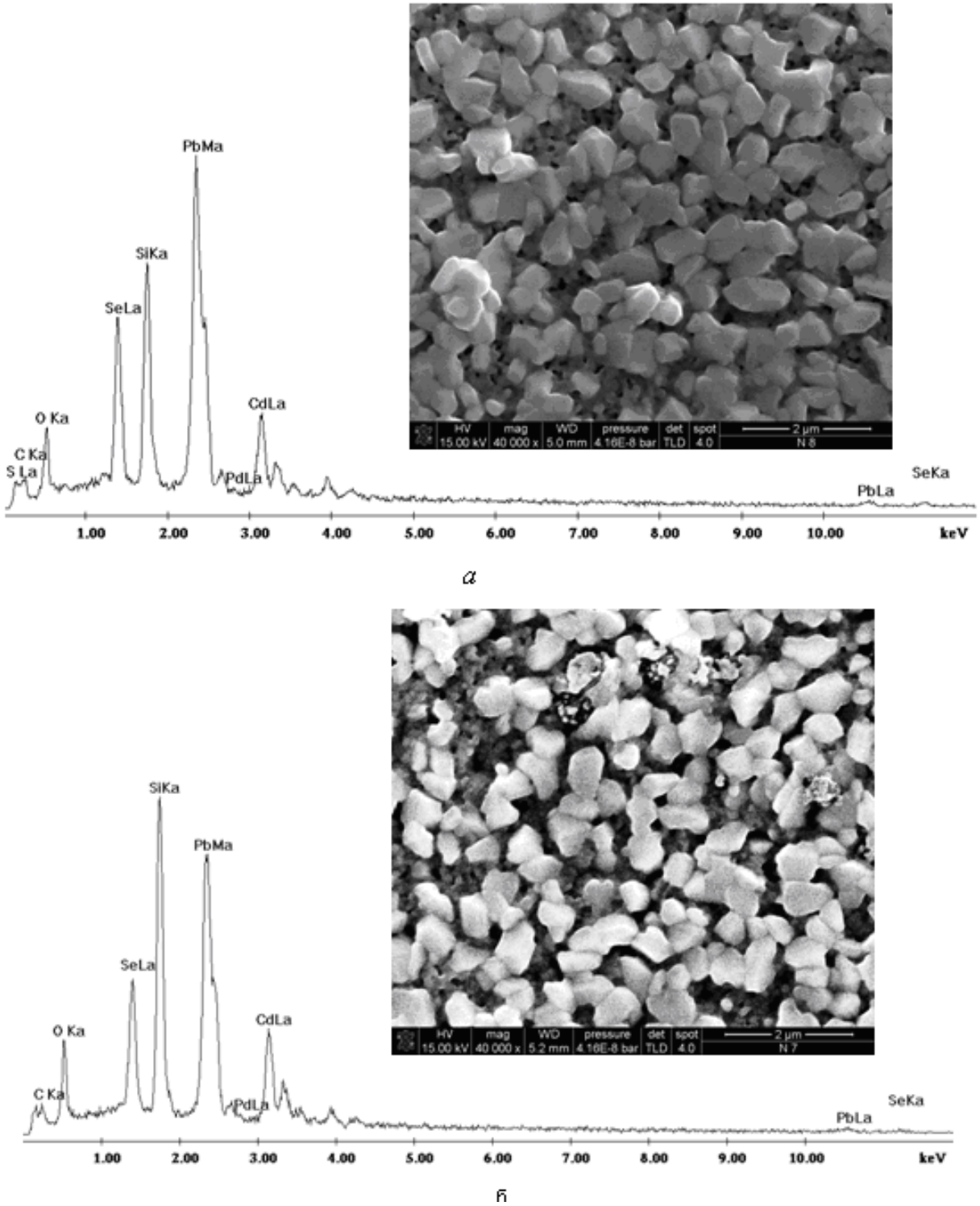

Рис. 7. Энерго-дисперсионный спектры и соответствующие им микрофотографии образцов пленок $Cd_{0,012}Pb_{0,988}Se$ (*а*) и $Cd_{0,043}Pb_{0,957}Se$

Анализ энерго-дисперсионных спектров показывает присутствие в слоях наряду с основными элементами Pb, Cd и Se примесей атомов O, S и C, как составляющих оксидных фаз, продуктов разложения селеномочевины и присутствия сульфита натрия в реакционной смеси.

Данные рентгено-спектрального анализа в целом подтверждают результаты рентгеновских исследований. Однако есть две обращающих на себя внимание особенности. Во всех случаях содержание кадмия в пленках превышает его количество в структуре твердого раствора. Если эти различия для низких концентраций соли кадмия в реакционной смеси составляют 1–5 мол. %, то с повышением концентрации соли в реакторе количество CdSe в слое резко увеличивается, и различия могут достигать 20–25 мол. %. Это связано с образованием в пленках индивидуальной фазы селенида кадмия. Вторая особенност – пленки $Cd_xPb_{1-x}Se$ характеризуются значительной нестехиометрией по селену, содержание которого по результатам рентгено-спектрального анализа в поверхностных слоях составляет 37,9–43,4 мол. %.

Выводы

1. Тонкие пленки $Cd_xPb_{1-x}Se$ являются перспективными материалами оптоэлектроники и сенсорной техники, значительно расширяя область их использования за счет регулирования состава.
2. Определена область совместного осаждения селенидов свинца и кадмия из водных растворов, содержащих соли кадмия, свинца, селеномочевину, йодистый аммоний, аммиак и гидроксид аммония.
3. Из цитратно-аммиачной системы при температуре 353 K получены пленки совместно осажденных PbSe и CdSe.
4. Показано, что при совместном химическом осаждении селенидов свинца и кадмия происходит формирование пересыщенных твердых растворов замещения $Cd_xPb_{1-x}Se$ ($0 < x < 0{,}219$). Данные рентгено-спектрального анализа подтверждают результаты рентгеновских исследований. Зависимость содержания селенида кадмия в составе твердого раствора от концентрации хлорида кадмия в реакционной смеси имеет экстремальный характер.

Примечания:

1. Taylor S. E. On time delays in lead salt semiconductor diode lasers / S.E. Taylor / Appl. Phys. A: Materials Science and Processing. 1986. V. 39. № 2. P. 91–94.
2. J.E. Hill, R.R. Chamberlin, “Process for marking conductive film”, Patent USA. N 3, 148, 084. from 08.09.1964.
3. Мухамедзянов Х.Н. Сравнительные фотоэлектрические характеристики наноструктурированных пленок $Pb_{1-x}Sn_xSe$, полученных совместным и послойным осаждением PbSe и SnSe / Х.Н. Мухамедзянов, Марков В.Ф., Маскаева Л.Н. / Физика техника полупроводников. 2014. Т.48. № 2. С. 278-282.
4. Курбатов Л.Н. Очерк истории приемников инфракрасного излучения на основе халькогенидов свинца / Л.Н. Курбатов / Вопросы оборонной техники. 1995. В. 1-2. С. 3.
5. Войтович Г.Д. Исследование оптических свойств, структуры и фазового состава слоев сульфида и селенида свинца / Г.Д. Войтович, М.С. Давыдов, А.И. Иванов, Г.П.Тихомиров / Оптико-механ. пром. 1966. № 12. С. 9–12.
6. Голубченко Н.В. Исследование микроструктуры и фазового состава поликристаллических слоев селенида свинца в процессе термического окисления / Н.В. Голубченко, В.А. Мошников, Д.Б. Чеснокова / Физика и химия стекла. 2006. Т. 32. № 3. С. 464-477.
7. Сергеева А.С. Термосенсибилизация химически осажденных пленок на основе твердых растворов $PbSe_yS_{1-y}$/ Сергеева А.С., Марков В.Ф., Маскаева Л.Н. / Физика и химия стекла. 2014. Т.40. № 2. С. 298-307.
8. Гамарц А.Е. Определение профиля диффузии кислорода в поликристаллических слоях селенида свинца методом ядерного микроанализа / А.Е. Гамарц, В.М. Лебедев, В.А. Мошников / Физика и техника полупроводников. 2004. Т. 38. В. 10. С. 1195-1197.
9. Томаев В.В. Эллипсометрический контроль параметров пленок селенида свинца при окислении / В.В. Томаев, М.Ф. Панов / Физика и химия стекла. 2006. Т. 32. № 3. С. 511-515.

10. Фреик Д.М. Изотермический отжиг пленок селенида свинца / Д.М. Фреик, Б.Ф. Костик, Л.И. Борик / Неорнан. материалы. 1984. Т. 20. № 5. С. 756-762.

11. Смирнова З.И. Модификация поверхности тонкопленочного селенида свинца путем выдержки в растворе соли олова(II) / Смирнова З.И., Маскаева Л.Н., Марков В.Ф., Воронин В.И., Кузнецов М.В. / Ж. Конденсированные среды и межфазные границы 2012. Т.14. № 2. С. 250-255.

12. Томаев В.В. Исследование продуктов окисления селенида свинца методом ИК спектроскопии / В.В. Томаев, И.В. Чернышева, П.А. Тихонов / Физика и химия стекла. 2007. Т. 33. № 6. С. 883-889.

13. Кирсанов А.Ю. Компьютерное моделирование процесса получения твердых растворов Pb1–xSnxSe гидрохимическим осаждением PbSe и SnSe / Кирсанов А.Ю., Марков В.Ф., Смирнова З.И., Маскаева Л.Н., / Успехи прикладной физики. 2013. Т.1. № 4. С. 516-519

14. Буткевич В.Г. Фотоприёмники и фотоприёмные устройства на основе поликристаллических и эпитаксиальных слоев халькогенидов свинца / В. Г. Буткевич, В.Д. Бочков / Прикладная физика. 2001. № 6. С. 66-112.

15. Юнович А.Э. Вынужденное излучение тонких пленок халькогенидов свинца при фотовозбуждении / А.Э. Юнович, В.П. Тен, М.С. Федоров / Физика и техника полупроводников. 1975. Т. 9. В. 5. С. 904-905.

16. Мухамедзянов Х.Н. Получение наноструктурированных высокофункциональных пленок селенида свинца / Х.Н. Мухамедзянов, М.П. Миронов, С.И. Ягодин, Л.Н. Маскаева, В.Ф. Марков / Цветные металлы. 2009. № 12. С. 57-60.

17. Серов И.Н. Анализ структурных характеристик нанокристаллических слоев селенида свинца / И.Н. Серов, М.А. Иошт, С.В. Кощеев / Микросистемная техника. 2004. №8. С. 17-20.

18. Смирнова З.И. Влияние йодсодержащей добавки на состав, структуру и морфологию химически осажденных пленок селенида свинца / Смирнова З.И., Баканов В.М., Маскаева Л.Н., Марков В.Ф., Воронин В.И. / Физика твердого тела. 2014. Т.56. Вып.12. С. 2468-2474

19. Урусов В.С. Твердые растворы в виде минералов / В.С. Урусов / Соросовский образовательный журнал. 1996. №11. С. 54-60.

20. Галески Ф. Вынужденное излучение тонких пленов PbSe при комнатной температуре / Ф. Галески, И.А. Дрозд, Л.Я. Лебедева / ФТП. 1977. Т. 11 В. 3. С. 568-570.

21. Воробель В.М. Электрофизические проявления структурных преобразований в слоях селенида кадмия / В.М. Воробель, В.С. Гриневич, В.А. Смынтина / Поверхность. Рентгеновские, синхротронные и нейтронные исследования. 2008. №10. С. 107-111.

22. Бачериков Ю.Ю. Фотолюминесценция наночастиц CdSe в пористом GaP / Ю.Ю. Бачериков. О.Б. Охрименко / ФТП. 2009. Т. 43. В.11. С. 1473-1476.

23. Гамарц А.Е. Фотолюминесценция в поликристаллических слоях $Pb_{1-x}Cd_xSe$ активированных в присутствии паров йода / А.Е. Гамарц, В.А. Мошников, Д.Б. Чеснокова / ФТП. 2006. Т. 40. В. 6. С. 683-685.

24. Непомнящий С.В. Фоточувствительность поликристаллических пленок $Pb_{1-x}Cd_xSe$ / С.В. Непомнящий, А.В. Пашкевич, Ю.Л. Шелехин / ФТП. 1984. Т. 18. В. 12. С. 2233-2235.

25. Дийков Л.К. Влияние УФ света на фоточувствительность поликристаллических пленок $Pb_{1-x}Cd_xSe$ / Л.К. Дийков, С.В. Непомнящий, А.В. Пашкевич / ФТП. 1983. Т. 18. В. 6. С. 1128-1130.

26. Гамарц А.Е. Поликристаллические слои $Cd_xPb_{1-x}Se$ с эффективной фотолюминесценцией. Модель зерна / А.Е. Гамарц, В.А. Мошников / Петербургский журнал электроники. 2005. № 4. С. 83-88.

27. Ильин В.А. Фоточувствительность поликристаллических пленок на основе $Pb_{1-x}Cd_xSe$ / В.А. Ильин, А.А. Петров, М.С. Писаревский / Петербургский журнал электроники. 2001. № 4. С. 93-100.

28. Спивак Ю.М. Особенности строения фоточувствительных поликристаллических слоев сетчатого типа на основе PbCdSe <I> / Ю.М. Спивак, В.А. Мошников / Поверхность. Рентгеновские, синхротронные и нейтронные исследования. 2010. №1. С. 97-102.

29. Мейтис Л. Введение в курс химического равновесия и кинетики / Л. Мейтис, пер. с англ. М.: Мир. 1984. 480 с. Перевод изд.: An introduction to chemical equilibrium and kinetics / L. Meites.

30. Чуфаров А.Ю., Зарубина Н.В., Форостяная Н.А., Ермаков А.Н., Григоров И.Г., Маскаева Л.Н., Марков В.Ф., Зайнуллин Ю.Г. Геометрии и состав тонких мультислойных пленок на основе селенидов кадмия и свинца / Поверхность. 2014. № 1. С. 71-76.

31. Rietveld H.M. A profile refinement method for nuclear and magnetic structures / J. Appl. Ctyst. 1969. V. 2. P. 65-71.

32. Марков В.Ф., Маскаева Л.Н. Особенности зародышеобразования и механизм роста пленок сульфидов металлов при осаждении тиокарбамидом / Изв.АН. Серия химическая. 2014. № 7. С. 1523-1532.

33. Марков В.Ф., Маскаева Л.Н. Расчет граничных условий образования твердой фазы сульфидов и селенидов осаждением тио- и селеномочевиной / Журнал физической химии. 2010. Т. 86. № 8. С. 1421-1426.

34. Физико-химические свойства полупроводниковых материалов. Справочник / Под ред. Новоселовой А.В., Лазарева В.В. М.: Наука, 1976. 339 с.

35. Шелимова Л.Е. Диаграммы состояния в полупроводниковом материаловедении. Системы на основе халькогенидов Si, Ge, Sn, Pb. М.: Наука. 1991. 368 с.

References

1. Taylor S. E. On time delays in lead salt semiconductor diode lasers / S.E. Taylor / Appl. Phys. A: Materials Science and Processing. 1986. V. 39. № 2. P. 91–94.

2. J.E. Hill, R.R. Chamberlin, “Process for marking conductive film”, Patent USA. N 3, 148, 084. from 08.09.1964.

3. Mukhamedzyanov Kh.N. Sravnitel'nye fotoelektricheskie kharakteristiki nano-strukturirovannykh plenok Pb1–xSnxSe, poluchennykh sovmestnym i posloinym osazhdeniem PbSe i SnSe / Kh.N. Mukhamedzyanov, Markov V.F., Maskaeva L.N. / Fizika tekhnika poluprovodnikov. 2014. T.48. № 2. S. 278-282.

4. Kurbatov L.N. Ocherk istorii priemnikov infrakrasnogo izlucheniya na osnove khal'kogenidov svintsa / L.N. Kurbatov / Voprosy oboronnoi tekhniki. 1995. V. 1-2. S. 3.

5. Voitovich G.D. Issledovanie opticheskikh svoistv, struktury i fazovogo sostava sloev sul'fida i selenida svintsa / G.D. Voitovich, M.S. Davydov, A.I. Ivanov, G.P.Tikhomirov / Optiko-mekhan. prom. 1966. № 12. S. 9–12.

6. Golubchenko N.V. Issledovanie mikrostruktury i fazovogo sostava polikristallicheskikh sloev selenida svintsa v protsesse termicheskogo okisleniya / N.V. Golubchenko, V.A. Moshnikov, D.B. Chesnokova / Fizika i khimiya stekla. 2006. T. 32. № 3. S. 464-477.

7. Sergeeva A.S. Termosensibilizatsiya khimicheski osazhdennykh plenok na osnove tverdykh rastvorov PbSeyS1–y/ Sergeeva A.S., Markov V.F., Maskaeva L.N. / Fizika i khimiya stekla. 2014. T.40. № 2. S 298-307

8. Gamarts A.E. Opredelenie profilya diffuzii kisloroda v polikristallicheskikh sloyakh selenida svintsa metodom yadernogo mikroanaliza / A.E. Gamarts, V.M. Lebedev, V.A. Moshnikov / Fizika i tekhnika poluprovodnikov. 2004. T. 38. V. 10. S. 1195-1197.

9. Tomaev V.V. Ellipsometricheskii kontrol' parametrov plenok selenida svintsa pri okislenii / V.V. Tomaev, M.F. Panov / Fizika i khimiya stekla. 2006. T. 32. № 3. S. 511-515.

10. Freik D.M. Izotermicheskii otzhig plenok selenida svintsa / D.M. Freik, B.F. Kostik, L.I. Borik / Neornan. materialy. 1984. T. 20. № 5. S. 756-762.

11. Smirnova Z.I. Modifikatsiya poverkhnosti tonkoplenochnogo selenida svintsa putem vyderzhki v rastvore soli olova(II) / Smirnova Z.I., Maskaeva L.N., Markov V.F., Voronin V.I., Kuznetsov M.V. / Zh. Kondensirovannye sredy i mezhfaznye granitsy 2012. T.14. № 2. S. 250-255.

12. Tomaev V.V. Issledovanie produktov okisleniya selenida svintsa metodom IK spektroskopii / V.V. Tomaev, I.V. Chernysheva, P.A. Tikhonov / Fizika i khimiya stekla. 2007. T. 33. № 6. S. 883-889.

13. Kirsanov A.Yu. Komp'yuternoe modelirovanie protsessa polucheniya tverdykh rastvorov Pb1–xSnxSe gidrokhimicheskim osazhdeniem PbSe i SnSe / Kirsanov A.Yu., Markov V.F., Smirnova Z.I., Maskaeva L.N., / Uspekhi prikladnoi fiziki. 2013. T.1. № 4. S. 516-519.

14. Butkevich V.G. Fotopriemniki i fotopriemnye ustroistva na osnove polikristallicheskikh i epitaksial'nykh sloev khal'kogenidov svintsa / V. G. Butkevich, V.D. Boch-kov / Prikladnaya fizika. 2001. № 6. S. 66-112.

15. Yunovich A.E. Vynuzhdennoe izluchenie tonkikh plenok khal'kogenidov svintsa pri fotovozbuzhdenii / A.E. Yunovich, V. P. Ten, M.S. Fedorov / Fizika i tekhnika poluprovodnikov. 1975. T. 9. V. 5. S. 904-905.

16. Mukhamedzyanov Kh.N. Poluchenie nanostrukturirovannykh vysokofunktsional'nykh plenok selenida svintsa / Kh.N. Mukhamedzyanov, M.P. Mironov, S.I. Yagodin, L.N. Maska-eva, V.F. Markov / Tsvetnye metally. 2009. № 12. S. 57-60.

Serov I.N. Analiz strukturnykh kharakteristik nanokristallicheskikh sloev selenida svintsa / I.N. Serov, M.A. Iosht, S.V. Koshcheev / Mikrosistemnaya tekhnika. 2004. №8. S. 17-20.

18. Smirnova Z.I. Vliyanie iodsoderzhashchei dobavki na sostav, strukturu i morfologiyu khimicheski osazhdennykh plenok selenida svintsa / Smirnova Z.I., Bakanov V.M.,

Maskaeva L.N., Markov V.F., Voronin V.I. / Fizika tverdogo tela. 2014. T.56. Vyp.12. S. 2468-2474.

19. Urusov V.S. Tverdye rastvory v vide mineralov / V.S. Urusov / Sorosovskii obrazovatel'nyi zhurnal. 1996. №11. S. 54-60.

20. Galeski F. Vynuzhdennoe izluchenie tonkikh plenov PbSe pri komnatnoi temperature / F. Galeski, I.A. Drozd, L.Ya. Lebedeva / FTP. 1977. T. 11 V. 3. S. 568-570.

21. Vorobel' V.M. Elektrofizicheskie proyavleniya strukturnykh preobrazovanii v sloyakh selenida kadmiya / V.M. Vorobel', V.S. Grinevich, V.A. Smyntina / Poverkhnost'. Rentgenovskie, sinkhrotronnye i neitronnye issledovaniya. 2008. №10. S. 107-111.

22. Bacherikov Yu.Yu. Fotolyuminestsentsiya nanochastits CdSe v poristom GaP / Yu.Yu. Bacherikov. O.B. Okhrimenko / FTP. 2009. T. 43. V.11. S. 1473-1476

23. Gamarts A.E. Fotolyuminestsentsiya v polikristallicheskikh sloyakh Pb1-xCdxSe aktivirovannykh v prisutstvii parov ioda / A.E. Gamarts, V.A. Moshnikov, D.B. Chesnokova / FTP. 2006. T. 40. V. 6. S. 683-685.

24. Nepomnyashchii S.V. Fotochuvstvitel'nost' polikristallicheskikh plenok Pb1–xCdxSe / S.V. Nepomnyashchii, A.V. Pashkevich, Yu.L. Shelekhin / FTP. 1984. T. 18. V. 12. S. 2233-2235.

25. Diikov L.K. Vliyanie UF sveta na fotochuvstvitel'nost' polikristallicheskikh plenok Pb1-xCdxSe / L.K. Diikov, S.V. Nepomnyashchii, A.V. Pashkevich / FTP. 1983. T. 18. V. 6. S. 1128-1130.

26. Gamarts A.E. Polikristallicheskie sloi CdxPb1–xSe s effektivnoi fotolyuminestsentsiei. Model' zerna / A.E. Gamarts, V.A. Moshnikov / Peterburgskii zhurnal elektroniki. 2005. № 4. S. 83-88.

27. Il'in V.A. Fotochuvstvitel'nost' polikristallicheskikh plenok na osnove Pb1-xCdxSe / V.A. Il'in, A.A. Petrov, M.S. Pisarevskii / Peterburgskii zhurnal elektroniki. 2001. № 4. S. 93-100.

28. Spivak Yu.M. Osobennosti stroeniya fotochuvstvitel'nykh polikristallicheskikh sloev setchatogo tipa na osnove PbCdSe <I> / Yu.M. Spivak, V.A. Moshnikov / Poverkh-nost'. Rentgenovskie, sinkhrotronnye i neitronnye issledovaniya. 2010. №1. S. 97-102.

29. Meitis L. Vvedenie v kurs khimicheskogo ravnovesiya i kinetiki / L. Meitis, per. s angl. M.: Mir. 1984. 480 s. Perevod izd.: An introduction to chemical equilibrium and kinetics / L. Meites.

30. Chufarov A.Yu., Zarubina N.V., Forostyanaya N.A., Ermakov A.N., Grigorov I.G. ,

Maskaeva L.N., Markov V.F., Zainullin Yu.G. Geometrii i sostav tonkikh mul'tisloinykh plenok na osnove selenidov kadmiya i svintsa / Poverkhnost'. 2014. № 1. S. 71-76

31. Rietveld H.M. A profile refinement method for nuclear and magnetic structures / J. Appl. Ctyst. 1969. V. 2. P. 65-71

32. Markov V.F., Maskaeva L.N. Osobennosti zarodysheobrazovaniya i mekhanizm rosta plenok sul'fidov metallov pri osazhdenii tiokarbamidom / Izv.AN. Seriya khimiche-skaya. 2014. № 7. S. 1523-1532

33. Markov V.F., Maskaeva L.N. Raschet granichnykh uslovii obrazovaniya tverdoi fa-zy sul'fidov i selenidov osazhdeniem tio- i selenomochevinoi / Zhurnal fizicheskoi khimii. 2010. T. 86. № 8. C. 1421-1426.
34. Fiziko-khimicheskie svoistva poluprovodnikovykh materialov. Spravochnik / Pod red. Novoselovoi A.V., Lazareva V.V. M.: Nauka, 1976. 339 s.
35. Shelimova L.E. Diagrammy sostoyaniya v poluprovodnikovom materialovedenii. Sistemy na osnove khal'kogenidov Si, Ge, Sn, Pb. M.: Nauka. 1991. 368 s.

УДК 546.815, 221

Состав, структура, морфология гидрохимически осажденных пленок в системе PbSe–CdSe

[1] Нина Викторовна Зарубина
[2] Иван Владимирович Зарубин
[3] Лариса Николаевна Маскаева
[4] Вячеслав Филиппович Марков

[1-4] Уральский федеральный университет имени первого Президента России Б.Н. Ельцина, Российская Федерация
620002, Россия, Свердловская область, Екатеринбург, ул. Мира, 19
[1] Аспирант
E-mail: nina6131@mail.ru
[2] Ведущий инженер
E-mail: ivan-carevich85@mail.ru
[3] Профессор, доктор химических наук
E-mail: mln@ural.ru
[4] Профессор, доктор химических наук
E-mail: v.f.markov@ustu.ru

Аннотация. С учетом критического зародыша рассчитана область совместного осаждения селенидов свинца и кадмия в реакционной системе “$Pb(CH_3COO)_2$ – $CdCl_2$ – $Na_3C_6H_5O_7$ – NH_4OH – $CSeN_2H_4$”. Гидрохимическим соосаждением селенидов свинца и кадмия получены тонкие пленки пересыщенных твердых растворов $Cd_xPb_{1-x}Se$ с кубической структурой *B*1 (NaCl). Установлены закономерности образования твердых растворов $Cd_xPb_{1-x}Se$ и кинетика их роста в зависимости от состава реакционной смеси. Методами рентгенофазового и энерго-дисперсионного анализов, электронно-микроскопическими исследованиями изучены структура, состав и морфология пленок PbSe–CdSe.

Ключевые слова: химическое осаждение; тонкие пленки; $Cd_xPb_{1-x}Se$; пересыщенные твердые растворы замещения.